Universidade de Aveiro Departamento de Biologia
2013

ANA ISABEL COSTA CALEJO

Regulação de Eventos Exocitóticos pela Via de Sinalização do cAMP

Regulation of Single Exocytotic Events by the cAMP Signaling Pathway

Dissertação apresentada à Universidade de Aveiro para cumprimento dos requisitos necessários à obtenção do grau de Doutor em Biologia, realizada sob a orientação científica da Doutora Maria Paula Polónia Gonçalves, Professora Associada do Departamento de Biologia da Universidade de Aveiro e do Doutor Robert Zorec, Professor Catedrático da Faculdade de Medicina da Universidade de Ljubljana

Apoio financeiro da FCT e do FSE no âmbito do III Quadro Comunitário de Apoio.

o júri

presidente

Prof. Doutor Carlos Alberto Diogo Soares Borrego
Professor Catedrático da Universidade de Aveiro

Prof. Doutor Robert Zorec (co-orientador)
Full Professor, Faculty of Medicine, Univerza v Ljubljani

Prof. Doutor Christopher Exley
Full Professor, The Birchall Centre, Lennard-Jones Laboratories, Keele University

Prof. Doutor Luís Manuel de Oliveira Martinho do Rosário
Professor Associado da Faculdade de Ciências e Tecnologia da Universidade de Coimbra

Prof. Doutora Maria Paula Polónia Gonçalves (orientadora)
Professora Associada da Universidade de Aveiro

Prof. Doutor Manuel António da Silva Santos
Professor Associado da Universidade de Aveiro

agradecimentos

Em primeiro lugar agradeço ao Departamento de Biologia e ao CESAM da Universidade de Aveiro. À Fundação para a Ciência e Tecnologia pelo financiamento sob a forma de uma Bolsa de Doutoramento (SFRH/BD/41271/2007) e Bilateral Agreement between Portugal and Slovenia – Proc.º 441.00 ESLOVÉNIA.

À Prof. Maria Paula Polónia Gonçalves um agradecimento pelo apoio e orientação científica desta tese de doutoramento, que tornaram possível este trabalho.

I would like to thank my co-mentor Prof. Robert Zorec. First for making me fell so welcome in his lab and also for all the support, guidance and encouragements during these last years.

To my great colleagues and friends Virgília and Jernej without their support, encouragement, guidance and friendship this work would never be possible.

To friends and colleagues in Ljubljana: Ajda, Bostjan, Alenka, Marusa, Sasa, Priyanka, Nina, Matejka, Marko, Maja, Vale, Lenka, Marko Kreft and Matjaz. Miss you all!

Aos meus amigos, do Porto e Aveiro, que estão sempre presentes nos momentos bons e mais difíceis, sempre com uma palavra amiga. Especialmente à Daniela e à Ana, obrigado por desde sempre serem minhas amigas.

Gostaria de agradecer também a toda a minha família, avós, tios e primos.

Agradeço à minha irmã por estar sempre do meu lado, sempre com apoio e uma palavra amiga. Ao meu mano que apesar de ainda ser pequeno para ter palavras de apoio, apoia pelo simples facto de estar lá.

Aos meus pais, agradeço pela muita paciência que sempre me dispensaram que foram tão decisivos na concretização deste trabalho. Pelo apoio em todos os momentos e decisões. Muito obrigado.

Por último um muito obrigado ao Filipe por em todos os momentos estar ao meu lado. Pela amizade que demonstrou em todas as ocasiões, sempre com uma palavra de força, encorajamento, apoio e com muita paciência. Por me ajudar e apoiar em todos os momentos e decisões.

palavras-chave

Exocitose regulada, lactotrofos da hipófise anterior, libertação de prolactina, propriedades do poro de fusão, sinalização por cAMP, canais HCN, citotoxicidade do alumínio

resumo

Permanece por esclarecer como a via de sinalização do cAMP modula a exocitose regulada.

Os principais objetivos deste trabalho foram: i) avaliar o efeito do cAMP nos eventos exocitóticos, nas propriedades dos poros de fusão e na secreção hormonal; ii) perceber o impacto da sinalização por cAMP-HCN na exocitose e nas propriedades do poro de fusão; e iii) estudar as propriedades do poro de fusão na presença de um agente neurotóxico comum, como o alumínio. Lactotrofos, isolados a partir da hipófise anterior de ratos Wistar machos, foram usados como modelo celular. Os eventos unitários de fusão exocitótica e a prolactina (PRL) libertada foram avaliados, respetivamente, em ensaios eletrofisiológicos efectuados segundo a técnica de contacto hermético no modo sobre a célula aderida à pipeta porta-elétrodo e com recurso a métodos imunológicos de deteção. Os níveis intracelulares de cAMP foram aumentados por 3-isobutil-1-metilxantina (IMBX), forscolina e N^6,2'-O-dibutiril adenosina-3',5'-monofosfato cíclico (dbcAMP). A expressão dos canais HCN foi determinada por Western-blot, qRT-PCR e imunocitoquímica em combinação com microscopia confocal. Culturas primárias de lactotrofos foram também transfetadas com DNA plasmídico que codifica HCN2 juntamente com a proteína-verde-fluorescente e um agente farmacológico foi usado para avaliar o efeito de cAMP-HCN na exocitose.

Observou-se que os lactotrofos responderam à forscolina e ao dbcAMP libertando PRL de um modo bifásico e dependente da concentração, uma vez que a secreção aumentou e diminuiu, respectivamente, na gama de baixas e altas concentrações. Os compostos que elevaram os níveis de cAMP aumentaram os eventos transientes e impediram a fusão completa. Além disso, o dbcAMP promoveu o aparecimento de eventos exocitóticos transientes de elevada periodicidade, cujos poros de fusão, de maior diâmetro, se mativeram abertos durante mais tempo. A expressão das quatro isoformas de HCN foi confirmada nos lactotrofos ao nível do mRNA e, tal como no coração, rim e hipófise, o mais abundante codifica a isoforma HCN2. Nos lactotrofos com sobre-expressão desta isoforma, o dbcAMP não só aumentou a frequência dos eventos transientes e a condutância dos poros, mas também a frequência dos eventos de fusão completa. Enquanto o bloqueador dos canais HCN, ZD7288, reduziu a frequência dos eventos transientes e de fusão completa desencadeados por dbcAMP e diminuiu o diâmetro dos poros de fusão. A simultânea diminuição da libertação de PRL, da frequência dos eventos transientes e do diâmetro dos poros de fusão representaram as principais alterações observados após pré-tratamento dos lactotrofos com concentração micromolar de alumínio.

Em conclusão, os resultados demonstram que elevados níveis de cAMP reduzem a secreção de PRL devido à estabilização dos poros de fusão no estado de maior abertura. Além disso, a via de sinalização cAMP-HCN afecta a actividade exocitótica e modifica as propriedades dos poros de fusão, que parecem ser igualmente importantes na citotoxicidade induzida por alumínio.

keywords

Regulated exocytosis, anteror pituitary lactotrophs, prolactin release, fusion pore properties, cAMP signaling, HCN channels, aluminium toxicity

abstract

How the second messenger cAMP modulates regulated exocytosis is still poorly understood.
The goals of this work were: i) to evaluate cAMP effect on single exocytotic events, fusion pore properties and hormone release; ii) to assess the impact of cAMP-HCN signaling on exocytosis and fusion pore properties; and iii) to study fusion pore properties in the presence of a common neurotoxic agent, such as aluminium.
Anterior pituitary lactotrophs isolated from male Wistar rats were used as the cell model. Electrophysiology in cell attached patch-clamp mode and immuno assays were used to monitor unitary exocytic fusion events and prolactin (PRL) release, respectively. Intracellular cAMP concentration was raised with 3-isobutyl-1-methylxanthine (IBMX), forskolin and N^6,2'-O-dibutyryl adenosine-3′,5′-cyclic monophosphate (dbcAMP). HCN channel expression was determined by using Western-blot, qRT-PCR and immunocytochemistry in combination with confocal microscopy. Primary cell cultures were also transfected with plasmid DNA encoding HCN2 together with enhanced-green-fluorescence protein and a pharmacological agent was applied to evaluate cAMP-HCN effects on exocytosis.
We observed that lactotrophs responded to forskolin and dbcAMP by releasing PRL in a biphasic dose-dependent manner, since secretion increased and decreased in the presence of low and high concentration ranges, respectively. cAMP-increasing agents enhanced transient events, while full-fusion events were prevented. Moreover, dbcAMP promoted the appearance of extreme periodic bursts of transient events that exhibited longer fusion pore life-time and wider diameters. The expression of the four HCN isoforms was confirmed at mRNA transcript level in lactotrophs and, like in heart, kidney and pituitary, the most abundant encodes HCN2 isoform. In HCN2 over-expressing lactotrophs, dbcAMP not only enhanced the frequency of transient events and pore conductance but also the frequency of full-fusion events. While, the HCN channel blocker, ZD7288, reduced the frequency of full-fusion and transient events elicited by dbcAMP and narrowed the fusion pore diameters. Finally, the simultaneous reduction on PRL release, transient events frequency and fusion pore diameters represented the main alterations observed after lactotrophs pre-treatment with micromolar aluminium concentration.
In conclusion, the results show that high cAMP reduces PRL secretion due to the stabilization of the wide fusion pore state. Additionally, cAMP-HCN signaling cascade affects exocytic activity and modifies fusion pore properties, which also appear to be relevant in the aluminium induced cytotoxicity.

Index

Abbreviations

AC	adenylyl cyclase
$AlCl_3$	aluminium chloride
AP	action potential
ATP	adenosine-5'-triphosphate
a.u.	arbitrary units
BSA	bovine serum albumin
$[Ca^{2+}]_i$	intracellular calcium concentration
cAMP	adenosine 3',5'- cyclic monophosphate
cDNA	complementary deoxyribonucleic acid
C_m	membrane capacitance
c_m	specific membrane capacitance
CNBD	cyclic nucleotide binding domain
C_v	vesicle capacitance
dbcAMP	N^6,2'-O dibutyryl cyclic adenosine monophosphate
DMSO	dimethyl sulfoxide
EGFP	enhanced green fluorescent protein
ELISA	enzyme-linked immunosorbent assay
Epac	exchange protein directly activated by cAMP
FP	forward primer
gDNA	genomic deoxyribonucleic acid
G_p	fusion pore conductance
HCN	hyperpolarization-activated cyclic nucleotide–gated channels
HEPES	4-(2-hydroxyethyl)piperazine-1-ethanesulfonic acid
IBMX	3-isobutyl-1-methylxanthine
I_h	hyperpolarization-activated currents
Im	imaginary part of the admittance trace
kDa	kilodalton
LDCV	large dense core vesicles
MW	molecular weight
PDE	phosphodiesterase
pDNA	plasmid deoxyribonucleic acid

PKA	protein kinase A
PRL	prolactin
qRT-PCR	quantitative real-time polymerase chain reaction
PBS	phosphate buffered-saline
PVDF	polyvinylidene fluoride
Re	real part of the admittance
RP	reverse primer
s.e.m.	standard error of the mean
SNARE	soluble N-ethylmaleimide-sensitive factor attachment protein receptor
SDS-PAGE	sodium dodecyl sulphate polyacrylamide gel electrophoresis
SSV	small synaptic vesicles
TBS	tris buffered saline
TBS-T	tris buffered saline and tween 20
ZD7288	4-ethylphenylamino-1,2-dimethyl-6-methylaminopyrimidinium chloride

Chapter I - Introduction and objectives

1 Introduction

Synopsis of exocytotic process

Exocytosis is a vital process for eukaryotic cell-to-cell communication, the currency of this information exchange in the whole body is hormonal release and synaptic transmission. These must be very precise and organized processes, or else they would destroy the highly efficient and differentiated structure of the eukaryotic cell. Exocytosis is based on the ability of secretory and synaptic vesicles to fuse with the plasma membrane and subsequently discharge their content, while endocytosis is essentially the reverse process, where the vesicle is recovered from the plasma membrane carrying material from the extracellular space. Researchers have extensively and continuously studied exocytosis and extraordinary progress has been made towards the understanding of this process but a lot remains unknown.

In secretory cells, exocytosis can occur via two different secretory pathways: the constitutive and the regulated (Burgess and Kelly, 1987; Orci *et al*., 1987). Orci *et al*., (1987) observed these two routes using electron microscopy by following a regulated hormone (insulin) and a constitutive protein (hemagglutinin). The constitutive pathway is ubiquitous in all eukaryotic cells and occurs mainly in preserving the plasma membrane integrity and identity. Therefore, in this exocytotic pathway there is no need for an external signal. On the other hand, regulated exocytosis is largely limited to specialized secretory cells, including neurons and neuroendocrine cells. In this case, the release can be controlled by extracellular and/or intracellular signals but commonly converges to a transient elevation of intracellular Ca^{2+}.

The first reports about regulated exocytosis appeared in the early 1950s. Katz and colleagues proposed a quantal release model for acetylcholine in neuromuscular junction (Fatt and Katz, 1952). They showed that each miniature end-plate potential follows the discharge of multi-molecular quantum of acetylcholine from the nerve terminal (Fatt and Katz, 1952). In this hypothesis, transmitters are stored in packages and released by a mechanism called regulated

exocytosis. A quantal package of transmitters is released into the extracellular medium, generating a signal (quantum), after Ca^{2+} entry into the presynaptic terminal (Katz, 1969). Later, it was also confirmed that this is not restricted to the cholinergic system, it occurs in several types of synapses and that transmitters are packed in structures called vesicles. These findings led to the proposal of two models in the early 1970s.

The Heuser and Reese model of regulated exocytosis postulates that vesicle fusion with the plasma membrane leads to the total release of the vesicle content and the vesicle membrane becomes fully incorporated into the plasma membrane (i.e. full-fusion exocytosis). Moreover, membrane balance is maintained with the retrieval of an equal amount of plasma membrane (i.e. endocytosis) (Heuser and Reese, 1973). Thereby, after formation of the fusion pore between the vesicle and plasma membrane, the release of the transmitter (quantum) occurred rapidly, as an all-or-nothing event.

An alternative exocytotic model was also proposed (Ceccarelli *et al.,* 1973), which is closer to Katz's initial idea (Katz, 1969). During exocytosis, vesicles momentarily fuse with the plasma membrane and are locally recycled to be reused again in the next round of exocytosis. This mode of exocytosis was later termed kiss-and-run (Fesce *et al*., 1994).

The field of exocytosis and vesicular release was renewed in early 1980s with the development of new techniques. Direct measurements of single vesicle fusion with the plasma membrane became possible with the high-resolution membrane capacitance patch clamp technique. Since biological membranes behave like electrical capacitors, membrane capacitance (C_m) is proportional to the area of the membrane. Therefore, high-resolution measurements of C_m, allow the detection of small changes in cell membrane surface area that reflect unitary fusion and fission events, corresponding to exocytosis and endocytosis, respectively (Neher and Marty, 1982). Another powerful method is amperometry, which is based on the electrochemical detection of released molecules from a single vesicle in real time (Wightman *et al*., 1991; Chow *et al*., 1992). Furthermore, high-resolution optical methods using different fluorescent markers have also been used to study unitary vesicle exocytosis and endocytosis (Betz and Bewick, 1992).

Researchers were able to monitor in real-time, single cells or membrane patches, with sufficient resolution to distinguish unitary fusion and fission events of vesicle, and concluded that vesicle fusion and content discharge are more complex processes than previously considered. For instance, discharge of vesicle content could be delayed relative to membrane fusion (Chow *et al*., 1992).

These data raised new challenges in the understanding of exocytosis and of fusion pore (a channel like structure formed between vesicle and plasma membranes during exocytosis). A new explanatory model was proposed. In this model, the fusion pore is formed for a short period of time, allowing only partial (or none) vesicular content release and can alternate between an open and a close state (Stenovec *et al.,* 2004; Vardjan *et al*., 2007). These transient events can appear in bursts, repetitively opening and closing of the fusion pore (Henkel *et al*., 2000; Weise *et al.,* 2000; Staal *et al.,* 2004; Stenovec *et al.,* 2004; Vardjan *et al*., 2007). Moreover, bursts can exhibit periodicity, i.e. relatively constant times between single events (Stenovec *et al*., 2004). Although there are differences between the original kiss-and-run and the latest mode, both modes are collectively called transient exocytosis in this work.

Transient and full fusion modes of exocytosis have been extensively documented during that last 40 years. Both modes were reported to coexist in the same cell, however, their relative abundance appears to be cell type specific, as demonstrated in neurons (Gandhi and Stevens, 2003; Harata *et al*., 2006), astrocytes (Chen *et al.*, 2005), chromaffin cells (Elhamdani *et al.,* 2006), posterior pituitary slices (Klyachko and Jackson, 2002) and lactotrophs (Vardjan *et al.,* 2007).

Regulated exocytosis has also been extensively studied at rest and during stimulation of cells. Even without application of an external stimulus, cells undergo regulated exocytosis (spontaneous activity) under physiological extracellular conditions. Spontaneous and stimulated exocytosis share some common properties, although recent studies suggest that the exocytotic molecular apparatus at spontaneous conditions differs from the one under stimulation (Hua *et al.,* 1998; Deák *et al.,* 2006; Pang *et al.,* 2006). The fusion of both plasma and vesicle membranes appears to be a very energetically unfavorable process. Not

only, the two opposing membranes are negatively charged (Kozlov and Markin, 1983) but also lipid-bilayer should to become a highly curved structure (Kralj-Iglic *et al.,* 1999). Proteins and lipids are required to promote fusion (Breckenridge and Almers, 1987; Han *et al.,* 2004; Rohrbough and Broadie*,* 2005; Churchward *et al*., 2005). Exocytosis is accomplished by these two components in a multipart mechanism where both regulate each other (Zimmerberg *et al*., 1991). In the exocytotic apparatus, soluble N-ethylmaleimide-sensitive factor attachment protein receptors (SNAREs) are thought to be the most prominent proteins to promote the fusion (review in Jahn, 2003; Li and Chin, 2003; Jahn and Scheller, 2006). SNAREs present in the vesicle and the plasma membrane interact with each other during several steps of exocytosis, bringing the two membranes in close contact and facilitating fusion (Michael *et al*., 2006; Schweizer and Ryan, 2006), due to the formation of the SNARE complex (Sollner *et al*., 1993). Sphingosine, inositol phospholipids and cholesterol are lipids, which involvement has been shown to facilitate Ca^{2+}-regulated exocytosis (Eberhard *et al*., 1990; Churchward *et al*., 2005; Darios *et al.*, 2009). Stimulated and spontaneous exocytosis also contrast in respect to the exocytic mode, fusion pore properties and release kinetics (Fulop *et al*., 2005; Elhamdani *et al*., 2006; Staal *et al.,* 2004; Stenovec *et al.*, 2004; Vardjan *et al*., 2007), which endorse whether they are differently triggered and regulated.

For fusion between the vesicle and the plasma membrane to occur a trigger signal is necessary, which normally is an increase in $[Ca^{2+}]_i$. Ca^{2+} signal may originate from intracellular pools (mainly endoplasmic reticulum and mitochondria) and/or from the extracellular environment, where the concentration of Ca^{2+} is several orders of magnitude higher than in the cytosol (Berridge *et al*., 2003). Initially, vesicle and plasma membranes merge to form a stalk that develops into a narrow fusion pore; which is still too narrow for vesicle content discharge. A subsequent expansion of the fusion pore takes place, and a channel-like structure connecting the vesicle lumen with the cell exterior is formed (Breckenridge and Almers, 1987; Spruce *et al.,* 1990). Finally, vesicular content is discharged from the vesicle into the extracellular space. Even though fusion pore formation and secretion are essentially related processes, they can be considered as two separate steps of the exocytic process. Prior to fusion with the plasma membrane

and cargo discharge, exocytotic vesicles are engaged in a complex multi-step process, the vesicle cycle. Briefly, this cycle involves at least trafficking to the plasma membrane, docking in membrane close proximity and priming before maturing as fusion-competent vesicles (review in Klenchin and Martin, 2000; Verhage and Sørensen, 2008). Most likely, the undocked group comprises the majority of vesicles, which corresponds to the “reserve pool”. Fusion-competent vesicles ("readily releasable pool") seem to be in minority and are usually sub-divided into fast and slow discharging according to the release latency after increase in $[Ca^{2+}]_i$ (review in Stojilkovic, 2005). Secretory vesicles involved in regulated exocytosis also differ significantly in terms of their size. In endocrine and neuroendocrine cells there are large dense-core vesicles (LDCVs, 200-500nm; Zorec *et al*., 1991; Angleson *et al*., 1999) and also small synaptic-like vesicles (SSVs, 25-80 nm; Takamori *et al*., 2006).

One of the most controversial topics about regulated exocytosis modulation is whether this is a post-fusionally process. First, the majority of studies focused on pre-fusion intracellular signaling, such as calcium concentration and the role of ionic channels (Rahamimoff *et al*., 1980; 1989). In the late 1990s, it was proposed that regulation of vesicular content release also occurred after fusion pore state (Rahamimoff and Fernandez, 1997). Later, Stenovec and co-workers (2004) showed that after potassium stimulation hormonal discharge and FM styryl dye loading into vesicles occurred within seconds, indicating that in lactotrophs stimulation increases the rate of vesicle cargo release, very likely at the stage when the fusion pore is already formed. Moreover, widening of pre-formed narrow fusion pores was clearly demonstrated to take place after stimulation allowing cargo discharge (Elhamdani *et al*., 2006; Vardjan *et al*., 2007). Miklavc and Frick (2011) proposed that after a narrow fusion pore is formed, Ca^{2+} enters via vesicle-associated Ca^{2+} channels into the cytosol, regulating exocytosis and secretion. These studies are strong evidence that modulation of regulated exocytosis is post-fusionally controlled by the fusion pore (Staal *et al.,* 2004; Stenovec *et al.,* 2004; Miklavc and Frick, 2011).

Cyclic AMP-dependent exocytosis

In addition to Ca^{2+}, other intracellular second messengers have also been shown to regulate exocytosis, like cyclic 3',5'-adenosine monophosphate (cAMP) (reviewed in Seino and Shibasaki, 2005). Cyclic AMP is synthesized from ATP by membrane-bound and soluble adenylyl cyclases (ACs) and it's degraded by phosphodiesterases (PDEs). The intracellular cAMP concentration is the result of a balance between cAMP production by ACs and degradation by PDEs, therefore, drugs that affect either synthesis or degradation of cAMP can alter its intracellular concentration. Cyclic AMP is an ubiquitous intracellular second messenger, the signals of which may be localized in distinct microdomains within the cell whereby they are involved in the regulation of a wide range of physiological processes in many types of cells (Zaccolo and Pozzan, 2003).

Measurements on bovine lactotrophs with the whole-cell patch-clamp mode showed that cAMP increases the magnitude and rate of Ca^{2+}-trigged exocytosis, however it had no effect in the absence of Ca^{2+} (Sikdar *et al*., 1990). cAMP was also shown to enhance the apparent sensitivity of vesicle to Ca^{2+} influx by increasing the number of vesicles with higher release probabilities (Sakaba and Neher, 2001). Chen and co-workers (2004) showed that cAMP increasing agents (forskolin and dibutyryl cAMP) mediate the secretion of the gonadotropin-releasing hormone from immortalized GT1-7 neurons in a L-type Ca^{2+} channel dependent manner. It is consensual that cross-talk between Ca^{2+} and cAMP signaling pathways in regulated exocytosis is crucial (Zaccolo and Pozzan, 2003). Even though, the majority of studies point to the fact that both cAMP and Ca^{2+} trigger and/or promote exocytosis, there are some cell models that represent the exception, like in renin (Grunberger *et al*., 2006) and leptin (Szkudelski *et al*., 2005) secretion. In the first case, renin secretion from juxtaglomerular cells is inhibited by Ca^{2+} while cAMP is the main promoter of release (Grunberger *et al.*, 2006). In leptin secretion, agonists of cAMP effectors diminish the release induced by glucose, alanine and leucine, while antagonists promote it, showing that in adipocytes cAMP inhibits secretion (Szkudelski *et al.,* 2005).

The complexity of cross-talk between Ca^{2+} and cAMP in regulated exocytosis impelled us in the year 2006, to start our work with the purpose to

elucidate the effect of cAMP on Ca^{2+}-regulated exocytosis in rat pituitary lactotrophs. Lactotrophs constitute 10-25% of anterior pituitary lobe and are, unlike other anterior pituitary cells, under tonic dopaminergic inhibitory control of the hypothalamus (Porter *et al.,* 1994; Freeman *et al*., 2000; Ben-Jonathan and Hnasko, 2001). Lactotrophs mainly secrete prolactin (PRL), which is perhaps best known for its role in lactation. However, it is now recognized that this hormone is the most versatile hormone regarding its range of actions, with over 300 separate biological functions, more than all other hormones from the pituitary combined (Bole-Feysot *et al.,* 1998 for review). After being synthesized, prolactin is stored in LDCV (Dannies, 2003; Huerta-Ocampo *et al.,* 2005). Lactotrophs fire action potentials (AP) independently of any external signal (Sankaranarayanan and Simasko, 1996). Thereby, *in vitro*, lactotrophs fire APs at rest (without any external signal), which causes transient elevation in $[Ca^{2+}]_i$ (Ben-Jonathan and Hnasko, 2001). Hence, basal prolactin secretion from lactotrophs is rather high, when in culture they exhibit a continued release of prolactin and respond to physiological stimulus by altering prolactin secretion (Ben-Jonathan and Hnasko, 2001). In lactotrophs, fusion of vesicles with the plasma membrane is primary triggered by an increase in $[Ca^{2+}]_i$, due to Ca^{2+} influx through activated L-type voltage-gated Ca^{2+} channels (see Stojilkovic *et al*., 2005 for review). Therefore, lactotrophs are very important and useful model to study exocytosis of hormones (Gonzalez-Iglesias *et al.,* 2006; Vardjan *et al.,* 2007).

Our first goal (Chapter II) was to understand the effect of cAMP on vesicle fusion and PRL release in lactotrophs. To increase intracellular levels of cAMP, well known cAMP-increasing agents were used: (i) 3-isobutyl-1-methylxanthine (IBMX) a PDE inhibitor, which blocks cAMP degradation increasing its intracellular levels; (ii) forskolin, an AC activator, which promotes the production of cAMP in cells and (iii) N^6,2'-O-dibutyryl cAMP (dbcAMP), a membrane permeable cAMP analog. We preformed electrophysiological studies in the cell-attached mode, which allowed us to gather information not only about the exocytic mode itself but also about the properties of the fusion pore. Meanwhile, using cell-attached patch-clamp approach it was shown that forskolin increases transient exocytotic mode in mammalian pancreatic β-cells (MacDonald *et al*., 2006; Braun *et al.*, 2009; Hanna

et al., 2009). In pituitary lactotroph cultures, prolactin release was quantified by using competitive enzyme immunoassay ELISA kit. Cells were incubated for 20 min in the extracellular solution (control) and in the extracellular containing 10 mM dbcAMP (+dbcAMP). In the presence of dbcAMP, PRL release was relatively low, 0.87±0.08 ng/ml/min, while in control condition was 1.61±0.12 ng/ml/min. This observation showed that cAMP does not always increase hormonal discharge in lactotrophs, as previously reported (Gonzalez-Iglesias *et al.,* 2006). Therefore, to understand in more detail cAMP-dependent PRL release, a new set of experiments were performed using a perfusion system. Besides, intracellular effects of cAMP on exocytosis were postulated to be mainly mediated by cAMP-dependent protein kinase A (PKA), in the late 1990s was shown that in mouse pancreatic β-cells cAMP stimulated exocytosis can occur via PKA-dependent and PKA-independent manner (Reström *et al*., 1997).

In 1998 the discovery of the cAMP receptor Epac (exchange protein directly activated by cAMP) or cAMP-GEF (cAMP-regulated guanine nucleotide exchange factor) was an important piece of the puzzle, critical for the understanding of cAMP-mediated cell signaling (de Rooij *et al.*, 1998; Kawasaki *et al.*, 1998). Epac contains a cAMP-binding domain that is homologous to the R subunit of PKA and a guanine exchange factor (GEF) domain (de Rooij *et al.*, 1998; Kawasaki *et al.*, 1998). In 2000 was shown that Epac directly contributes to regulated exocytosis (Ozaki *et al*., 2000). Mei and co-workers showed that both Epac and PKA are activated by cAMP, but they can have opposing effects (Mei *et al*., 2002). Moreover, the ability of cAMP to mobilize Ca^{2+} from intracellular stores is mainly mediated by Epac (Kang *et al*., 2001) and it is implicated in insulin secretion in β-cells (Kang *et al*., 2003). It was also demonstrated that Epac-mediated signaling cascade requires much higher concentrations of cAMP to be activated than the cascade activated by cAMP-PKA (Shimomura *et al.,* 2004). Evidence indicates the role of Epac in the stimulation of exocytosis by cAMP in different cells types (review in Seino and Shibasaki, 2005), including neuroendocrine cells (Sedej *et al*., 2005). Sedej *et al*. (2005) showed that in pituitary melanotrophs both PKA and Epac mechanisms are involved in Ca^{2+}-dependent exocytosis in spontaneous and cAMP stimulated conditions. In human sperm, Ca^{2+}-triggered exocytosis is an

Epac-dependent process and Epac alone is sufficient to reach maximal acrosomal release (Branham *et al*., 2006). It was also found that in β-cells Epac and PKA selectively regulate exocytosis of SSVs and LDCVs, respectively, and that Epac regulates exocytosis more rapidly than PKA (Hatakeyama *et al*., 2006). Moreover, PKA is essential but not sufficient to induce compound exocytosis and both PKA and Epac agonists increase the number of exocytotic sites (Kwan *et al.,* 2007).

During this time, Gonzalez-Iglesias *et al*. (2006) observed that cAMP-dependent PRL secretion by pituitary lactotrophs occurs in a PKA- and Epac-independent manner. They used several PKA inhibitors and a specific Epac-receptor agonist (8-pCPT-2'-O-Me-cAMP) to show that PRL release is not affected by these two pathways, in both spontaneous and cAMP-stimulated conditions. In addition, they hypothesized that the cAMP effect on electrical activity of lactotrophs, voltage-gated Ca^{2+}-influx and PRL release might be related to ion channels, most likely hyperpolarization-activated cation channels (Gonzalez-Iglesias *et al*., 2006). In acrosomal exocytosis of human sperm Epac was considered a potential cAMP effector, since both PKA and cyclic nucleotide channels were previously shown to have no effect (Branham *et al*., 2006). There are many contradictory studies on the putative HCN channels effects on exocytosis and transmitter release. For instance HCN channels appear not to be involved in GABAergic transmission (Saitow *et al.,* 2005). Conversely, they have been implicated on the modulation of glutamatergic synapse at Crayfish neuromuscular junction (Beaumont and Zucker, 2000); dorsal root ganglion neuronal secretion (Yu *et al.,* 2003), glucagon secretion by α-TC6 cells lines (Zhang *et al.,* 2008) and insulin secretion by rat pancreatic β-cells (Zhang *et al.,* 2009). Moreover, over-expression of HCN2 increased insulin secretion but only under low glucose concentration, while HCN2 suppression had no effect on secretion at both, low and high glucose concentration in pancreatic β-cells (Zhang *et al.,* 2009). Therefore, this pathway is still very poorly understood and appears more complex than initially believed.

Involvement of hyperpolarization-activated cyclic nucleotide–gated (HCN) channels on exocytosis

It has been known since the late 1970s that cAMP modulates ion channels, like hyperpolarization-activated cyclic nucleotide-gated (HCN) channels (Brown *et al.,* 1979). They were not studied extensively in the context of regulated exocytosis since efforts were mostly dedicated to clarify the relevance of the two aforementioned pathways. We studied the role of HCN channels activation in PRL secretion, given that they appear to be a far more probable candidate to mediate cAMP-dependent effects on exocytosis (Gonzalez-Iglesias *et al*., 2006).

Direct interaction of cAMP with the cyclic nucleotide binding domain (CNBD) facilitates channels activation, due to suppressing the inhibitory effect of the CNBD and shifting activation curve to more positive voltages (Wainger *et al*., 2001). This leads to an influx of extracellular cations into the cytoplasm and consequent depolarization of the plasma membrane. HCN channels are voltage dependent and open and close at hyperpolarizing and depolarizing membrane potential, respectively. In their open state they are permeable to both K^+ and Na^+ (e.g. hyperpolarization-activated currents, I_h) (review in Wahl-Schott and Biel, 2009), but they also allow Ca^{2+} influx (Zhong *et al*., 2004; Michels *et al.,* 2008). HCN channels are homo- or hetero-tetramerically organized and have four known homologs isoforms (HCN1, 2, 3 and 4) in mammals, that differ in activation speed and cAMP sensibility (Kaupp and Seifert, 2001). Generally, the biophysics properties of native channels are a mixture of those determined for pure homo-oligomers and their localization to membrane micro-domains is important for their expression of functional properties (Barbuti *et al*., 2004).

Hyperpolarization-activated currents have been demonstrated in most neuroendocrine cells, including lactotrophs (Gonzalez-Iglesias *et al*., 2006b). In immortalized pituitary cells, HCN are under tonic activation by basal levels cAMP, since cAMP inhibition affects I_h but stimulation with forskolin add no effect (Kretschmannova *et al.,* 2006). Thus, we checked if HCN channel isoforms are present in the pituitary gland. In Chapter III we present a comparative study on the protein and mRNA expression profile of the four HCN isoforms in several excitable and non-excitable tissues. This work was accomplished using Western-blot

technique in whole tissue extracts and membrane and cytosolic fractions of different tissues. qRT-PCR scanning was used to assess the mRNA expression of each HCN isoform using specific primers. This study led to the assumption that post-transduction processes are important for the heterogeneity and complexity of native channels. Meanwhile Kretschmannova *et al*. (2012), using qRT-PCR and Western-blot, showed also that all HCN mRNA isoforms are present in pituitary cells but only HCN2, 3 and 4 proteins are expressed in normal and immortalized cells. They also showed that basal cAMP production is sufficient to activate HCN channels in pituitary cells and depletion of PIP2 by phospholipase C has the opposite effect (Kretschmannova *et al*., 2012). Furthermore, HCN channels facilitate spontaneous excitability of these cells by direct binding of cAMP (reviewed in Stojilkovic *et al*., 2012).

Taking into consideration the aforementioned information, our next goal was to assess if cAMP-activated HCN channels are involved in the exocytic process by modulating fusion pore properties. For this purpose we started by confirming the expression of these channels in lactotrophs. The HCN1-4 mRNAs were detected in cells by using qRT-PCR (Fig. I.1).

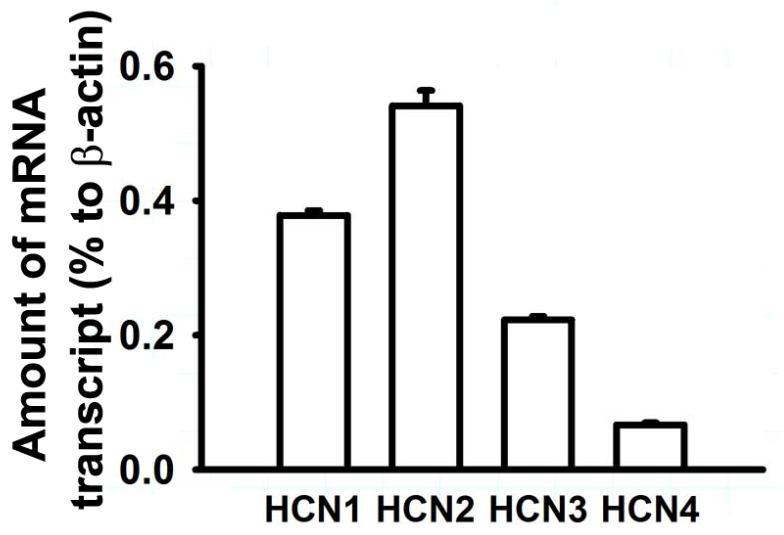

Figure I.1: Quantitative analysis of expression of HCN isoforms in lactotrophs.

Total RNA and genomic DNA (gDNA) were extracted from frozen lactotrophs using AllPrep DNA/RNA/Protein Mini kit (QIAGEN) according to the manufacturer's protocol.

Total RNA (2 µg) was reverse-transcribed to cDNA using Superscript II™ RT enzyme (Invitrogen) and oligo dT (12-18) primers as manufacturer's recommendations. First-strand cDNA templates were then used to PCR amplification of the gene of interest using the appropriate primers, chosen according to previous studies (El-Kholy *et al*., 2007). Real-time PCR was performed in triplicate using Platinium® SYBR Green Supermix UDG (Invitrogen) and analyzed using a 7500 real-time PCR system (Applied Biosystems) following the manufacturer's recommendations. Melt curve analysis was performed on the PCR products at the end of each PCR run to ensure that a single product was amplified. Levels for HCN isoforms and β-actin mRNA transcripts were determined by using standard curves. Levels of mRNA of HCN are expressed relative to the housekeeping mRNA β-actin. The data are expressed as the percentage ratio between the quantities of HCN and β-actin mRNA (n = 3). Data are expressed as the mean ± s.e.m..

Next, our work was dedicated to determine the sub-cellular localization of HCN2 isoform (most abundant mRNA transcript in lactotrophs), by using immunocytochemistry in combination with confocal microscopy.

Then, we studied the effects of these channels on the modulation of exocytosis by monitoring membrane capacitance in the cell-attached mode and using dbcAMP as the stimulus for exocytosis. We addressed this question by using both a genetic and a pharmacologic approach. Lactotrophs were transfected with plasmid DNA to promote the over-expression of HCN2 isoform. We inhibited HCN channel specific current with 4-ethylphenylamino-1,2-dimethyl-6-methylaminopyrimidinium chloride (ZD7288). We also assessed the basal level of PRL release on non-transfected (control) and transfected lactotrophs that over-express HCN2 (+HCN2) (Fig. I.2a).

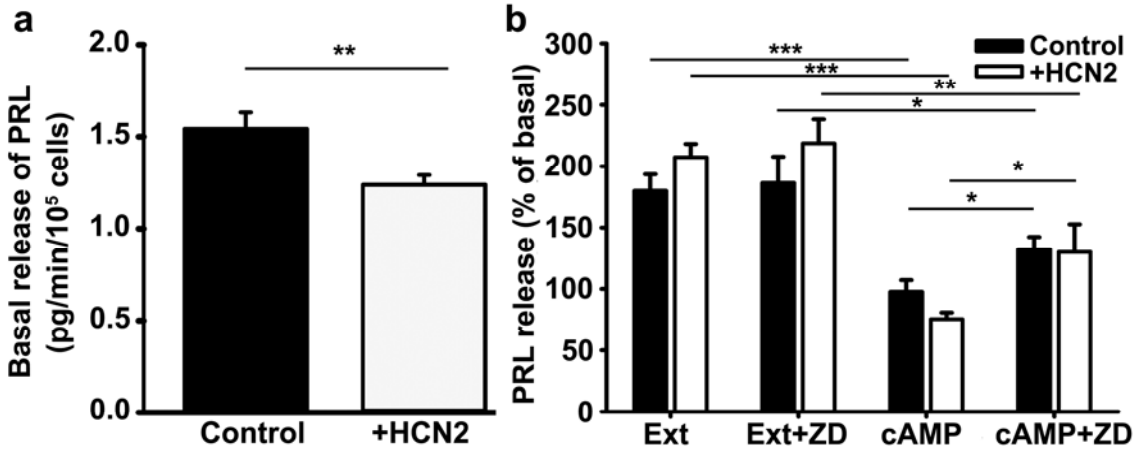

Figure I.2: HCN channels modify prolactin release in pituitary lactotrophs.

(**a**) Control and HCN2-over expressing (with transfection rate of 30%) lactotrophs were incubated for 6 h in DMEM (where $CaCl_2$ concentration is 1.8 mM) at 37 °C. (**b**) Coverslips were incubated for 20 min with extracellular solution (10 mM HEPES/NaOH (pH 7.4), 10 mM D-glucose, 130 mM NaCl, 8 mM $CaCl_2$, 1 mM $MgCl_2$, and 5 mM KCl) supplemented or not with 100 µM ZD7288 (Ext or Ext+ZD, respectively). Media were collected and cells were incubated again for 20 min with 10 mM dbcAMP supplemented or not with 100 µM ZD7288 (cAMP or cAMP+ZD). Collected media were aliquoted and preserved at -20 ºC. Prolactin quantification was performed by using Rat Prolactin EIA Kit (SPIbio) according to the manufacturer's guidelines, as previously described (Calejo *et al*., 2010). Values are expressed as mean ± s.e.m., from two independent experiments performed in triplicates. *<P0.05; ** P<0.01 and ***P<0.001.

Lactotrophs over-expressing HCN2 exhibited a reduced ability to secrete PRL given that basal release decreased from 1.54 ± 0.09 pg/min/10^5 to 1.24 ± 0.05 pg/min/10^5 cells (P<0.01;Fig. I.2a), in cell cultures in which transfection did not exceed 30%, as determined by inspection of EGFP fluorescent cells with confocal microscope. Both control and transfected cells responded to the increase in extracellular Ca^{2+} by doubling of release PRL (Fig. I.2b). Stimulation by dbcAMP caused an even more pronounced reduction of PRL release in transfected than in non-transfected cells (Fig. I.2b). HCN channel blockage by ZD7288 increased the

amount of prolactin release induced by cAMP and its effect was more evident in transfected cell cultures (Fig. I.2b).

Cyclic AMP seems to have a very important inhibitory effect on prolactin release from anterior pituitary lactotrophs, furthermore, this effect is influenced by HCN channels. The most relevant results on the involvement of cAMP-activated HCN channels in the modulation of fusion pore properties are presented in Chapter IV.

Role of exocytosis in aluminium induced toxicity

The so far mentioned studies regarding exocytosis, were conducted in animal models or animal cell lines, but exocytosis is a common process also to plant cells (Battey *et al.,* 1999). In plants, the exocytosis cycle is essentially similar to the one in animals, resulting in the formation of a fusion pore through which vesicle cargo is released. Using whole cell patch clamp technique in aleurone protoplasts Tester and Zorec, (1992) observed that plant cells share with animal cells a common Ca^{2+} mechanism to regulate exocytosis. Moreover, it was also shown in plants that exocytosis can occur, with complete fusion between the vesicle and the plasma membrane or with a transient fusion pore (Thiel and Battey, 1998). Several other components have been found to be common in the exocytotic apparatus between animal and plant organisms, like SNARE proteins (review in Battey *et al.,* 1999).

Aluminium appears to affect exocytosis in evolutionary distant organisms. In animals it has been shown to interfere with several steps of neurotransmission (review in Gonçalves and Silva, 2007). Aluminium has been considered a highly neurotoxic agent (Simonsen *et al*., 1994) that impairs Ca^{2+}-dependent release of classical neurotransmitters, such as acetylcholine, gamma-aminobutyric acid, glutamate and noradrenaline. Aluminium is also toxic to plants (review in Panda *et al.,* 2009). In this case, one of the major mechanisms involves the inhibition of root growth (review in Horst *et al*., 2010), which might be related to disturbances in growth factors secretion and of intracellular Ca^{2+} homeostasis. Exocytosis is in plants the main supplier of membrane and wall material for growth (Miller *et al*., 1997). Additionally, exocytosis is not only important for cell growth but also to

secret material outside the cell wall (Battey *et al.*, 1999). It has been shown that aluminium exposure impairs secretion of mucilage (Puthota *et al*., 1991) and phytosiderophore (Chang *et al*., 1998).

These observations strongly suggest that aluminium could impair secretion at a final step of exocytosis. It is also well documented that aluminium affects several components of the cAMP signaling cascade. Exley and Birchall (1992) have proposed that aluminium can be responsible for second-messenger systems disruption, most likely the G-protein function. Moreover, aluminium binds to G proteins and modifies GTPase activity (Matzel *et al*., 1996). It has also been shown that AC activity is stimulated by aluminium fluoride (Sternweis and Gilman, 1982) that might be relevant for its toxicity action (Ebstein *et al*., 1986). In addition, it was also shown that aluminium increases cyclic AMP levels in brain cortex (Johnson and Jope, 1987; Johnson *et al.,* 1989).

Therefore, we analyzed the effect of aluminium on the fusion pore properties. Recently we showed that incubation of pituitary lactotrophs with 30 μM $AlCl_3$ for 24 h does not induce cell death (Calejo *et al.,* 2010). The most relevant results on the effect of this sub-lethal concentration of $AlCl_3$ in prolactin release and modulation of fusion pore properties are presented in Chapter V.

2 Objectives

The main purpose of this thesis was to depict how cAMP signaling pathway impacts exocytosis with high-resolution changes in C_m, in order to describe how alteration of fusion pore properties contributes to modulation of regulated exocytosis and hormone release by cAMP.

This main purpose was achieved by accomplishing to following specific goals:

I. Evaluation of the effect of cAMP on the secretion of prolactin by cells in culture. Description of cAMP induced single exocytotic events. Characterization of the post-fusion modulation of fusion pore properties (Chapter II).

II. Identification of the main cAMP signaling pathway involved on post-fusion modulation of exocytosis. Comparative analysis of the expression of the four isoforms of HCN channels in different tissues and identification of the most abundant isoform in lactotrophs. Localization of HCN channels at sub-cellular level in cell cultures. Demonstration of the involvement of HCN channels in the regulation of cAMP induced fusion events (Chapters III and IV).

III. Assessment of pathophysiological consequences of the alteration of fusion pore properties by using the aluminium induced neurotoxicity paradigm. Quantitative analysis of the impact of $AlCl_3$ exposure on prolactin release and on the parameters of single exocytotic events in cell cultures (Chapter V).

Chapter II - cAMP-mediated stabilization of fusion pores in cultured rat pituitary lactotrophs

NOTE: The results in this chapter were accepted for publication as: Calejo A.I.*, Jorgačevski J, Kucka M., Kreft M., Gonçalves P.P., Stojilkovic S., Zorec R. cAMP-mediated stabilization of fusion pores in cultured rat pituitary lactotrophs (2013) J Neuroscience. * I have not performed the experiments included in Fig. II.1.

1 Abstract

Regulated exocytosis mediates the release of hormones and transmitters. The last step of this process is represented by the merge between the vesicle and the plasma membranes, and the formation of a fusion pore. Once formed, the initially stable and narrow fusion pore may reversibly widen (transient exocytosis) or fully open (full-fusion exocytosis). Exocytosis is typically triggered by an elevation in cytosolic calcium activity. However, other second messengers, such as cyclic AMP (cAMP), have been reported to modulate secretion. The way in which cAMP influences the transitions between different fusion pore states remains unclear. Here, hormone release studies show that prolactin release from isolated rat lactotrophs stimulated by forskolin, an activator of adenylyl cyclases, and by membrane-permeable cAMP analog (dbcAMP), exhibit a biphasic concentration dependency. While at lower concentrations (2-10 µM forskolin and 2.5-5 mM dbcAMP) these agents stimulate prolactin release, an inhibition is measured at higher concentrations (50 µM forskolin and 10-15 mM dbcAMP). By using high-resolution capacitance (C_m) measurements, we recorded discrete increases in C_m, which represent elementary exocytic events. An elevation of cAMP leaves the frequency of full-fusion events unchanged, while increasing the frequency of transient events. These exhibited a wider fusion pore as measured by increased fusion pore conductance and a prolonged fusion pore dwell-time. The probability of observing rhythmic reopening of transient fusion pores was elevated by dbcAMP. In conclusion, cAMP-mediated stabilization of wide fusion pores prevents vesicles from proceeding to the full-fusion stage of exocytosis, which hinders vesicle content discharge at high cAMP concentrations.

Key words: lactotrophs, exocytosis, cAMP, membrane capacitance, fusion pore, prolactin release

2 Introduction

Regulated exocytosis mediates the release of hormones and transmitters stored in vesicles (Jahn *et al.,* 2003). This process ends with the merge of the vesicle membrane and the plasma membrane, leading to the formation of a stable and narrow fusion pore, through which secretions exit the cell (Spruce *at al.,* 1990; Lollike *et al.,* 1995; Vardjan *et al*., 2007). An increase in cytosolic calcium concentration ($[Ca^{2+}]_i$) leads to the fusion pore diameter increase, which eventually either fully opens (full-fusion exocytosis) or reversibly closes (transient exocytosis; Vardjan *et al*., 2007; Jorgačevski *et al*., 2010). Fluctuations between fusion pore states with different diameters have been reported, lasting from milliseconds to minutes before full-fusion (Fernandez *et al.,* 1984; Vardjan *et al*., 2007; Jorgačevski *et al*., 2010). These fluctuations can exhibit remarkable rhythmicity (Henkel *et al*., 2000; Stenovec *et al*., 2004; Vardjan *et al*., 2007), but their nature remains elusive.

Changes in $[Ca^{2+}]_i$ are likely to play a role in regulating the transitions between stages of exocytosis (Alés *et al*., 1999; Jorgačevski *et al*., 2008). Additionally, elevations in cAMP affect exocytosis (Renström *et al*., 1997; Sikdar *et al.*, 1998; Cochilla *et al*., 2000; Kostic *et al*., 2002; Sedej *et al*., 2005; Gonzalez-Iglesias *et al*., 2006), but it is less clear exactly which exocytic stages are modulated by cAMP. In lactotrophs, cAMP facilitates hormone release via several mechanisms (Gonzalez-Iglesias *et al*., 2006, 2008; Stojilkovic *et al*., 2010), also by affecting the exocytic machinery (Sikdar *et al.,* 1990). Interestingly, cAMP may shift full-fusion to transient exocytosis, as shown in insulin-secreting cells (Hanna *et al*., 2009). In contrast, in melanotrophs, cAMP mediates preferential fusion of larger vesicles without increasing the frequency of events (Sikdar *et al*., 1998).

To investigate the nature of the transitions between stages vesicles undergo in regulated exocytosis, we studied peptidergic vesicles of rat pituitary lactotrophs, cells in which unitary exocytic events can be studied (Stenovec *et al.,* 2004; Jorgačevski *et al*., 2008). We first asked how elevations in intracellular cAMP affect hormone release from the population of lactotrophs. The results revealed a biphasic effect of cAMP. At relatively low cAMP elevations, prolactin

release was augmented, whereas a decreased release in prolactin was recorded at higher cAMP levels. Next, the cell-attached patch clamp was used to monitor discrete changes in membrane capacitance (C_m), which represent unitary exocytic events (Neher and Marty, 1982) and permit the measurements of fusion pore conductance (G_p) and the fusion pore dwell-time (Lollike and Lindau, 1999; Jorgačevski *et al*., 2008; Jorgačevski *et al.,* 2011). Elevations in cAMP increase the frequency of transient, but not full-fusion events. Transient fusion pore openings exhibited increased G_p and prolonged fusion pore dwell-time. Moreover, cAMP increased the probability of rhythmic reopenings of transient fusion pores. Although cAMP increased the frequency of unitary exocytic events, cAMP-mediated stabilization of widely open transient fusion pores may hinder the discharge of vesicle contents.

3 Materials and Methods

3.1 Cell cultures

Lactotrophs were isolated from adult male Wistar rats as described (Ben-Tabou *et al.,* 1994). Briefly, cells were plated on glass coverslips coated with poly-L-lysine and maintained in the feeding medium (high-glucose Dulbecco's modified Eagle's medium supplemented with 10 percent newborn calf serum, 1.5 µM bovine serum albumin and 2 mM L-glutamine) in an atmosphere of humidified air (95 percent) and CO_2 (5 percent) at 37 °C. The feeding medium was replaced every other day. The animals were euthanized in accordance with the International Guiding Principles for Biomedical Research Involving Animals developed by the Council for International Organizations of Medical Sciences and the Directive on Conditions for Issue of License for Animal Experiments for Scientific Research Purposes (Official Gazette of the Republic of Slovenia 40/85 and 22/87), and by the NICHD Animal Care and Use Committee. The procedures using animals were approved by the Veterinary Administration of the Republic of Slovenia (approval no. 3440-29/2006). Experiments were carried out at room temperature one to four days after the isolation.

3.2 Prolactin-release and cAMP measurements

Prolactin (PRL) and cAMP release was monitored using cell column perifusion experiments. Briefly, 1.2 x 10^7 cells were incubated with pre-swollen cytodex-1 beads in 60 mm petri dishes for 18 h. The beads were then transferred to 0.5 ml chambers and perifused with Hanks' M199 containing 25 mM HEPES, 0.1 percent BSA and penicillin (100 units/ml)/streptomycin (100 µg/ml) for 2.5 h at a flow rate of 0.8 ml/min and at 37 °C to establish stable basal secretion. Fractions were collected at 1 min intervals and later assayed for PRL and cAMP contents using radioimmunoassay. The primary antibody and standard for PRL assay were purchased from the National Pituitary Agency and Dr. AF Parlow (Harbor-UCLA Medical Center, Torrance, USA). Cyclic AMP was determined using specific

antiserum provided by Albert Baukal (NICHD, Bethesda, USA). ^{125}I-PRL and ^{125}I-cAMP were purchased from PerkinElmer Life Sciences (Boston, USA).

3.3 Electrophysiology

Glass pipettes were fire-polished and heavily coated with Sylgard® (Midland, USA). The resistance of pipettes was 3–6 MΩ. Cell-attached capacitance measurements were performed with a dual-phase lock-in patch-clamp amplifier (SWAM IIC; Celica, Ljubljana, Slovenia) as described (Vardjan *et al*., 2007, Jorgačevski *et al*., 2010). A sine wave voltage (1591 Hz, 111 mV r.m.s.) was applied to the pipette, while holding the pipette potential at 0 mV. The phase of the dual-phase lock-in amplifier was adjusted and checked at regular intervals as described previously (Vardjan *et al*., 2007; Jorgačevski *et al*., 2010). We performed capacitance measurements under non-stimulated conditions and after stimulation with different cAMP-increasing agents: 1 mM IBMX (3-isobutyl-1-methylxanthine, a phosphodiesterase inhibitor to increase cytosolic cAMP concentration), 10 mM dbcAMP (N^6,2'-O-dibutyryl adenosine-3′,5′-cyclic monophosphate, a membrane permeable cAMP analog) and 1 µM forskolin (adenylyl cyclase activator). dbcAMP and IBMX were added as a bolus of the stock solutions, which were prepared in extracellular solution. Stimulation with forskolin was performed by a 30 min pre-incubation of cells with forskolin.

3.4 Data analysis

Electrophysiological recordings were analyzed in the custom-made software (CellAn, Celica, Slovenia) written for MATLAB (Math Works, Natick, USA). For transient fusion events, vesicle capacitance (C_v) and fusion pore conductance (G_p) were calculated from the imaginary (Im) and the real (Re) part of the admittance signals, as reported (Lollike and Lindau, 1999): $C_v=[(Re^2 + Im^2)/Im]/\omega$, where ω is the angular frequency ($\omega=2\pi f$, f is the sine-wave frequency, 1591 Hz) and $G_p=(Re^2 + Im^2)/Re$. Fusion pore radius was estimated by using the equation $G_p=(\pi r^2)/(\rho\lambda)$, where r denotes fusion pore radius, ρ the estimated resistivity of the saline (100 Ωcm), and λ the length of a gap junction channel (15 nm; Spruce *et al*.,

1990). Vesicle diameter was calculated by using specific membrane capacitance (c_m) of 8 fF/µm^{-2}. A burst was considered to consist of no less than five transient events, with no more than 5 s between the ensuing events. Transient events in a burst were considered periodic when times between the ensuing events were normally distributed (Shapiro-Wilk normality test) and the coefficient of variation of the Gaussian curve fitted to the data was less than 0.2. All statistics were performed with Sigma Plot® (Systat Software; San Jose, USA). Results are presented as mean ± standard error of the mean (s.e.m.). Statistical significance was evaluated by using Student's t-test for normally and Man-Whitney for non-normally distributed data. Considering $P<0.05$ (*), $P<0.01$ (**).

3.5 Solutions

The extracellular solution consisted of 10 mM HEPES/NaOH (pH 7.4), 10 mM D-glucose, 130 mM NaCl, 8 mM $CaCl_2$, 1 mM $MgCl_2$, and 5 mM KCl. Unless stated otherwise, all chemicals of highest purity available were purchased from Sigma-Aldrich (St. Louis, USA).

4 RESULTS

4.1 The effect of cAMP-increasing agents on cAMP and PRL release in pituitary cells

cAMP is a secondary messenger capable of enhancing hormone release by promoting Ca^{2+} influx into cells or by directly modulating specific steps in the secretory pathway (reviewed in Seino and Shibasaki, 2005). Previously we have confirmed a linear relationship between intracellular and extracellular cyclic nucleotide concentrations in lactotrophs treated with cAMP-increasing agents (Gonzalez-Iglesias *et al*., 2006). Forskolin, an adenylyl cyclase activator, dose-dependently (added to the culture medium at 2, 10, and 50 µM; see Fig. II.1a) increased the concentration of release cAMP in cultured cells, as reported (Gonzalez-Iglesias *et al*., 2006). To determine whether forskolin also affects the release of hormones from lactotrophs, we measured PRL release from perifused pituitary lactotrophs when forskolin was applied for a period of 30 min (Fig. II.1b). At lower concentrations of forskolin (2 µM and 10 µM), PRL release was enhanced immediately after the addition of forskolin and reached a steady-state that was 1.6-fold higher than in controls. However, at higher concentration of forskolin (50 µM) PRL release increased only after a delay of 30 min (Fig.II.1b). Because different concentrations of forskolin had different effects on PRL release from lactotrophs, we wanted to determine whether this effect was specific for forskolin. Next, we used dbcAMP, a membrane permeable cAMP analog. In Fig. II.1c, the results show that dbcAMP increased PRL release by 1.5-fold at 2.5 and 5 mM. However, the addition of 10 mM dbcAMP decreased the rate of PRL release, which reached levels lower than those recorded in controls. At 15 mM dbcAMP, the rate of PRL release continued to decrease but reverted to partial recovery upon rinsing dbcAMP from the bath.

These results indicate that cAMP potentiates PRL release at relatively low concentrations, while at higher cAMP concentrations it inhibits PRL release. Therefore, our next goal was to study how cAMP-increasing agents affect the exocytic machinery directly. To this end, we recorded unitary exocytic events by

the high-resolution membrane capacitance technique (Neher and Marty, 1982; Zorec *et al.*, 1991).

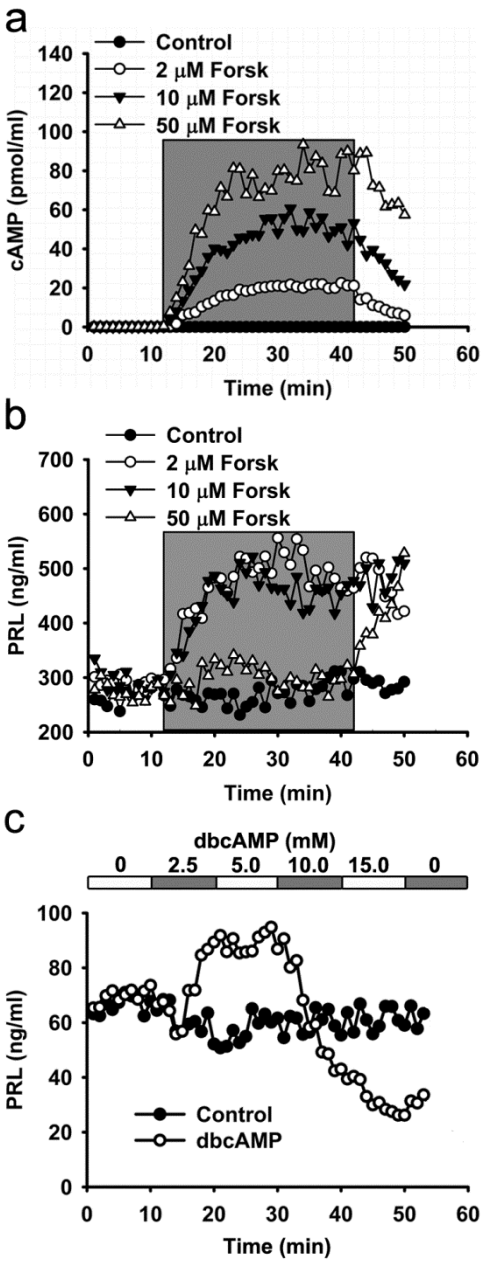

Figure II.1: Elevation in cAMP cytosolic concentration increases prolactin (PRL) release from perifused pituitary lactotrophs.

Cultured pituitary lactotrophs were perifused with extracellular solutions containing different concentrations of forskolin, an adenylyl cyclase activator, and dbcAMP (N^6,2'-O-dibutyryl adenosine-3′,5′-cyclic monophosphate). Samples were collected every minute and analyzed for either cAMP or PRL. **(a)** Dose-dependent effect of forskolin on cAMP

release in perifused lactotrophs. The grey part denotes the period of forskolin application. **(b)** Dose-dependent effect of forskolin on PRL release from perifused lactotrophs. The grey part denotes the period of forskolin application. **(c)** The effect of different concentrations of dbcAMP on the PRL release from perifused lactotrophs. The top x-axis shows the concentrations of applied dbcAMP. Shown are representative experiments from four independent experiments.

4.2 cAMP increases the frequency of transient exocytic events

Although single fusion events can be studied in single cells (Kreft and Zorec, 1997; Vardjan *et al*., 2007; Jorgačevski *et al*., 2008), few studies address the question of how cAMP modulates unitary exocytotic events (Sikdar *et al*., 1998; Hanna *et al*., 2009). Here, we studied the effects of cAMP on the occurrence and on the properties of the unitary exocytic events of PRL-containing vesicles. We used the cell-attached patch-clamp technique to monitor membrane capacitance (C_m), a parameter linearly related to the plasma membrane surface area in control conditions (extracellular solution) and in the presence of different cAMP-increasing agents. To elevate cAMP levels we applied: IBMX, a non-specific phosphodiesterase inhibitor (1 mM), and forskolin (1 μM), in two separate sets of experiments. Both of which have been shown to increase cAMP and PRL release from lactotrophs (Fig. II.1b, Gonzalez-Iglesias *et al*., 2006). We performed an additional set of experiments where we applied 10 mM dbcAMP, which inhibits PRL release (Fig. II.1c).

The recordings were made from 50 membrane patches, each on a different cell, with a total recording time of 13.9 hours (3.2 hours at control conditions and 10.7 hours at stimulated conditions) and at an average time of 1000 s per recording. We observed the presence of discrete irreversible upward and downward steps in C_m, likely indicating full-fusion exocytosis and endocytosis, respectively (Heuser and Reese, 1973; Neher and Marty, 1982; see Fig. II.2a). We also recorded reversible steps in C_m that likely represent transient exocytosis (Alvarez de Toledo *et al.,* 1993; Fesce *et al*., 1994; Jorgačevski *et al*., 2008; see Fig. II.2b). Transient exocytic events, observed in the imaginary part of the admittance trace (Im), often exhibited a crosstalk, observed on the real part of the

admittance trace (Re), indicating the presence of a narrow fusion pore (Lollike and Lindau, 1999; see Fig. II.2b). For these events we calculated the vesicle capacitance (C_v) and fusion pore conductance (G_p), as described in Materials and Methods (see Fig. II.2c; Lollike and Lindau, 1999). The average C_v amplitude of exocytic events recorded in control and in stimulated conditions was 0.88 ± 0.03 fF (range 0.2–4 fF).

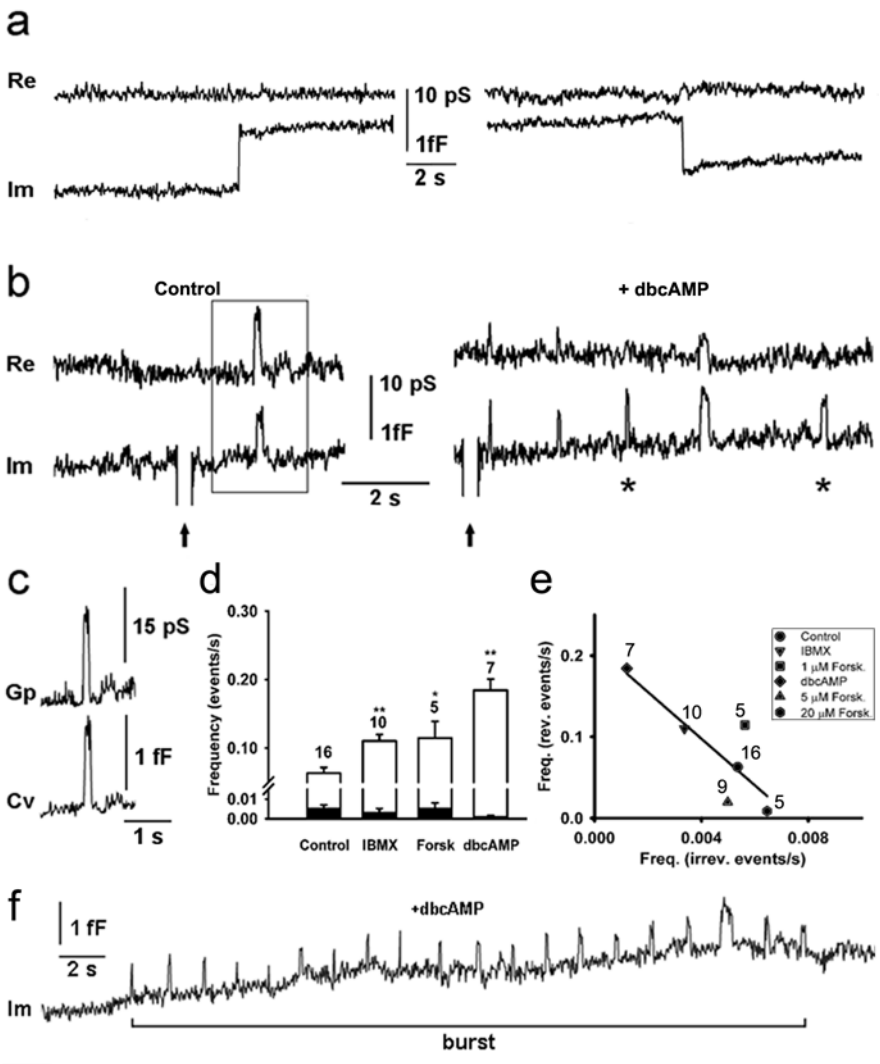

Figure II.2: cAMP-increasing agents augment the frequency of reversible but not the irreversible discrete capacitance steps.

The irreversible events are represented by discrete upward or downward step in the imaginary admittance trace (Im), which is proportional to the membrane capacitance. Reversible events consist of an upward and a subsequent downward discrete step in Im, which follows within 5 s. **(a)** A representative example of irreversible upward (left) and downward steps (right) in Im trace and the corresponding real part of the admittance trace (Re, top). **(b)** Reversible events in Im before (Control, left) and after the stimulation by dbcAMP (10mM, +dbcAMP, right). Note that some of the reversible events in Im trace

exhibit projections to the Re trace, while the others were devoid of projections (asterisks). Arrows denote calibration pulses in Im, used to adjust the phase of the lock-in amplifier. **(c)** Projected reversible events were used to calculate fusion pore conductance (G_p) and vesicle capacitance (C_v), as described in the Materials and Methods section. Shown is a representative example framed in panel b. **(d)** The average frequency of irreversible upward events (full bars) in controls was 0.005 ± 0.002 s^{-1} (n=16). The addition of phosphodiesterase inhibitor (IBMX, 1 mM), an agent to activate adenylyl cyclase (forskolin 1 µM, Forsk), and a membrane permeable cAMP analog (dbcAMP, 10 mM) did not affect (P>0.05) the frequency of irreversible upward events, (0.003 ± 0.002 s^{-1}, 0.006 ± 0.002 s^{-1} and 0.001 ± 0.001 s^{-1}) respectively. The average frequency of reversible events (open bars) increased from 0.06 ± 0.01 s^{-1} in controls to 0.11 ± 0.01 s^{-1} (P<0.01; IBMX), 0.11 ± 0.02 s^{-1} (P<0.05; forskolin) and 0.18 ± 0.02 s^{-1} (P<0.01; dbcAMP). Values are means ± s.e.m. Numbers above error bars indicate the number of patches. **(e)** We observed negative relationships between the average frequency of irreversible upward events and the average frequency of reversible events for each condition, which was best fitted with the linear regression: y (the average frequency of reversible events)=(-21 ± 9) × x (the average frequency of irreversible up-ward events) + (0.20 ± 0.04) with the correlation coefficient, r=0.85. **(f)** Representative Im trace, showing a burst of reversible events. We defined a burst as a minimum of five reversible events with less than 5 s between ensuing reversible events.

By assuming specific membrane capacitance of 8 fF/µm^{-2} and spherical geometry of vesicles, the amplitude corresponds to vesicle diameter of 176 ± 10 nm, which is in agreement with previously published results on PRL-containing vesicles (Smets *et al*., 1987; Angleson *et al*., 1999; Vardjan *et al*., 2007, Jorgačevski *et al*., 2008, 2011).

The occurrence of irreversible upward events did not significantly change after the addition of any of the cAMP-increasing agents (Fig. II.2d, black bars; see Table II.1). However, both IBMX and forskolin applications increased the occurrence of transient exocytic events twofold, from 0.06 ± 0.01 s^{-1} to 0.11 ± 0.01 s^{-1} (P<0.01) and to 0.11 ± 0.02 s^{-1} (P<0.05), respectively (Fig. II.2d, open bars). The stimulation with dbcAMP elicited an even greater increase in the frequency of transient exocytic events, to 0.18 ± 0.02 s^{-1} (Fig. II.2d, open bars P<0.01). Observed changes were not an artifact of the vehicle (20 mM DMSO) because control experiments where we added the vehicle without cAMP increasing agents did not affect the frequency of transient exocytic events (data not shown).

The inverse linear relation between the occurrence of reversible (transient) vs. irreversible (full-fusion) exocytic events indicates that cAMP-stimulation

augments the former while inhibiting the latter events (Fig. II.2e), which is consistent with the view that cAMP up-regulates the transient mode of exocytosis (Hanna *et al.,* 2009). We also observed that the nature of appearance of transient exocytic events was different after stimulation. Prior to the stimulation transient exocytic events usually occurred as independent events, while after the addition of dbcAMP, they often appeared in bursts (Fig. II.2f).

Figure II.3a shows the C_v amplitude distribution of transient exocytic events recorded in a representative patch of membrane. Note the unchanged C_v amplitude before and after dbcAMP application (Gaussian mean 1.09 ± 0.05 fF; n=11 and 1.08 ± 0.01 fF; n=64), indicating that dbcAMP-stimulation modulated the properties of a pre-existing fusion pore. To determine whether transient events in C_m represent the repetitive fusion pore opening of a single vesicle, we compared the C_v amplitudes of upward and downward steps in this recording. Regression lines for control (n=11 events, filled circles) and dbcAMP-stimulated conditions (n=64 events, open circles) had slopes close to 1 (1.0 ± 0.1 and 0.8 ± 0.1, respectively; see Fig. II.3aii) and high correlation coefficients (r=0.95 and r=0.78, respectively; see Fig. II.3aii). These results are consistent with the view that transient exocytic events represent a single vesicle interacting with the plasma membrane. To further test if this is valid for all patches, we compared the average upward and downward amplitudes in C_v in controls (n=16 cells) and after cAMP-stimulation (n=21 cells). Similarly as for the single patch, the results were best fitted with the regression line with the slope near one (0.97 ± 0.04 for control and 1.04 ± 0.02 after stimulation) and with even higher correlation coefficients (r=0.99 and 0.99, respectively; see Fig. II.3b). We also investigated whether the stimulation by cAMP affects the distribution of C_v amplitudes of transient exocytic events. Figure II.3c shows that in controls, the distribution of C_v amplitudes consisted of two peaks (with mean amplitudes of 0.58 ± 0.01 fF and 1.44 ± 0.02 fF), indicating two populations of vesicles interacting with the plasma membrane. However, following stimulation by cAMP, the predominant vesicle population that interacted with the plasma membrane exhibited a lower C_v amplitude of 0.61 ± 0.01 fF.

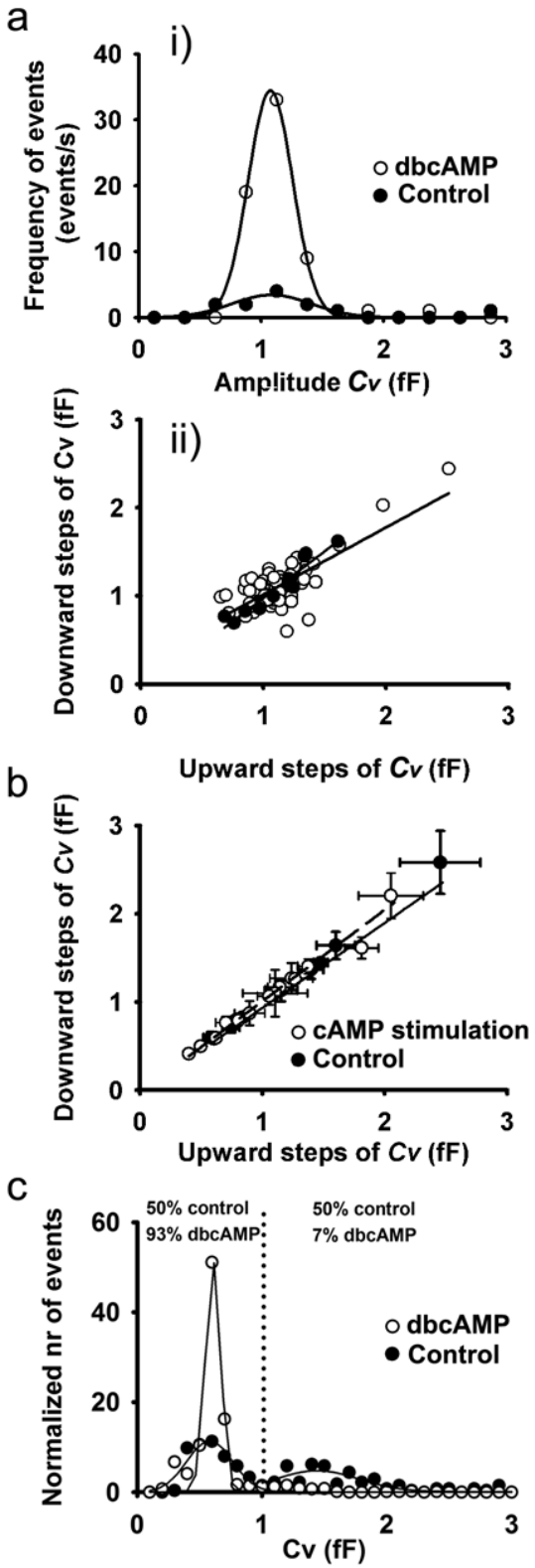

Figure II.3: Reversible events mirror repetitive fusion of single vesicle.

(a)(i) The distributions of vesicle membrane capacitance (C_v) amplitudes of reversible events from a representative patch, before and after the stimulation with dbcAMP, were similar. Lines show fitted Gaussian curves with means of 1.09 ± 0.05 fF (control,

correlation coefficient r=0.92; n=11 events) and 1.08 ± 0.01 fF (dbcAMP, r=0.99; n=64 events), respectively. **(ii)** The relationship between amplitudes of the downward and the preceding upward C_v steps of reversible events: the regression line represents the best fit with parameters: y (C_v amplitude of the downward step)=(1.0 ± 0.1) × x (C_v amplitude of the upward step) + (-0.1 ± 0.1) (r=0.95, n=11 events) before stimulation and the regression line y (C_v amplitude of the downward step)=(0.8 ± 0.1) × x (C_v amplitude of the upward step) + (0.26 ± 0.10) (r=0.76, n=64 events) after the stimulation (open circles). The slopes of both regression lines were similar (P=0.2). **(b)** The relationship between the average C_v amplitudes of downward vs. upward discrete steps of reversible events in distinct membrane patches before and after the addition of cAMP-increasing agents. The solid line represents linear fit of the controls: y (the average C_v amplitudes of down-ward steps)=(0.97 ± 0.04) × x (the average C_v amplitudes of upward steps) + (-0.03 ± 0.15) (r=0.99, n=9 cells) and the dashed line represents linear fit to the data obtained after the addition of cAMP-increasing agents: y (the average C_v amplitudes of upward steps)=(1.04 ± 0.02) × x (the average C_v amplitudes of downward steps) + (-0.03 ± 0.05) (r= 0.99, n=16 cells). The slopes of both regression lines were similar (P=0.3). Values are means ± s.e.m. **(c)** Distribution of C_v amplitudes of all events in control conditions shows two population best fitted with Gaussian curves with means: 0.58 ± 0.01 fF (r=0.82) and 1.44 ± 0.02 fF (r=0.80), each corresponding to 50 percent of all events in control conditions. After dbcAMP, we only observed one population best fitted with Gaussian curve with mean 0.61 ± 0.01 fF (r=0.99) that represents 93 percent of all events after dbcAMP.

This population of vesicles represented 50 percent of all vesicles interacting with the plasma membrane in controls, whereas it increased to 93 percent following cAMP stimulation.

These results indicate that stimulation by cAMP primarily affects smaller peptidergic vesicles, which are engaged in transient mode of exocytosis.

4.3 cAMP affects the fusion pore diameter and dwell-time

In the transient mode of exocytosis, vesicle cargo discharge can be constrained by a narrow fusion pore and by the relatively short effective fusion pore dwell-time (Barg *et al*., 2002; Tsuboi and Rutter, 2003; Stenovec *et al*., 2004; Obermüller *et al*., 2005). Therefore, our next aim was to determine if cAMP-increasing agents alter the fusion pore geometry. Thus, we calculated fusion pore conductance (G_p; see Fig. II.2c; Lollike and Lindau, 1999; see Materials and Methods), a parameter related to the fusion pore diameter (Breckenridge and Almers, 1987). However, G_p can only be calculated for transient fusion events

exhibiting a significant crosstalk between the Im (proportional to the vesicle capacitance C_v) and the Re traces. In this case, a relatively narrow fusion pore acts as a resistor which produces a measurable projection to the Re part of the admittance signal (reflecting the conductance of the fusion pore; Lollike and Lindau, 1999).

The majority of transient fusion events, observed in controls and in dbcAMP- stimulated conditions exhibited wide fusion pores. Stimulation with dbcAMP increased the percentage of transient exocytic events with wide fusion pores from 67 percent to 99 percent (Table II.1).

Table II.1: Types of unitary exocytic events in controls and in the presence of dbcAMP.

Type of exocytic events	Percentage of different exocytic events		
	Full-fusion events (No. of events/all events)	Transient events with wide fusion pores (No. of events/all events)	Transient events with narrow fusion pores (No. of events/all events)
Control	8.3% (n=25/300)	66.6% (n=200/300)	25.0% (n=75/300)
+dbcAMP	0.6% (n=7/1152)	98.5% (n=1136/1152)	0.9% (n=9/1152)

Transient exocytic events with narrow fusion pores decreased from 25 percent in controls to approximately 1 percent after treatment with dbcAMP (Table II.1). In addition, the percentage of full-fusion events decreased after stimulation with dbcAMP from 8 percent (control) to less than 1 percent (Table II.1).

To learn about the influence of each of the cAMP-enhancing agents on G_p in detail, we analyzed the average G_p in each set of experiments, respectively (Fig. II.4a). Following the treatment with IBMX, the average G_p was 21 ± 1 pS (n=139 events), similar to the average G_p in controls (23 ± 2 pS; n=75 events; see Fig. II.4a).

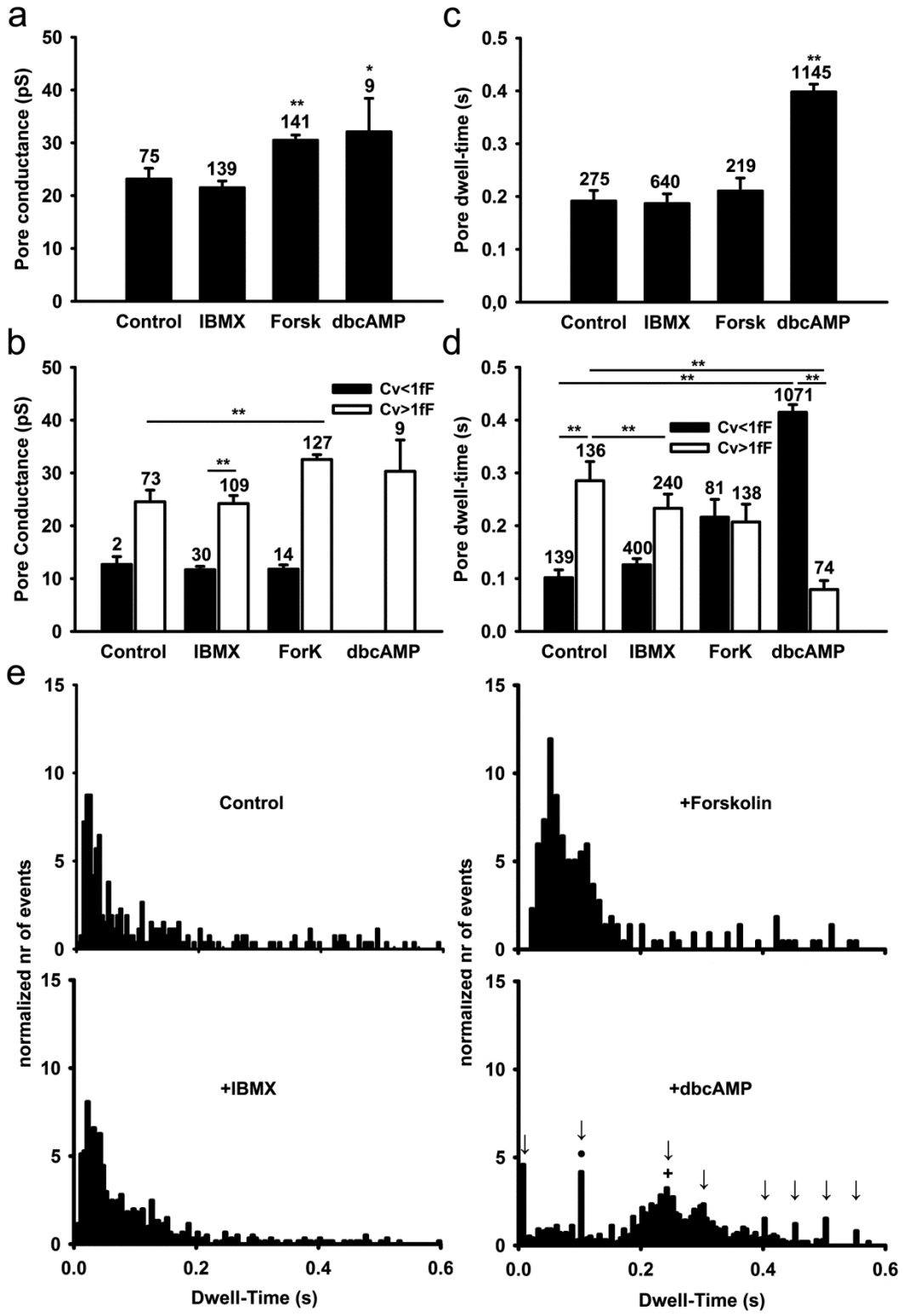

Figure II.4: cAMP-increasing agents affect the fusion pore conductance and the pore dwell-time.

(a) The average fusion pore conductance (G_p), determined for reversible events with measurable crosstalk between Re and Im traces in controls was 23 ± 2 pS (n=75 events).

The addition of IBMX, forskolin, and dbcAMP increased the average G_p to 21 ± 1 pS (n=139 events; P=0.3), 30 ± 1 pS (141 events; P<0.001), and 32 ± 6 pS (n=9 events; P<0.05), respectively. Values are means ± s.e.m. **(b)** The average fusion pore dwell-time of controls was 0.19 ± 0.02 s (n=275 events) and remained unchanged after the addition of IBMX and forskolin (0.19 ± 0.02 s; n=640 events and 0.21 ± 0.02 s; n=219 events, respectively). DbcAMP treatment increased the average fusion pore dwell-time to 0.40 ± 0.02 s (n=1145 events, P<0.001). Values are means ± s.e.m. **(c)** Fusion pore conductance displayed as a function of C_v > 1 fF (white columns) and C_v < 1 fF (black columns). **(d)** Changes in fusion pore dwell-time displayed as a function of C_v > 1 fF (white columns) and C_v < 1 fF (black columns). **(e)** The frequency distribution of fusion pore dwell-times in controls and after the addition of cAMP increasing agents. Arrows in the panel showing the distribution of fusion pore dwell-times after the addition of dbcAMP (+dbcAMP) point to the modal values of the dwell-times, which belong to the respective bursts. Two modal dwell-times, which are marked with the cross and the dot, denote two bursts, shown in panels a and b of Fig. II.5.

However, a significant increase in the average G_p was observed following the treatment by forskolin and dbcAMP; 30 ± 1 pS (n=141; P<0.01) and 32 ± 6 pS (n=9; P<0.05; see Fig II.4a), respectively. Interestingly, if we analyzed the cAMP-mediated change in fusion pore conductance as a function of C_v, the results revealed that larger vesicles with C_v > 1 fF exhibited larger G_p than events with C_v < 1fF (Fig. II.4b).

The dwell-time of transient fusion pore openings was measured as the time between the upward and the ensuing downward step in C_m, as reported (Vardjan *et al*., 2007; Jorgačevski *et al*., 2008). Stimulation with IBMX or forskolin did not affect the average fusion pore dwell-time (0.19 ± 0.02 s in control vs. 0.19 ± 0.02 s with IBMX and 0.21 ± 0.02 s with forskolin). However, stimulation with dbcAMP doubled the average fusion pore dwell-time to 0.40 ± 0.02 s (Fig. II.4c; P<0.01). The probability of the open fusion state, which we calculated as the sum of all fusion pore dwell-times divided by the total recording time, increased after dbcAMP stimulation threefold, from 0.02 (n=16 cells) to 0.07 (n=7 cells). In contrast, IBMX (n=10 cells) and forskolin (n=5 cells) stimulation did not significantly affect the probability of open fusion pore state (0.02 and 0.03, respectively). Moreover, the cAMP-mediated effects of fusion pore dwell-time depended on the C_v amplitude. In controls, fusion pore dwell-time was shorter for events with C_v < 1fF than with C_v > 1fF (Fig. II.4d).

Frequency histograms of fusion pore dwell-time (Fig. II.4e) show that in controls and after simulation with IBMX, distributions of fusion pore dwell-times are similar (modal peaks at ~0.03 s). However, after stimulation with forskolin, fusion pore dwell-time distribution shifted to higher values (note a second peak at ~0.07 s). After stimulation with dbcAMP, the distribution of fusion pore dwell-times was different. Instead of a single or double mode distribution, we observed several modes (Fig. II.4e, bottom right). Each of the modal peaks (highlighted by arrows on Fig. II.4e, lower right panel) denotes a particular burst of events. Multimodality was observed also for separated data of C_v < 1fF and C_v > 1fF (data not shown).The prolonged fusion pore dwell-time, observed after the stimulation with forskolin and dbcAMP, is consistent with previous reports (Ohara-Imaizumi *et al*., 2002; Gandhi and Stevens, 2003; Perrais *et al*., 2004; Thorn and Parker, 2005). Our results indicate that the stimulation with low concentration of IBMX and forskolin is not sufficient to affect fusion pore dwell-time. On the other hand, the increased of the mean dwell-time after dbcAMP stimulation is similar to the reported value after depolarization with KCl (Vardjan *et al*., 2007).

4.4 The addition of dbcAMP elicits periodicity of transient fusion events within a burst

The increased intracellular level of cAMP elicited the periodicity of transient fusion events, which appeared in bursts (Fig. II.2f and Fig. II.5a, b). Within a burst, the transient fusion pore events represent repetitive reopening of the single vesicle fusion pore as indicated by practically identical C_v amplitudes (see also Fig. II.2f). Moreover, fusion pore dwell-times of the repetitive reversible events in the same burst were relatively constant, contributing to the distinct modal peaks seen in Fig. II.4e (lower right panel; see also Henkel *et al*., 2000; Stenovec *et al*., 2004). To study periodicity of transient fusion events in more detail, we determined the burst parameters. We considered a burst to be composed of at list five transient events, with at most 5 s in between ensuing events. In controls, 42 percent of transient fusion events occurred in bursts (n=115 events in bursts). The percentage of events appearing in bursts increased to 53 percent (n=338 events in bursts) after

IBMX stimulation and to 70 percent (n=153 events in bursts) after forskolin stimulation. After dbcAMP stimulation, almost all events appeared in bursts (~94 percent; n=1078 events in bursts). We then measured the time between ensuing events within bursts. The distribution of these, prior to stimulation, was complex (Fig. II.5c).

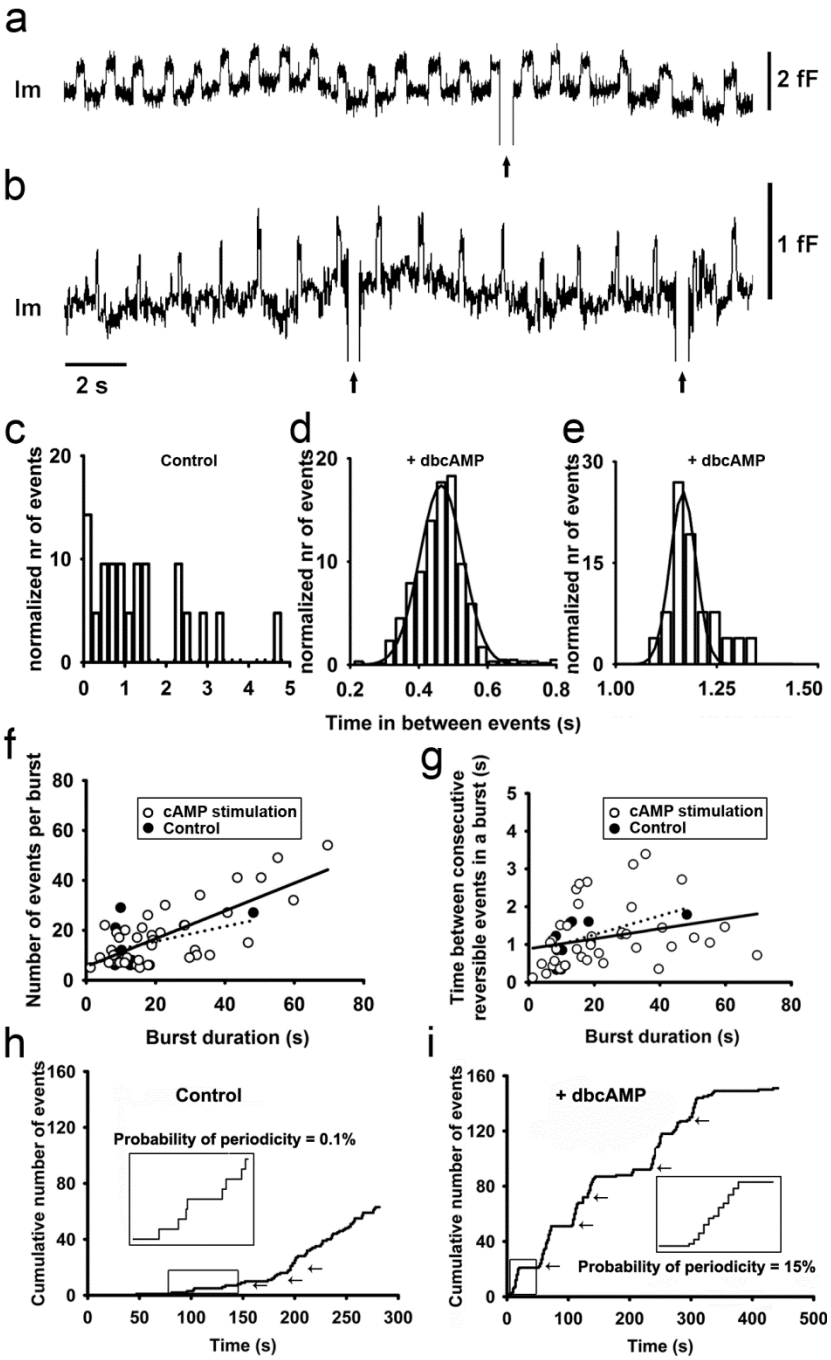

Figure II.5: The addition of dbcAMP results in rhythmic reopening of the same fusion pore.

(a, b) Two epochs of the representative Im traces showing rhythmic fusion pore activity in

two different cells after the addition of dbcAMP. This activity was part of two bursts (see Fig. II.1e for definition) with durations of 180 s and 41s s. **(c, d, e)** Representative histograms of times in between ensuing transient exocytic events within a burst in controls **(c)** and after the addition of dbcAMP **(d, e)**. The histogram of controls shows a random distribution, while histograms after the addition of dbcAMP (which are partially shown in panels a, b) appear normally distributed and were fitted with Gaussian curves with the means of 0.465 ± 0.001 s (n=645 events) and 1.166 ± 0.002 s (n=26 events), respectively. **(f)** The number of reversible events in a burst depends on the burst duration. The control data points were fitted with the regression line (dotted line) with parameters: y (number of events per burst)=(0.30 ± 0.27) × x (burst duration in s) + (10 ± 6) (correlation coefficient r=0.41, n=8 bursts, P=0.3) and after stimulation with cAMP (solid line): y (number of events per burst)=(0.56 ± 0.08) × x (burst duration in s) + (6 ± 2) (correlation coefficient r=0.76, n=44 bursts, P<0.001). Note that the number of bursts of controls is much reduced. **(g)** The time between consecutive reversible events in a burst did not depend on the burst duration. Control data points were fitted with the regression line (dotted line) with parameters: y (time between consecutive reversible events in a burst in s)=(0.025 ± 0.015) × x (burst duration in s) + (0.8 ± 0.3) (correlation coefficient r=0.57, n=8 bursts, P=0.1) and after cAMP stimulation data points were fitted with the regression line (solid line) with parameters: y (time between consecutive reversible events in a burst in s)=(0.013 ± 0.007) × x (burst duration in s) + (0.9 ± 0.2) (correlation coefficient r=0.27, n=44 bursts, P=0.08). Note that the burst duration of controls was typically shorter than 20 s. **(h)** The cumulative number of reversible events as a function of time in a representative control cell. Arrows denote bursts of reversible events. The inset shows a magnified epoch (marked in fig. with rectangle) where the time between ensuing reversible events is random. **(i)** The cumulative number of reversible events as a function of time in a representative cell after the addition of dbcAMP. Arrows denote bursts of reversible events. Inset shows a magnified burst (marked in fig. with rectangle) with remarkably constant time between ensuing reversible events.

In contrast, stimulation with dbcAMP resulted in a bell-shaped distribution (Fig. II.5d and e), indicating that the fusion pores reopened at predictable times within a given patch of membrane where the periodic behavior was recorded. To confirm the periodicity, we fitted the distributions with Gaussian curves (Fig. II.5d and e) with means 0.465 ± 0.001 s and 1.166 ± 0.002 s. Similar values were reported previously (Stenovec *et al*., 2004).

Then we analyzed the relationship between the number of transient fusion events within a burst and the duration of the burst (Fig. II.5f). In bursts after cAMP stimulation we observed that the number of transient fusion events was correlated with the duration of the burst (r=0.76; n=44 bursts), with the average frequency of 0.56 ± 0.08 events/s in bursts. Figure II.5f shows that the majority of bursts that occurred after the addition of cAMP-increasing agents had increased number of

events per burst, and prolonged burst durations, compared to controls. The average number of transient fusion events in a burst increased; from 14 ± 4 events in controls (n=115 events in 8 bursts) to 17 ± 3 events after addition of IBMX (n=338 events in 19 bursts), to 29 ± 20 events after addition of forskolin (n=153 events in 8 bursts) and to 27 ± 6 events after addition of dbcAMP (n=1078 events in 17 bursts). The average burst duration was similar in control and in IBMX-stimulated condition (~18 s), whereas after forskolin- and dbcAMP-stimulations, burst durations were prolonged (~24 s and ~33 s, respectively; data not shown). We also analyzed the relationship between the time between consecutive transient events within a burst and burst duration, which showed a poor correlation (r=0.29; n=50 bursts) and slope near 0 (0.01 ± 0.007; Fig. II.5g). Note also that the majority of bursts recorded in the presence of elevated cAMP exhibit longer periods between consecutive transient events in addition to the prolonged burst durations, compared to controls (Fig. II.5g). Therefore, the burst duration is related to the number but not the time in between consecutive transient fusion events. Panels h and i of Fig. II.5 show cumulative numbers of transient events in two representative recordings. The appearance of bursts both in control and in dbcAMP-stimulated conditions are highlighted in insets, respectively. In controls, the time between consecutive events is rarely periodic with the probability of periodicity of 0.1 percent, calculated as the time in which reversible events were periodic, divided by the total time of recordings (see Materials and Methods). However, the inset of the dbcAMP- stimulated recording shows highly periodic transient exocytic events. The overall probability of periodicity after the addition of dbcAMP was 15 percent, much more than in spontaneous conditions, where it was 0.1 percent.

These results indicate that dbcAMP-stimulation not only increases the frequency of transient exocytic events, but also affects the nature of their appearance – transient exocytic events become periodic, with periodic fusion pore dwell-times and more frequently appear in bursts.

4.5 cAMP stabilizes transient, widely open fusion pores

The results shown in Table II.1 demonstrate that dbcAMP decreases the fraction of transient exocytic events with relatively narrow (measurable) fusion pores. Moreover, the remaining transient exocytic events with measurable fusion pores exhibit increased diameters, compared to controls (Fig. II.4a). Both results indicate that the addition of dbcAMP promote wider fusion pores. Previously we observed that fusion pore diameter is related to the diameter of vesicles (Jorgačevski *et al*., 2010). To check the possibility that the elevation of cAMP influences previously observed relationship, we plotted C_v and the respective G_p for each event in controls and after the addition of cAMP-increasing agents (Fig. II.6a). The data points were best fitted with linear regressions with the following slopes: 2.3 ± 0.5 pS/fF (control) and 7.0 ± 0.5 pS/fF (cAMP- increasing agents) ($P<0.001$). These results show that a vesicle of a given C_v (diameter) may attain a threefold larger G_p (wider fusion pore) in the presence of a cAMP-increasing agent (Fig. II.6a).

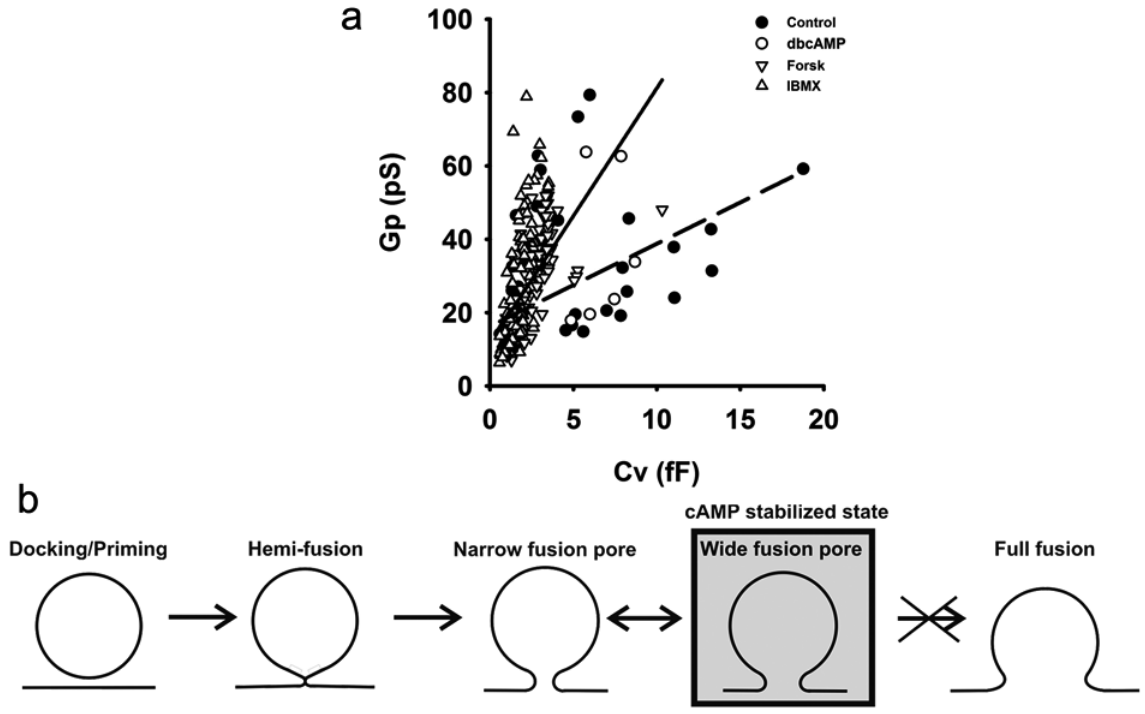

Figure II.6: The presence of cAMP increasing agents affects the relationship between the fusion pore diameter and the vesicle diameter.

(a) Scatter plot diagram of fusion pore conductance vs. vesicle capacitance of respective reversible events in controls (full circles) and after the addition of cAMP increasing agents

(empty symbols). Respective data points were best fitted with: y (G_p)=(2.3 ± 0.5) × x (C_v) + (16 ± 2) (control, dashed line, r=0.48) and y (G_p)=(7.0 ± 0.5) × x (C_v) + (11 ± 1) (cAMP-increasing agents, solid line, r=0.61). Both slopes are significantly different from each other ($P<0.001$). Significance was tested using one-way ANCOVA for two independent samples. **(b)** Model describing the effect of cAMP on exocytotic cycle of lactotroph vesicles.

5 Discussion

Regulated exocytosis consists of several distinct stages (Coorssen and Zorec, 2012). The key finding of this work is that cAMP stabilizes a stage, where the vesicle fusion pore transiently opens to relatively wide diameters, but has a reduced probability to enter into the full-fusion exocytic stage (Fig. II.6b). Stabilization of a particular stage may represent a rate-limiting step for vesicle cargo release, implying that secretion can be regulated at the post-fusion state (Rahamimoff and Fernandez, 1997; Barg *et al*., 2002; Tsuboi and Rutter, 2003; Obermüller *et al*., 2005; Hanna *et al*., 2009; Thorn, 2009; Jorgačevski *et al*., 2011). This condition can be attained by regulating fusion pore gating (kinetics) and by regulating fusion pore diameter (Staal *et al*., 2004; Stenovec *et al*., 2004; Vardjan *et al*., 2007; Jorgačevski *et al*., 2008; Zhang and Jackson, 2008; Jorgačevski *et al*., 2010), as demonstrated in the present work for cAMP-modulation of regulated exocytosis.

Hormone-release studies have shown that cAMP-elevating agents stimulate PRL release from pituitary cells at relatively low forskolin and dbcAMP concentrations, whereas at higher concentrations an inhibition of PRL release was recorded (Fig. II.1). The latter finding contrasts with previous studies, where IBMX increases the content of cAMP in cells and also the release of PRL in a dose-dependent manner (Gonzalez-Iglesias *et al*., 2006). In the present work, elevated forskolin (50 µM) and dbcAMP (>10 mM) concentrations are inhibitory for PRL release (Fig. II.1). Among many possible mechanisms, the inhibition of PRL release at elevated levels of cAMP may be due to direct cAMP-mediated modulation of the exocytic machinery (Sikdar *et al*., 1990, 1998; Hanna *et al*., 2009).

5.1 cAMP increases the occurrence of transient exocytic events

As shown previously (Zorec *et al*., 1991; Jorgačevski *et al*., 2008, 2011), we recorded unitary exocytic events in lactotrophs (Figs. II.2 and II.5). The amplitude of ~1 fF of these events is consistent with the view that they represent peptidergic

vesicles interacting with the plasma membrane (Jorgačevski *et al*., 2011). Two kinds of discrete increases in C_m were present: irreversible, representing full-fusion, and reversible, representing the transient mode of exocytosis (Fig. II.2). Interestingly, cAMP-increasing agents did not increase the frequency of the former, but only the frequency of the latter (Figs. II.2 and II.3). The increased frequency of transient events is consistent with the increased PRL release recorded in these cells (Fig. II.1). Furthermore, transient exocytic events exhibited wider fusion pore diameters and prolonged fusion pore dwell-times (Fig. II.4), all facilitating the exit of vesicle cargo into the extracellular space. However, the relative reduction of the occurrence of discrete irreversible steps in C_m observed in the presence of cAMP-elevating agents (Fig. II.2e), indicates that vesicle discharge may not attain full rates because it is hindered by the inability of transient exocytic events transiting into the full-fusion stage of regulated exocytosis (Fig. II.6b). This condition is likely reflected in reduced rates of PRL release recorded at relatively high dbcAMP concentrations (Fig. II.1). These results are in agreement with the decrease in cAMP-dependent full-fusion events in β-cells (Hanna *et al*., 2009). As in our experiments, where cAMP-increasing agents increase the frequency of transient exocytic events (Fig. II.2d, e), a similar augmentation of the occurrence of transient exocytotic events was observed in PC12, chromaffin, and pancreatic β-cells (Wang *et al*., 2003; MacDonald *et al*., 2006; Hanna *et al*., 2009), but not in islet cells (Hatakeyama *et al*., 2006). Furthermore, Cochilla and co-workers (2000) have shown that the increase of intracellular cAMP does not affect the number of plasma membrane fusion sites. Thus, the enhanced, cAMP-stimulated PRL release observed (Fig. II.1b; Gonzalez-Iglesias *et al*., 2006) is due to the increased secretion of prolactin per fusion site, possibly via more efficient vesicle discharge (i.e. increased frequency of reversible exocytic events and increased G_p; Figs. II.2d and II.4a). Most likely, the afore mentioned cAMP-stimulated PRL release cannot be attributed to the compound exocytosis (Vardjan *et al.,* 2009), since the results on the vesicle sizes (estimated from C_v; Fig. II.3) do not support this conclusion.

The fusion pore has long been considered an unstable intermediate leading to complete merger of the vesicle membrane with the plasma membrane (Heuser

and Reese, 1973). However, recent evidence indicates that the fusion pore can exhibit remarkable stability and can fluctuate between several open and closed states (Vardjan *et al*., 2007; Jorgačevski *et al*., 2010). The results in this study show that cAMP may stabilize one of these intermediates, that is, transient fusion pore openings with relatively wide diameters and prolonged dwell-times. However, this intermediate unlikely proceeds to the full-fusion stage of exocytosis (Fig. II.6b) and thus represents a hindrance for the fastest rates of PRL release. A similar stabilization, albeit with fusion pore narrowing, was observed in lactotrophs transfected with Munc 18-1 mutants (Jorgačevski *et al.,* 2011) and in lactotrophs exposed to Al^{3+} (p. 119).

The increase of intracellular cAMP resulted in fusion of larger vesicles in melanotrophs (Sikdar *et al*., 1998). Our results show that the amplitudes of C_v of transient events are similar in control and cAMP conditions in a given patch of membrane (Figs. II.2b, f and II.3). However, when we plotted the C_v amplitudes of all recorded events, the amplitudes of C_v appeared to consist of two vesicle populations being engaged in regulated exocytosis. The recalculated average vesicle diameters were 145 nm and 225 nm (see Materials and Methods), corresponding well with the size of prolactin containing vesicles (Smets *et al*., 1987; Angleson *et al*., 1999). Stimulation with cAMP-increasing agents increased the occurrence of the smaller amplitude vesicles (Fig. II.4c). Why cAMP-mediated effects are related to mainly the smaller sized vesicles interacting with the plasma membrane is unclear, but may relate to the observation that fusion pore diameter attained at equilibrium depends on vesicle diameter and on the intrinsic shape of membrane constituents in the region of the fusion pore (Jorgačevski *et al*., 2010). The latter could be affected by cAMP-dependent alteration of the local phospholipid environment (Su *et al.,* 2012), while size dependent modulation of vesicles of different diameters was observed in cells treated by Munc 18-1 mutations (Jorgačevski *et al.,* 2011).

5.2 cAMP-increasing agents elevate the fusion pore conductance and invoke rhythmicity

The release of vesicle content through a transient fusion pore depends on the effective diameter and the lifetime of the fusion pore. Previous studies have shown that KCl and hyposmotic stimulation affects both parameters in rat lactotrophs (Vardjan *et al*., 2007; Jorgačevski *et al*., 2008). In the present work, 25 percent of transient events, measured in control conditions, exhibited fusion pores, with the diameters < 3 nm (a limitation of our experimental setup; see Debus and Lindau, 2000; Table II.1) as reported and too narrow for the exit of PRL from the vesicle (Vardjan *et al*., 2007). Stimulation with cAMP-increasing agents decreased the percentage of narrow fusion pores and increased the average fusion pore diameter of measurable fusion pores (Table II.1; Fig. II.4). Only stimulation with IBMX failed to result in a statistically significant increase of the average fusion pore diameter. This failure could be due to the slower time course of the cAMP increase that follows this type of stimulation. The other possibility is that the level of cAMP concentration achieved with this stimulation is below the level of that achieved with forskolin and dbcAMP. In agreement with these two notions, stimulation with dbcAMP had the most robust effects on the kinetics and conductance of the fusion events (Figs. II.4, II.5, II.6). MacDonald *et al.* (2006) failed to observe changes in G_p following the stimulation with 5 μM of forskolin, which could be due to the different concentration used or due to the different cell model.

5.3 Rhythmicity of transient fusion events

Our results show that the average fusion pore dwell-time significantly increased only following the stimulation with dbcAMP (Figs. II.4 and II.6a). This result may reflect the fact that the intracellular cAMP concentration must reach a threshold value in order to increase the fusion pore dwell-time. The distribution of fusion pore dwell-times show that in controls the modal peak is similar to the one reported (Stenovec *et al*., 2004) and is not changed after the stimulation with IBMX

(Fig. II.4c). Stimulation with forskolin shifted the modal peak dwell-time to a higher value. On the other hand, stimulation with dbcAMP resulted in several modal values, which represent the distribution of fusion pore dwell-times within bursts (Figs. II.2f, II.5a, II.5b) and are similar to the observations of stimulated fission pore open states (Henkel *et al*., 2000). Moreover, time in between ensuing exocytic events was regular and could be fitted with a Gaussian curve (Figs. II.5d and e). Amperometric measurements in giant dopamine neurons of freshwater snail showed a similar phenomenon: a bursting of periodic exocytotic events (Chen *et al.*, 1996). The physiological significance of this periodic exocytic activity is still unknown but may involve cationic fluxes through the fusion pore and the vesicle membrane, as previously modeled (Kabaso *et al*., 2012).

In conclusion, the regulation of cAMP-mediated PRL-release is much more complicated than initially believed. Even though the increase in cAMP to a certain level stimulates PRL- release, at much higher levels of cAMP, the PRL release is significantly reduced mainly because of a decrease in the full-fusion exocytic events. We attribute transient increase in PRL release to stabilized fusion pores, which open more frequently, have on average prolonged dwell-time and wider diameters, but are unable to transit into the full-fusion exocytic state.

6 References

Alés E, Tabares L, Poyato JM, Valero V, Lindau M, Alvarez de Toledo G (1999). High calcium concentrations shift the mode of exocytosis to the kiss-and-run mechanism. *Nat Cell Biol* 1:40–44.

Alvarez de Toledo G, Fernández-Chacón R, Fernández J (1993). Release of secretory products during transient vesicle fusion. *Nature* 363:554–558.

Angleson J, Cochilla A, Kilic G, Nussinovitch I, Betz W (1999). Regulation of dense core release from neuroendocrine cells revealed by imaging single exocytotic events. *Nat Neurosci* 2:440–446.

Barg S, Olofsson C, Schriever-Abeln J, Wendt A, Gebre-Medhin S, Renstrom E, Rorsman P (2002). Delay between fusion pore opening and peptide release from large-dense-core vesicles from neuroendocrine cells. *Neuron* 33:287–299.

Ben-Tabou S, Keller E, Nussinovitch I (1994). Mechanosensitivity of voltage-gated calcium currents in rat anterior pituitary cells. *J Physiol* 476:29–39.

Breckenridge LJ, Almers W (1987). Currents through the fusion pore that forms during exocytosis of a secretory vesicle. *Nature* 328:814–817.

Chen G, Gutman DA, Zerby SE, Ewing AG (1996). Electrochemical monitoring of bursting exocytotic events from the giant dopamine neuron of Planorbis corneus. *Brain Res* 733:119–124.

Cochilla AJ, Angleson JK, Betz WJ (2000). Differential regulation of granule-to-granule and granule-to-plasma membrane fusion during secretion from rat pituitary lactotrophs. *J Cell Biol* 150:839–848.

Coorssen JR, Zorec R (2012). Regulated exocytosis per partes. *Cell Calcium* 52:191–195.

Debus K, Lindau M (2000). Resolution of patch capacitance recordings and of fusion pore conductances in small vesicles. *Biophys J* 78:2983–2997.

Fernandez J, Neher E, Gomperts B (1984). Capacitance measurements reveal stepwise fusion events in degranulating mast cells. *Nature* 312:453–455.

Fesce R, Grohovaz F, Valtorta F, Meldolesi J (1994). Neurotransmitter release: fusion or “kiss-and-run”? *Trends Cell Biol* 4:1–4.

Gandhi S, Stevens C (2003). Three modes of synaptic vesicular recycling revealed by single-vesicle imaging. *Nature* 423:607–613.

Gonzalez-Iglesias AE, Jiang Y, Tomic M, Kretschmannova K, Andric SA, Zemkova H, Stojilkovic SS (2006). Dependence of electrical activity and calcium influx-controlled prolactin release on adenylyl cyclase signalling pathway in pituitary lactotrophs. *Mol Endocrinol* 20:2231–2246.

Gonzalez-Iglesias AE, Murano T, Li S, Tomic M, Stojilkovic SS (2008). Dopamine inhibits prolactin release in pituitary lactotrophs through pertussis toxin-sensitive and -insensitive signaling pathways. *Endocrinology* 149:1470–1479.

Hanna ST, Pigeau GM, Galvanovskis J, Clark A, Rorsman P, MacDonald PE (2009). Kiss-and-run exocytosis and fusion pores of secretory vesicles in human β-cells. *Pflugers Arch - Eur J Physiol* 457:1343–1350.

Hatakeyama H, Kishimoto T, Nemoto T, Kasai H, Takahashi N (2006). Rapid glucose sensing by protein kinase A for insulin exocytosis in mouse pancreatic islets*. J Physiol* 570:271–282.

Henkel AW, Meiri H, Horstmann H, Lindau M, Almers W (2000). Rhythmic opening and closing of vesicles during constitutive exo- and endocytosis in chromaffin cells. *EMBO J* 19:84–93.

Heuser J, Reese T (1973). Evidence for recycling of synaptic vesicle membrane during transmitter release at the frog neuromuscular junction. *J Cell Biol* 57:315–344.

Jahn R, Lang T, Südhof T (2003). Membrane fusion. *Cell* 112:519–533.

Jorgačevski J, Stenovec M, Kreft M, Bajić A, Rituper B, Vardjan N, Stojilkovic S, Zorec R (2008). Hypotonicity and peptide discharge from a single vesicle. *Am J Physiol Cell Physiol* 295:624–631.

Jorgačevski J, Fošnarič M, Vardjan N, Stenovec M, Potokar M, Kreft M, Kralj-Iglič V, Iglič A, Zorec R (2010). Fusion pore stability of peptidergic vesicles. *Mol Membr Biol* 27:65–80.

Jorgačevski J, Potokar M, Grilc S, Kreft M, Liu W, Barclay WF, Buckers J, Medda R, Hell SH, Parpura V, Burgoyne RD, Zorec R (2011). Munc18-1 Tuning of Vesicle Merger and Fusion Pore Properties. *J Neurosci* 31:9055–9066.

Kabaso D, Calejo AI, Jorgačevski J, Kreft M, Zorec R, Iglič A (2012). Fusion pore diameter regulation by cations modulating local membrane anisotropy. *Scientific World Journal*, Article ID 983138, 7 pages doi:10.1100/2012/983138

Kostic TS, Tomic M, Andric SA, Stojilkovic SS (2002). Calcium-independent and cAMP-dependent modulation of soluble guanylyl cyclase activity by G protein-couple receptors in pitiitary cells. *J Biol Chem* 277:16412–16418.

Kreft M, Zorec R (1997). Cell-attached measurements of attofarad capacitance steps in rat melanotrophs. *Pflugers Arch* 434:212–214.

Lollike K, Borregaard N, Lindau M (1995). The exocytotic fusion pore of small granules has a conductance similar to an ion channel. *J Cell Biol* 129:99–104.

Lollike K, Lindau M (1999). Membrane capacitance techniques to monitor granule exocytosis in neutrophils. *J Immunol Methods* 232:111–120.

MacDonald PE, Braun M, Galvanovskis J, Rorsman P (2006). Release of small transmitters through kiss-and-run fusion pores in rat pancreatic β cells. *Cell Metabolism* 4:283–290.

Neher E, Marty A (1982). Discrete changes of cell membrane capacitance observed under conditions of enhanced secretion in bovine adrenal chromaffin cells. *Proc Natl Acad Sci USA* 79:6712–6716.

Obermüller S, Lindqvist A, Karanauskaite J, Galvanovskis J, Rorsman P, Barg S (2005). Selective nucleotide-release from dense-core granules in insulin-secreting cells. *J Cell Sci* 118:4271–4282.

Ohara-Imaizumi M, Nakamichi Y, Tanaka T, Katsuta H, Ishida H, Nagamatsu S (2002). Monitoring of exocytosis and endocytosis of insulin secretory granules in the pancreatic beta-cell line MIN6 using pH-sensitive green fluorescent protein (pHluorin) and confocal laser microscopy. *Biochem J* 363:73–80.

Perrais D, Kleppe I, Taraska J, Almers W (2004). Recapture after exocytosis causes differential retention of protein in granules of bovine chromaffin cells. *J Physiol* 560:413–428.

Rahamimoff R, Fernandez JM (1997). Pre- and post-fusion regulation of transmitter release. *Neuron* 18:17–27.

Renström E, Eliasson L, Rorsman P (1997). Protein kinase A-dependent and -independent stimulation of exocytosis by cAMP in mouse pancreatic B-cells. *J Physiol* 502:105–118.

Sedej S, Rose T, Rupnik M (2005). cAMP increases Ca^{2+}-dependent exocytosis through both PKA and Epac2 in mouse melanotrophs from pituitary slices. *J Physiol* 567:799–813.

Seino S, Shibasaki T (2005). PKA-dependent and PKA-independent pathways for cAMP-regulated exocyosis. *Physiol Rev* 85:1303–1342.

Su WM, Han GS, Casciano J, Carman GM (2012). Protein Kinase A-mediated Phosphorylation of Pah1p Phosphatidate Phosphatase Functions in Conjunction with the Pho85p-Pho80p and Cdc28p-Cyclin B Kinases to Regulate Lipid Synthesis in Yeast. *J Biol Chem* 40:33364–33376.

Sikdar SK, Zorec R, Mason WT (1990). cAMP directly facilitates Ca-induced exocytosis in bovine lactotrophs. *FEBS Lett* 273:150–154.

Sikdar SK, Kreft M, Zorec R (1998). Modulation of unitary exocytotic event amplitude by cAMP in rat melanotrophs. *J Physiol* 511:851–859.

Smets G, Velkeniers B, Finne E, Baldys A, Gepts W, Vanhaelst L (1987). Postnatal development of growth hormone and prolactin cells in male and female rat pituitary. An immunocytochemical light and electron microscopic study. *J Histochem Cytochem* 35:335–341.

Spruce A, Breckenridge L, Lee A, Almers W (1990). Properties of the fusion pore that forms during exocytosis of a mast cell secretory vesicle. *Neuron* 4:643–654.

Staal R, Mosharov E, Sulzer D (2004). Dopamine neurons release transmitter via a flickering fusion pore. *Nat Neurosci* 7:341–346.

Stenovec M, Kreft M, Poberaj I, Betz W, Zorec R (2004). Slow spontaneous secretion from single large dense-core vesicles monitored in neuroendocrine cells. *FASEB J* 18:1270–1272.

Stojilkovic SS, Tabak J, Bertram R (2010). Ion channels and signaling in the pituitary gland. *Endocr Rev* 31:845–915.

Thorn P (2009). New insights into the control of secretion. *Commun Integr Biol* 2:315–317.

Thorn P, Parker I (2005). Two phases of zymogen granule lifetime in mouse pancreas: Ghost granules linger after exocytosis of contents. *J Physiol* 563:433–442.

Tsuboi T, Rutter G (2003). Multiple forms of "kiss-and-run" exocytosis revealed by evanescent wave microscopy. *Curr Biol* 13:563–567.

Vardjan N, Stenovec M, Jorgačevski J, Kreft M, Zorec R (2007). Subnanometer fusion pores in spontaneous exocytosis of peptidergic vesicles. *J Neurosci* 27:4737–4746.

Vardjan N, Jorgačevski J, Stenovec M, Kreft M, Zorec R (2009). Compound exocytosis in pituitary cells. *Ann N Y Acad Sci* 1152:63–75.

Wang CT, Lu JC, Bai J, Chang PY, Martin TFJ, Chapman ER, Jackson MB (2003). Different domains of synaptotagmin control the choice between kiss-and-run and full fusion. *Nature* 424:943–947.

Zhang Z, Jackson MB (2008). Temperature dependence of fusion kinetics and fusion pores in Ca^{2+}-triggered exocytosis from PC12 cells. *J Gen Physiol* 131:117–124.

Zorec R, Sikdar SK, Mason WT (1991). Increased Cytosolic Calcium Stimulates Exocytosis in Bovine Lactotrophs*. J Gen Physiol* 97:473–497.

Chapter III - Differences in the expression pattern of HCN isoforms among mammalian tissues – sources and implications

NOTE: The results in this chapter were submitted for publication as: Calejo A.I., Reverendo M., Silva V.S., Pereira P.M., Santos M.A.S., Zorec R., Gonçalves P.P. Differences in the expression pattern of HCN isoforms among mammalian tissues – sources and implicationsds (2013) Mol Bio Rep.

1 Abstract

Hyperpolarization-activated cyclic nucleotide-gated (HCN) channels play a critical role in a broad range of cell types, but the expression of the various HCN isoforms is still poorly understood. In the present study we have compared the expression of HCN isoforms in rat excitable and non-excitable tissues at both the mRNA and protein levels. Real-time PCR and Western blot analysis revealed distinct expression patterns of the four HCN isoforms in brain, heart, pituitary and kidney, with inconsistent mRNA-protein expression correlation. The HCN2 was the most abundant mRNA transcript in all tissues (95.6%, 78.0% and 59.0% in kidney heart and pituitary, respectively) except in the brain (42.0%), whereas HCN4 was the most abundant protein isoform. Our results suggest that HCN channels are mostly produced by the HCN4 isoform in heart, which contrasts with the sharp differences in the isoform stoichiometry in pituitary (15 HCN4 : 2 HCN2 : 1 HCN1 : 1 HCN3), kidney (24 HCN4 : 2 HCN3 : 1 HCN2 : 1 HCN1) and brain (3 HCN4 : 2 HCN2 : 1 HCN1 : 1 HCN3). Moreover, deviations of the electrophoretic molecular weight (MW) of the HCN isoforms relative to the theoretical MW were observed, suggesting that N-glycosylation and enzymatic proteolysis influences HCN channel surface expression. We hypothesize that selective cleavage of HCN channels by membrane bound metalloendopeptidases could account for the multiplicity of properties of native HCN channels in different tissues.

Key words: HCN channels, rat, western-blot, quantitative real-time PCR

2 Introduction

The study of the hyperpolarization-activated, cyclic nucleotide-gated (HCN) channels re-emerged with enhanced interest given the unequivocal evidence of its importance as therapeutic targets (Postea and Biel, 2011). HCN channel-based therapies have been anticipated due to their intrinsic properties as biological pacemakers (Biel *et al.,* 2009). It is not surprising that the present relevance of HCN channels in physiological and pathophysiological conditions is mainly linked with heart and brain tissues. These channels were first described as hyperpolarization activated or funny currents (Ih/If) in cardiac sinoatrial node cells in 1979 (Brown *et al.,* 1979) and the four known HCN isoforms were cloned from brain in 1998 (Santoro *et al*., 1998).The mammalian HCN isoforms (HCN1, HCN2, HCN3 and HCN4) share ~80 % of homology between them (Monteggia *et al*., 2000) and differ mainly in activation kinetics and sensitivity to cAMP (Kaupp and Seifert, 2001). HCN channels exhibit common features like activation in the negative voltage range, closure at positive potentials and modulation by cyclic nucleotides, which appear to be directly linked to generation of rhythmic electrical activity in excitable tissues (Kaupp and Seifert, 2001). The hyperpolarization-activated currents are generated by the permeability primarily to Na^+ and K^+, however they may also be permeable to Ca^{2+} in some cell types (Zhong *et al*., 2004).

The expression pattern of HCN channels, at protein and mRNA levels, has been characterized in brain and heart cells (Robinson and Siegelbaum, 2003; Herrmann *et al.,* 2007). All HCN isoforms were found in different cells types of these two organs, though their expression levels are variable and complex. This complexity is mainly generated *in vivo* and *in vitro* by isoform co-assembly in heterotetramers (Accili *et al*., 2002). Furthermore, *in vivo* post-translational modifications (e.g. glycosylation) are known to occur in HCN channels (Much *et al.,* 2003; Hegle *et al*., 2010) and there is also association with other proteins (Lewis *et al*., 2010).

HCN channels are often described as being predominantly expressed in neurons and heart cells, but they may exhibit a broader distribution throughout

different organs than previously predicted. Hurtado *et al.* (2010) confirmed the expression of the HCN3 isoform using immunocytochemistry and real-time PCR and revealed its important role in peristalsis of the pelvis-kidney junction. Interestingly, the human embryonic kidney (HEK) 293 cell line is extensively used to study HCN channels activity (Varghese *et al*., 2006). Recent studies show expression of HCN isoforms in pancreas (El-Kholy *et al*., 2007), pituitary gland (Kretschmannova *et al.,* 2012) and bladder (He *et al*., 2012; Xue *et al*., 2012). Therefore, it is important to clarify the relevance of HCN channels related pathologies and their physiological role in cell types beyond the excitable cells. In this context, the clarification of the expression patterns of HCN channels isoforms in different organs is important to determine their involvement in other inherited and/or acquired channelopathies. Although there are reports on the molecular expression of HCN isoform transcripts and on functional expression of HCN currents in excitable and non-excitable cells (Monteggia *et al*., 2000; Marionneau *et al*., 2005; Aponte *et al*., 2006; El-Kholy *et al.,* 2007; Horwitz *et al*., 2010; Cho *et al*., 2011, Greener *et al*., 2011; Poller *et al*., 2011; He *et al*., 2012; Kretschmannova *et al*., 2012; Xue *et al.,* 2012), to our knowledge, a comparative analysis of the molecular expression of the four HCN isoforms in excitable and non-excitable tissues has not been reported yet. Here we use two techniques, Western blot analysis and Real-time PCR, to detect and quantify the expression of HCN isoforms in non-excitable tissues and to compare their expression levels between excitable and non-excitable cells. We have identified distinct expression patterns of full-length and fragmented polypeptide chains of the HCN isoforms, suggesting that specific proteolytic cleavage of HCN subunits occur *in vivo*.

3 Materials and Methods

3.1 Sample collection

Adult male Wistar rats were handled in accordance with EU guidelines for accommodation and care of animals used for experimental and other scientific purposes (2007/526/EC). The collected organs were quickly sliced, washed with phosphate buffered saline (PBS: 137 mM NaCl, 10 mM Na_2HPO_4, 2.7 mM KCl, 1.8 mM KH_2PO_4), immediately frozen in liquid N_2 and stored at -80 ºC.

3.2 Real-time PCR

Total RNA and genomic DNA (gDNA) were extracted using AllPrep DNA/RNA/Protein Mini kit (QIAGEN). RNA quantity and quality were assessed using the Nanodrop and Agilent 2100 bioanalyzer systems, respectively. The total RNA was reverse-transcribed to cDNA using Superscript II™ RT enzyme (Invitrogen) and oligo dT (12-18) primers. First-strand cDNA templates were used for PCR amplification of genes. Real-time PCR (qRT-PCR) was performed in triplicate using Platinium® SYBR Green Supermix UDG (Invitrogen) and analysed using a 7500 real-time PCR system (Applied Biosystems). Forward primers (FP) and reverse primers (RP) were chosen according to El-Kholy *et al.,* (2007):

HCN1	FP - CACCAGCAGCTGTGCAGAGA	RP-CAAGAATCATAAATTCGAAGCAAAAC
HCN2	FP- GGGAATCGACTCCGAGGTCTAC	RP- AGACTGAGGATCTTGGTGAAACG
HCN3	FP- AACGTGGCCATAGCCTTGAC	RP- GCTGAGCGTCTAGCAGATCGA
HCN4	FP- GCTCCAAACTGCCGTCTAATTT	RP- GAAGAAGGGAGCAAGAAAAAGAAGA
β-actin	FP- TAGCCATCCAGGCTGTGTTG	RP- GGAGCGCGTAACCCTCATAG

Melt curve analysis was performed on the PCR products at the end of each PCR run to ensure that a single product was amplified. Standard dilution curves for cDNA and gDNA were produced for each primer set and their amplification efficiencies calculated from cDNA standard curves. RT-minus and non-template controls were performed for all samples. The relative abundance of HCN isoform transcripts was calculated using gDNA standard curves of each tissue and β-actin as normalization control.

3.3 Western-blot

Frozen tissues were either processed according to the manufacturer's protocol to extract membrane and cytosolic fraction separately (ProteoExtract®Transmembrane Protein Extraction Kit, Novagen), or homogenized in RIPA buffer (50 mM Tris, 150 mM NaCl, 1% NP-40, 0.5% Na-desoxycolate and 0.1% SDS), supplemented with protease inhibitor cocktail (Roche), incubated for 10 min and centrifuged at 15,000×g to collect the total protein fraction. Protein concentration was determined by the Bradford method (Bio-Rad). Proteins were separated by SDS-PAGE using 4–15% polyacrylamide gel (Bio-Rad) and transferred to polyvinylidene fluoride membranes (PVDF, Amersham Biosciences, UK). Blocked membranes were incubated overnight at 4 °C with polyclonal rabbit antibodies against HCN1-4 isoforms (1:200, Alamone, Israel) in 5% non-fat milk/TBS (Tris Buffered Saline; 150 mM NaCl, 50 mM Tris-HCl pH 7.6)/ 0.1% Tween. The epitopes in the amino acid chains of isoforms recognized by the specific antibodies are shown in Figure III.1. Membranes were incubated with secondary antibody (1:10,000; Irdye680 Red anti-rabbit IgG, Odyssey). The Li-Cor Biosciences Odyssey infrared imaging system (Lincoln, NE) was used for membrane scanning and quantification of fluorescence emission at 700 nm. Na^+K^+-ATPase (polyclonal rabbit; 1:500; Abcam) was used as control for protein loading and normalization of data. The molecular weight (MW) of HCN isoforms were determined from calibration curves using pre-stained, broad range SDS-PAGE MW standards (Bio-Rad).

4 Results

We have quantified the expression of the HCN isoforms in adult rat heart, brain, pituitary and kidney by qRT-PCR and Western blotting. Non-template controls were performed and the amplification efficiency of the primers was similar (1.90, 1.97, 1.94, 1.90 and 1.94 for β-actin, HCN1, HCN2, HCN3 and HCN4, respectively), as determined by analysis of the cDNA standard curves. For Western blot experiments negative controls were performed using antigens for HCN1, HCN2, HCN3 and HCN4.

4.1 Distribution of HCN isoforms in excitable and non-excitable tissues

In heart tissue the expression of all transcripts was confirmed by qRT-PCR and the two most abundant transcripts were the HCN2 and HCN4, 78.0% and 19.2% of the HCN transcripts, respectively (Fig. III.2a). A relatively low level of expression (sum of 4.6%) was obtained for HCN transcripts, compared with the β-actin transcript (housekeeping constitutive gene). To verify the expression of the HCN isoforms in heart tissue, we have performed a Western blot analysis of the total organ lysate (Fig. III.2a). All HCN isoforms, namely the 102 kDa (HCN1), the 95 kDa (HCN2), the 87 kDa (HCN3) and the 129 kDa (HCN4) were detected using antibodies targeted to isoform specific epitopes (Fig. III.1). As expected from the mRNA quantification data the HCN2 protein was not the most abundant isoform and produced a weak signal at 93±3 kDa. No significant differences were detected in the amount of HCN1, HCN2 and HCN3 isoforms at the protein level (2%, 2% and 1% of the total amount of immunoreactive proteins, respectively). Conversely, a strong signal at 87±1 kDa was obtained with the HCN4 specific antibody, showing that HCN4 is the most abundant isoform in heart tissue. The presence of a relatively weaker signal at 65±1 kDa suggests that HCN4 was fragmented.

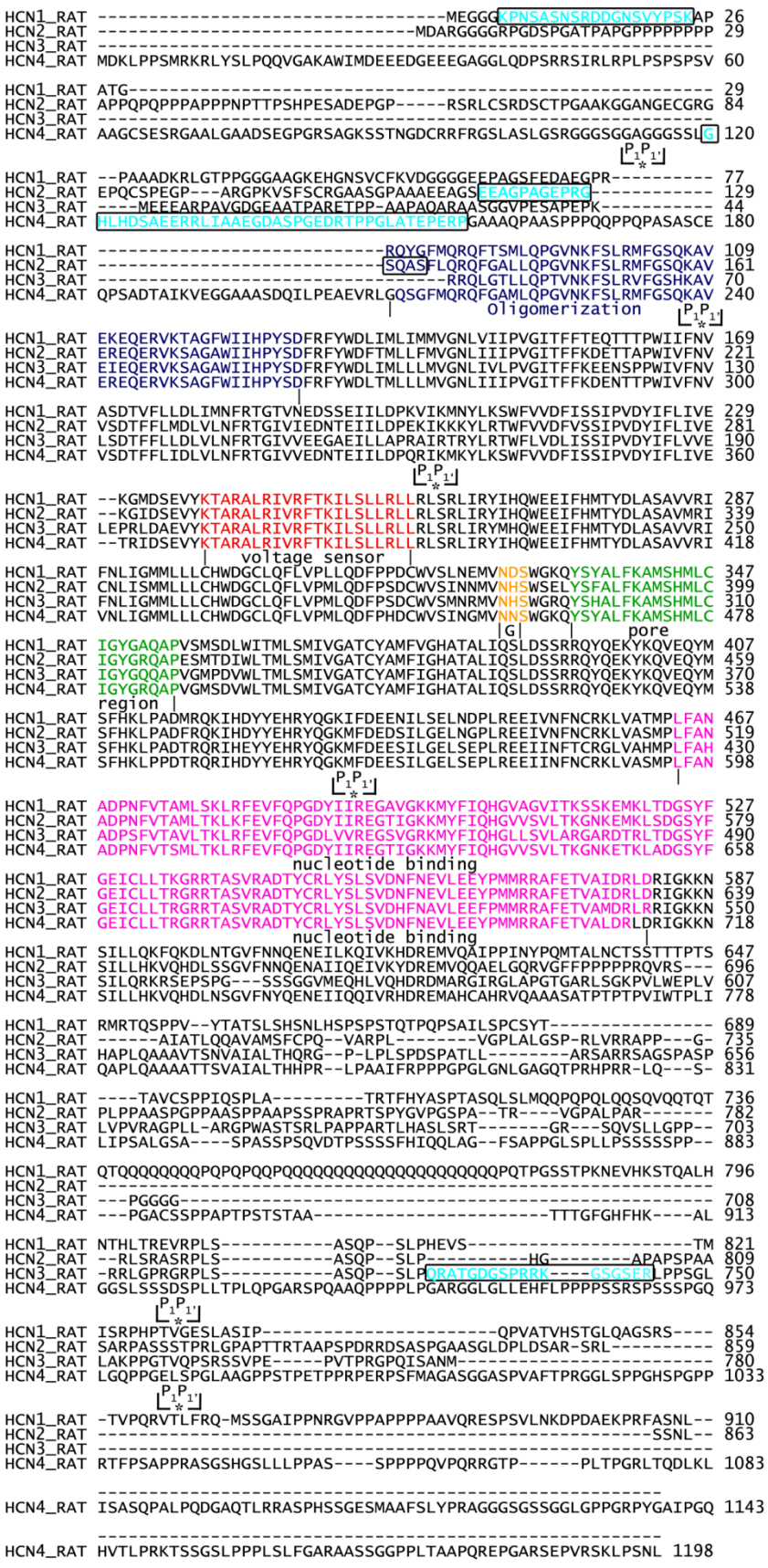
HCN1_RAT
HCN2_RAT
HCN3_RAT
HCN4_RAT
Oligomerization
voltage sensor
pore
region
nucleotide binding
nucleotide binding

Figure III.1: Alignment of amino acid sequences of rat HCN isoforms.

HCN isoform amino acid sequences were assessed in UniProt (Q9JKB0 for HCN1_RAT, Q9JKA9 for HCN2_RAT, Q9JKA8 for HCN3_RAT and Q9JKA7 for HCN4_RAT). The alignment of amino acid sequences was performed using ClustalW. Specific domains are shown in different colors: blue, oligomerization region; red, voltage sensor region; orange, N-glycan binding site; green, pore region and pink, nucleotide binding region. The epitopes in the amino acid chains recognized by specific anti-bodies against HCN1-4 are assigned in boxes. PeptideCutter online tool (http://*www.expasy.com*) was used to predict potential cleavage sites by proteases and their relative solvent accessibility predicted using the program PredictProtein (http://*www.predictprotein.org/*). HCN isoforms were revealed as potential substrates for metalloendopeptidases with PROSITE PS00142 (http://prosite.expasy.org/). Putative cleavage sites in high scored (≥8 in 10 grade scale) regions of the amino acid chains are marked according to Schechter and Berger, (1968): amino acid residues undergoing cleavage (*) are designated P1 in the N-terminal direction from the cleaved bond and P1' in the C-terminal direction.

Since we used protease inhibitors in the RIPA buffer it is likely that such proteolysis may not be related with sample degradation. Indeed, evidence that specific cleavage of HCN might happen *in vivo* is supported by the identification of putative cleavage sites by metalloendopeptidases in solvent accessible regions of the amino acid sequences by bioinformatics tools (PeptideCutter and PredictProtein) (Fig. III.1). Moreover, the experimentally determined MW appeared to be lower than the theoretical values. The cleavage of HCN4 by metalloendopeptidases at Gly112-Ala113, Lys562-Met563 and Ser920-Asp921 could generate fragments with 87±1 kDa and 65±1 kDa. Antibodies against HCN1 and HCN3 also produced immunoreactive bands at 89±2 kDa and 80±6 kDa, respectively, supporting fragmentation of HCN1 and HCN3 at Arg801-Glu802 and Thr757-Val758 by metalloendopeptidases.

The expression profiling of HCN isoforms in pituitary tissue revealed that the HCN2 transcript and HCN4 protein are the most abundant (Fig. III.2b), as in heart tissue (Fig. III.2a). However, a relatively low level of total expression (sum of 2.9%) was obtained for HCN transcripts in pituitary tissue when compared with heart tissue. Notably, the highly expressed HCN4 protein corresponded to the lowest average mRNA expression value obtained in this tissue (HCN2, 59.0%; HCN1, 20.1%; HCN3, 13.9%; and HCN4, 6.9%). Major immunoreactive bands at 93±1 kDa (HCN1), 95±1 kDa (HCN2), 93±0 kDa (HCN3) and 70±1 kDa (HCN4)

were detected, although other lower MW immunopositive bands were also observed (Fig. III.2b). The relative contribution of each immunopositive polypeptide chain to the total amount of HCN protein was also very different. In the case of HCN1 and HCN2, equimolar amounts of long (93±1 kDa and 95±1 kDa) and short (24±0 kDa and 23±0 kDa) polypeptide chains were present. Conversely, short polypeptide chains of HCN3 (23±0 kDa) and HCN4 (27±4 kDa) only represented 28% and 12% of the total amount of the respective isoform. The experimentally determined MW of the longer polypeptide chain of HCN3 (93±0 kDa) was slightly higher than the theoretical one (87 kDa). Since the introduction of a N-glycan at the S5 pore linker of HCN1-4 occurs during channel maturation and its cleavage by PNGaseF decreases MW by 10-20 kDa (Much *et al*., 2003; Hegle *et al*., 2010), we confirmed the presence of the glycosylation consensus "Asn-X-Ser" in the amino acid sequences (Fig. III.1). Accordingly, the obtained results seem to indicate that HCN3 is mostly present in the form of glycosylated polypeptide chains. On the other hand, the experimental MW of the HCN4 long polypeptide chain was 70±1 kDa, which is lower than the theoretical one (129 kDa). Thereby, the primary structure of HCN isoforms were re-examined in order to identify potential endopeptidase cleavage sites generating 93±1 kDa (HCN1), 70±1 kDa (HCN4) and ~25 kDa (HCN1-4) fragments. Based on fragment sizes, localization of immunoreactive epitopes and solvent exposure scores potential cleavage sites were mapped between amino acid residues: Lys199-Val200 and Glu802-Val803 (HCN1); Lys160-Ala161 (HCN2); Lys394-Met395 and Thr757-Val758 (HCN3); and Gly112-Ala113, Lys238-Ala239 and Lys562-Met563 (HCN4) (Fig. III.1). Thus, the discrepancies between experimental MW of HCN isoforms and the theoretical ones can be explained by considering specific cleavage of glycosylated and non-glycosylated polypeptide chains. For instance, the 93±1 kDa immunoreactive band produced by anti-HCN1 antibody could represent a proteolytic fragment of the glycosylated HCN1 encompassing the amino acid residues Met1-Glu802.

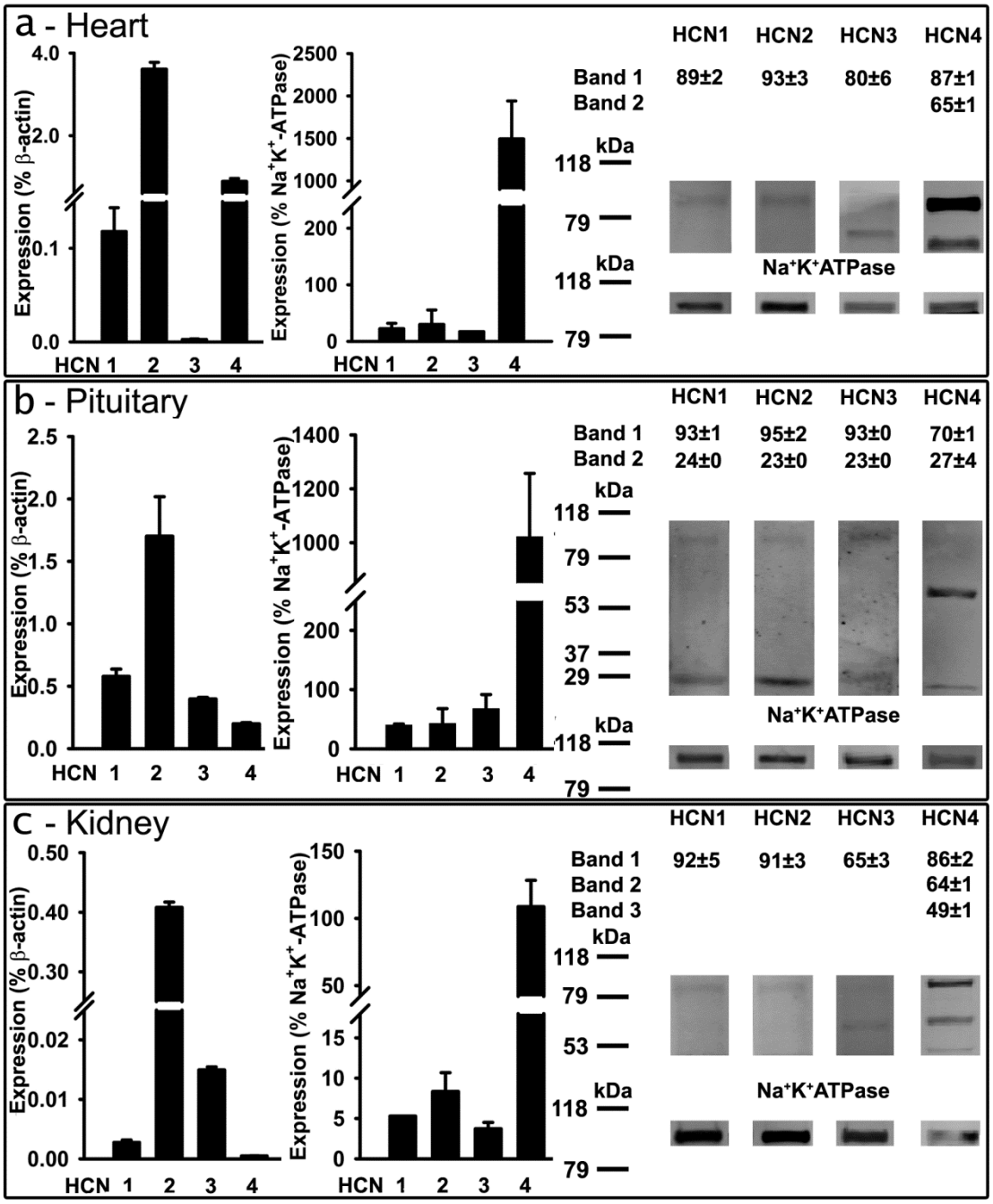

Figure III.2: Expression of HCN isoforms in rat heart, pituitary and kidney.

The expression of HCN isoforms was confirmed in the tissues analysed. Quantitative real-time PCR (qPCR) and Western blotting were performed as described in methods, with total lysates of heart **(a)**, pituitary **(b)** and kidney **(c)**. For quantitative analysis of HCN isoform mRNA transcripts (left panel) and their expression at protein level (middle panel) β-actin gene and Na^+K^+-ATPase were used as housekeeping constitutive gene and protein loading control, respectively. Representative Western blots of HCN isoforms in tissue total lysates and the MW's of the respective immunoreactive bands are displayed in right panel. Data are expressed as the mean ± s.e.m. of at least 3 experiments.

Likewise, proteolysis of HCN4 would produce a 70±1 kDa immunoreactive band, encompassing the amino acid residues Ala113 to Lys562. Actually, the specific antibodies reacted with HCN isoforms, producing also one immunoreactive band around the 25 kDa region. Small fragments were also detected when total brain lysates were used instead. The relative abundances of the HCN isoforms in brain lysate were 24% (HCN1), 25% (HCN2), 14% (HCN3) and 36% (HCN4), when compared with the expression of Na^+K^+-ATPase used as protein loading control. It is likely that these immunoreactive bands could be generated by proteolysis, given that all isoforms have putative cleavage sites for metalloendopeptidases close to the epitopes recognized by the specific antibodies (Lys199-Val200, HCN1; Lys160-Ala161, HCN2; Lys394-Met395, HCN3; and Lys238-Ala239, HCN4).

Until now only the expression of HCN in excitable tissues has been studied. Figure III.2c shows the relative mRNA and protein levels in kidney, a non-excitable tissue. The analysis revealed the presence of all HCN isoforms. Like in heart and pituitary tissue, the HCN2 and HCN4 appeared to be the most abundant mRNA transcripts and polypeptide chains, respectively. Once again, the highly expressed HCN4 protein corresponds to the lowest average mRNA expression level obtained (HCN2, 95.6%; HCN3, 3.5%; HCN1, 0.7%; and HCN4, 0.2%). However, the quantification of mRNA expression levels relative to the housekeeping gene performed in different tissues showed that the total amount of mRNA transcripts in kidney was of the same order of magnitude than in liver but 2 orders of magnitude smaller than in brain (brain>>heart>pituitary>liver=kidney). Major immunoreactive bands at 92±5 kDa (HCN1), 91±3 kDa (HCN2), 65±3 kDa (HCN3) and 86±2 kDa (HCN4) were detected (Fig. III.2c). The protein levels of HCN isoforms in liver lysate were 2% (HCN1), 4% (HCN2), 9% (HCN3) and 85% (HCN4), when compared with the expression of Na^+K^+-ATPase used as protein loading control. In the case of the anti-HCN4 antibody, two other immunopositive bands (64±1 and 49±1 kDa) were also observed. The least expressed isoforms HCN3, HCN1 and HCN2 only represented 3%, 4% and 6% of the total amount of immunoreactive proteins, respectively. It is likely that the immunoreactive bands at 86±2 kDa, 64±1 kDa and 49±1 kDa represent HCN4 fragments produced by

metalloendopeptidases (putative cleavage sites: Gly112-Ala113, Lys562-Met563 and Ser920-Asp921) (Fig. III.1). The apparently underestimated MW values of HCN1 (92±5 kDa) and HCN3 (65±3 kDa) seem to suggest that both forms, glycosylated and non-glycosylated, are substrates of metalloendopeptidases (putative cleavage sites: Glu802-Val803, Ala162-Ile163 and Thr757-Val758) in kidney.

4.2 Subcellular distribution of full length and proteolytic fragments of HCN isoforms

The Western blot analysis of the HCN isoforms performed in total lysates of different tissues (Fig. III.2) suggested that the tendency of the isoforms to be mainly glycosylated and/or proteolysed is variable. N-linked glycosylation is a determinant of HCN channels targeting the plasma membrane, whose function may be abrogated by proteolytic processing (Much *et al*., 2003; Ye *et al*., 2009; Hegle *et al.*, 2010).

To evaluate the expression levels of HCN isoforms in the membrane fraction, Western blots of membrane and cytosolic extracts of kidney and brain were carried out (Fig. III.3). Brain has been the tissue prototype for studying the subcellular expression and subunit composition of HCN channels (Herrmann *et al.,* 2007). As expected, the mRNA and protein corresponding to all isoforms were observed in the brain. We were surprised by the fact that the most abundant mRNA transcript was HCN1 (57.1%) instead of HCN2 (42.0%) since previous data showed that the HCN2 transcript was the most prominent (Fig. III.2). Only a single 92±0 kDa immunoreactive band was detected in the kidney membrane extract (Fig. III.3a). Still, all three HCN4 immunopositive bands (86±2 kDa, 64±1 kDa and 49±1 kDa) previously observed in the total lysate (Fig. III.2c) were also present in the cytosolic extract (Fig. III.3a). These results suggest that HCN fragmentation occurs in the cytoplasm rather than during protein preparation. However, when brain membrane extracts were immunoblotted, full-length HCN isoforms and proteolytic fragments of HCN2-4 were detected (Fig. III.3b). In brain tissue HCN1-3 isoforms at the cell surface appeared to be mainly glycosylated since the MW of

the major immunoreactive bands (121±4 kDa, HCN1; 119±5 kDa, HCN2 and 94±0 kDa, HCN3) were systematically higher than the theoretical ones (102 kDa, HCN1; 95 kDa, HCN2; 87 kDa, HCN3).

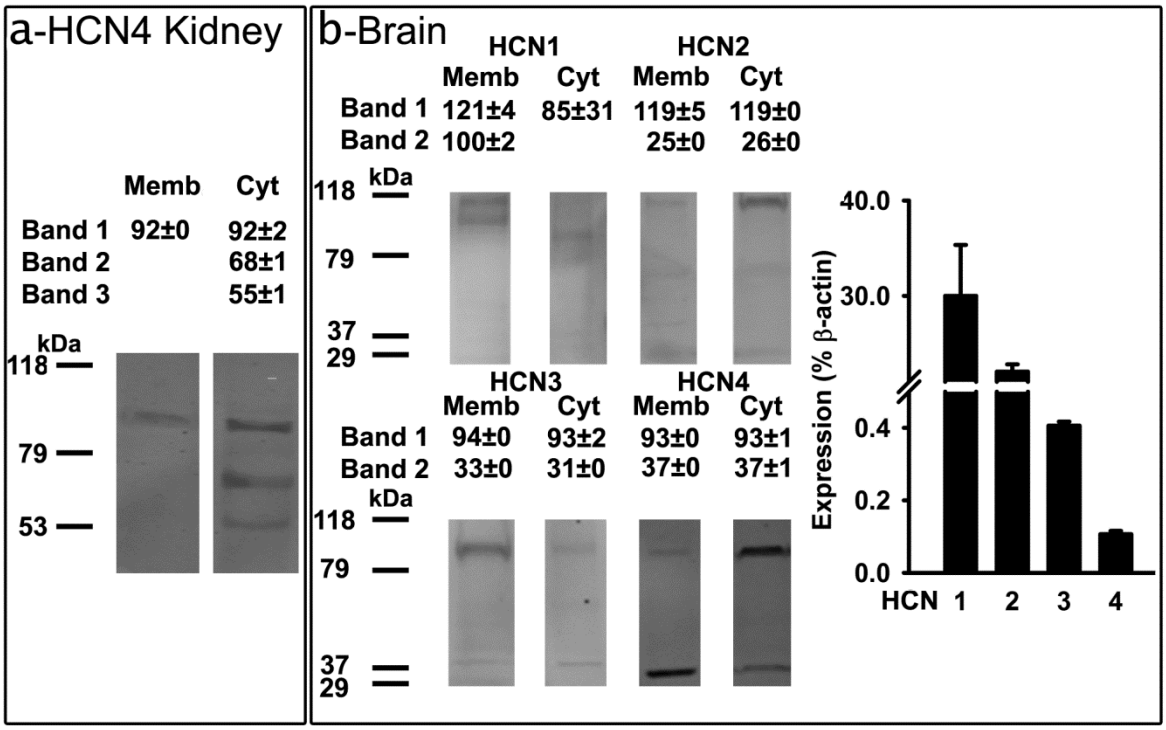

Figure III.3: Plasma membrane and cytosolic pools of HCN isoforms.

Samples for qPCR and Western blot (plasma membrane and cytosolic fractions) from rat kidney **(a)** and brain **(b)** were prepared as described in methods. Representative Western blots of membrane and cytosolic fractions of HCN isoforms and the MW's of the respective immunoreative bands are displayed. The presence of HCN isoforms in brain tissue was confirmed by quantitative analysis of mRNA transcripts. Data are expressed as the mean ± s.e.m. of at least 3 experiments.

These results are consistent with previous reports showing that in the brain HCN1 and HCN2 are predominantly glycosylated (Much *et al*., 2003). Anti-HCN2 antibody also revealed a lower MW band (25±0 kDa, membrane; 26±0 kDa cytosol). Anti-HCN3 and anti-HCN4 antibodies showed the presence of two immunoreactive bands in membrane and cytosolic extracts, suggesting that the glycosylated forms of the full-length HCN3 (94±0 kDa, membrane; 93±2 kDa, cytosol) and their proteolytic fragments (33±0 kDa, membrane; 31±0 kDa, cytosol) were detected. Similarly the glycosylated HCN4 (93±0 kDa, membrane; 93±1 kDa,

cytosol) and proteolytic fragments (37±0 kDa, membrane; 37±1 kDa, cytosol) were observed.

Table III.1: Apparent molecular weights in kDa of HCN isoforms in excitable and non-excitable tissues.

	HCN1	HCN2	HCN3	HCN4
Excitable tissues				
Brain	121±4; 98±13	118±1; 29±4	92±2; 32±1	90±3; 35±2
Pituitary	93±1; 24±0	95±1; 23±0	93±0; 23±0	68±3; 24±4
Heart	89±2	93±3	80±1	89±1; 66±1
Pancreas	62±2	57±0	60±2	58±1
Non-excitable tissues				
Kidney	91±5	91±3	75±10	90±2; 66±2; 52±3
Liver	91±1	92±2	56±0	68±3; 50±1

The average MW of the immunoreative bands are expressed as the mean ± s.e.m. of at least 3 experiments.

Table III.1 shows that the MW of HCN4 was underestimated in all analysed tissues relative to the theoretical value (129 kDa), suggesting that selective enzymatic cleavage may play a central role in the functional processing and compartmentalization of HCN isoforms. Therefore, a comparative analysis of all full-length amino acid sequences of HCN isoforms and of their putative proteolytic fragments was carried out using PSORT II (Table III.2). As expected, the plasma membrane was the predictable localization (k = 23) for the full-length amino acid sequences of all HCN isoforms. The tendency of the proteolytic fragments to be targeted to the plasma membrane appeared to be dissimilar, presently interpreted as reflecting the actuality of functional domain regions of the amino acid sequences. All HCN fragments immunoblotted with MW lower than 50 kDa were predicted to be absent in the plasma membrane (Table III.2). In non-excitable tissues, Western blots for specific membrane/cytosolic proteins did not reveal the presence of immunoreactive bands with MW lower than 60 kDa. Intriguingly, brain membrane extract probed with the anti-HCN2, 3 and 4 antibodies revealed the presence of immunoreactive bands at 25±0, 33±0 and 37±0 kDa (Fig. III.3b).

Therefore, HCN fragments predicted to lack targeting sequence to plasma membrane in brain membrane fraction were present, suggesting that *in vivo* proteolytic processing of HCN channels at the cell surface takes place in brain tissue.

Table III.2: Localization of full-length and fragments of HCN isoforms in plasma membrane.

Predicted Localization	Preferential (k=23; p>39%)	Possible (4.3%<p<38%)	Improbable (p<4.3%)
HCN1	Met1-Leu910 (102 kDa) Met1-Glu802 (91 kDa) Met1-Lys431 (49 kDa)		Met1-Val200 (22 kDa)
HCN2	Met1-Leu863 (95 kDa) Met1-Lys483 (55 kDa)		Met1-Lys160 (20 kDa)
HCN3	Ala1-Met780 (87 kDa)	Ala162-Met780 (68 kDa)	Lys394-Met780 (38 kDa)
HCN4		Met1-Ser920 (98 kDa) Met1-Lys562 (63 kDa)	Met1-Lys238 (25 kDa)

Localization at the plasma membrane was predicted using PSORT II online tool (*http://psort.hgc.jp/form2.html*), which considers the k-nearest neighbour (k-NN) algorithm to assess the probability of subcellular location (k=9/23; Horton and Nakai, 1997). “p” denotes for the probability to be localized in the plasma membrane.

5 Discussion

In this study we have characterized the mRNA and protein expression patterns of the HCN isoforms in excitable and non-excitable tissues and the putative proteolytic cleavage of HCN subunits at the plasma membrane. The data suggest that HCN channels might be regulated by membrane bound metalloendopeptidases.

The HCN isoforms were detected at mRNA and protein levels and their relative abundance was variable among tissues. When compared with a housekeeping gene (β-actin) the relative number of mRNA copies was higher in excitable (brain, 52.59% >> heart, 4.63% > pituitary, 2.88%) than in non-excitable tissues (kidney, 0.43% and liver, 0.35%). HCN1 and HCN2 were the predominant isoforms in brain (HCN1>HCN2>>HCN3>HCN4) and HCN2 and HCN4 in heart (HCN2>HCN4>>HCN1>HCN3). These results are in line with those previously reported, where the highest number of HCN mRNA copies in brain and heart correspond to HCN1/HCN2 and HCN2/HCN4, respectively (El-Kholy *et al*., 2007). The expression levels of the isoforms were more similar in pituitary tissue (HCN2>HCN1>HCN3>HCN4), while the amount of HCN2 mRNA was at least twenty-fold higher than the amount of HCN3 mRNA in kidney and liver tissue, where HCN1 and HCN4 were only present in vestigial amounts. Accordingly, Kretschmannova *et al*. (2012) observed that HCN2 mRNA transcript was predominant in pituitary cells. The obtained results suggest that mRNA expression profile is tissue specific for excitable tissues and distinct from the prevailing one in non-excitable tissues. This conclusion is also supported by qRT-PCR of HCN transcripts in other tissues and cell cultures. Basket cells in the hippocampus co-express HCN1 and HCN2, but lack detectable expression of HCN3 and HCN4 (Aponte *et al.,* 2006). In wild-type mouse cochlea, the total number of copies of mRNA decrease from HCN2 to HCN3 (HCN2>HCN1>HCN4>HCN3) (Horwitz *et al*., 2010). The amount of HCN1 mRNA is the lowest in rat lateral habenular complex where HCN2-4 are expressed in equivalent amounts (Poller *et al*., 2011). Greener *et al*. (2011) performed an extensive study of the mRNA expression profile of HCN isoforms in different components of the human atrioventricular

conduction axis and observed that HCN4 is the most abundant isoform. Regarding HCN protein isoform expression the scenario was very different. The HCN4 isoform was the most abundant in all tissues (Figs. III.2 and III.3). Expression of the HCN4 isoform was at least 100-, 27-, 24-, 15-, 4- and 3-fold higher than either HCN1 or HCN3 in heart, liver, pituitary, kidney, pancreas and brain tissue, respectively. The relative expression of the other HCN isoforms at protein level was very similar. These results are in agreement with those reported by Xue *et al*. (2012) showing that HCN4 is the most abundant isoform in the human bladder interstitial cells of Cajal, but contrast with those of He *et al*. (2012) noticing HCN4 as the least abundant isoform in rat urinary bladder. Actually, expression of HCN isoforms is variable at different postnatal ages (Cho *et al.,* 2011) and in distinct compartments of mouse heart (Marionneau *et al*., 2005). We assessed the mRNA-protein expression correlation of HCN isoforms among different tissues; the highest positive correlation (r^2 = 0.6658) was for HCN4. The mRNA and protein expression of HCN isoforms appeared negatively correlated in each tissue (Figs. III.2 and III.3). The number of mRNA copies does not reflect the number of functional protein molecules, and thereby complementary mRNA and protein expression studies should be conducted when analysing HCN gene function. There are several biological processes that could account for the lack of correlation between mRNA and protein expression, namely different protein translation efficiencies due to different mRNA secondary structures, the variability of protein half-life, splicing, translational modifications, translational regulation and protein complex formation.

The variability of HCN isoform expression patterns at the protein level should impact the structure of HCN channels and their functional properties, given that they are thought to be either homo- or heterotetramers that display different properties (Ulens and Tytgat, 2001; Altomare *et al*., 2003; Michels *et al.,* 2005; Whitaker *et al*., 2007). Although the subunit composition of HCN channels was not analysed, the protein expression profiling of the HCN presented in this study suggest significant differences in subunit composition of HCN channels due to the heterogeneity of isoform stoichiometry in different tissues. Likely HCN channels are mostly built by HCN4 in heart, which contrasts with the isoform stoichiometry in

brain (3 HCN4 : 2 HCN2 : 1 HCN1 : 1 HCN3) and in pancreas (4 HCN4 : 3 HCN1 : 2 HCN2 : 1 HCN3). Curiously, more similar stoichiometry patterns of HCN isoforms were exhibited in the liver (27 HCN4 : 3 HCN3 : 2 HCN2 : 1 HCN1), kidney (24 HCN4 : 2 HCN3 : 1 HCN2 : 1 HCN1) and pituitary (15 HCN4 : 2 HCN2 : 1 HCN1 : 1 HCN3). Much *et al*. (2003) depicted overlapping expression in plasma membrane for isoforms HCN1/HCN2, HCN1/HCN3, HCN1/HCN4, HCN2/HCN4 and HCN3/HCN4 in HEK239 cells, and demonstrated that HCN3 does not form functional channels with HCN2. Whether the properties of HCN channels depend on the specific subunit composition was also investigated in other models, such as rabbit sinoatrial node (Altomare *et al.*, 2003), Xenopus oocytes (Ulens and Tytgat, 2001) and human atrial myocytes (Michels *et al*., 2005). These studies revealed that the isoform combination is tissue specific, although all possible combinations of at least two different HCN isoforms could be found, that are differently modulated by cyclic nucleotides and accessory proteins.

Analysis of HCN subcellular distribution revealed that the differential localization within specific neurons and subcellular compartments is dependent on cell type (Robinson and Siegelbaum, 2003; Herrmann *et al*., 2007). In this study differential extraction of proteins from tissue lysates was successfully applied to show the membrane and cytosolic localization of immunoreactive bands by applying antibodies targeted to specific epitopes of HCN1-4 (Fig. III.3). Surprisingly, not only immunopositive bands corresponding to full-length polypeptide chains of all isoforms were observed at the membrane, but also small polypeptide chain fragments have been detected in this subcellular fraction. Major 20-40 kDa immunoreactive bands were unequivocally noticed in membrane extracts of brain by specific antibodies against HCN2-4 isoforms (Fig. III.3b). Actually, all antibodies produced immunoreactive bands in a wide range of kDa regions (from 20 to 120 kDa) (Figs. III.2 and III.3, Table III.1). Accordingly, a disparity of MW for HCN isoforms (60 -160 kDa) has been obtained by other authors with samples from different sources (Altomare *et al*., 2003; Much *et al*., 2003; Whitaker *et al*., 2007; Ye and Nerbonne, 2009; Hegle *et al*., 2010; Cho *et al.*, 2011; He *et al*., 2012; Kretschmannova *et al*., 2012; Xue *et al.*, 2012). We got important information concerning the relative proportion of full-length and

fragmented polypeptide chains for each HCN isoform and tissue. HCN2 and HCN4 were mostly detected as immunoreactive bands of full-length chains and protein fragments, respectively. Cleavage of HCN isoforms appeared to be more prominent in non-excitable tissues than in excitable tissues, although the relative proportion of full-length and fragmented polypeptide chains did not exceed 40% in brain and heart. Our data do not exclude the possibility that technical limitations contributed to the discrepancies between experimentally determined MW and those based on sequence analysis. On the contrary, evidence that proteolysis and glycosylation of HCN isoforms occur *in vivo* is supported by the fact that in mouse heart lysates the HCN2 fragment with 60 kDa is not a product of degradation of the extract preparation (Ye and Nerbonne, 2009) and glycosylated HCN1 and HCN2 being predominant in brain (Much *et al*., 2003). Moreover, inhibition of N-linked glycosylation or HCN2 mutation in the glycosylation site prevent surface membrane expression, suggesting that glycosylation is required for cell surface trafficking of HCN channels (Much *et al*., 2003). Independently of the precise mechanism responsible for the fragmentation of HCN proteins, our data are indicative of specific cleavage of HCN isoforms being physiologically meaningful.

The schematic diagram of HCN1-4 isoforms shown in Figure III.4 proposes a model in which the data can be explained if one considers that the glycosylated and non-glycosylated configurations of HCN isoforms are substrates of membrane bound metalloendopeptidases. They exhibit consensus sequences at polypeptide chain regions with high probability of being processed by proteases (Fig. III.1). Interestingly, the putative cleavage sites generating fragments of MW close to the experimentally determined values were positioned in specific regions (between the oligomerization and voltage-sensor domains, as well as between the ion conducting pore and the cyclic nucleotide binding domains) in all HCN isoforms. Additional cleavage sites were predicted to be localized nearby the C-terminal of HCN1, HCN3 and HCN4, whereas HCN4 also appears to be cleaved at the N-terminal. The hypothesis of whether removal of specific regions of the polypeptide chain of HCN isoforms is an important event in the regulation of HCN channel properties has been analysed by different approaches in several experimental models.

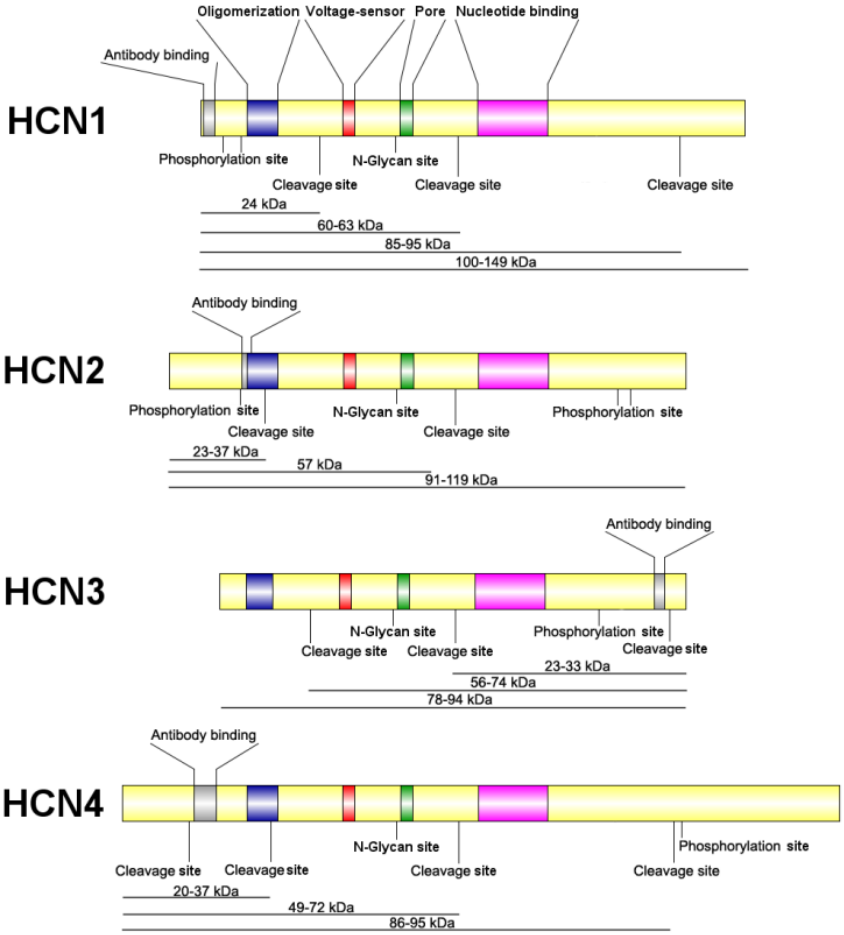

Figure III.4: Schematic diagram of HCN1-4 isoforms.

The schematic diagrams of HCN isoforms were constructed using Domain Graph (DOG version 2.0) software. Oligomerization, voltage-sensor, pore and nucleotide binding regions, as well as specific functional sites (phosphorylation, cleavage and N-glycosylation) are assigned according to the annotations provided in UniProt (Q9JKB0 for HCN1_RAT, Q9JKA9 for HCN2_RAT, Q9JKA8 for HCN3_RAT and Q9JKA7 for HCN4_RAT). The location of the epitopes recognized by specific anti-bodies against HCN1-4 is also provided. The diagrams are annotated in order to illustrate the polypeptide chain regions that correspond to the observed MW immunopositive bands of full-length and proteolytic fragments.

The N-terminal of HCN1 and HCN2 are essential for expression on the cell surface of homo and heteromeric channels and for interaction between subunits (Proenza *et al.,* 2002). Removal or mutation at highly conserved residues of C-terminal containing the cyclic nucleotide binding domain of HCN2 disrupt channel trafficking and expression of functional homomeric channels but heteromeric complexes with

HCN4 can still function (Ye and Nerbonne, 2009). Moreover, the properties of the heteromultimeric channels (midpoint of activation, speed of activation and voltage shift in response to cAMP) seem to be differently affected by the composition in isoforms (Ulens and Tytgat, 2001; Altomare *et al*., 2003; Michels *et al*., 2005; Whitaker *et al*., 2007). The above mentioned studies provided evidence that selective cleavage of isoforms can modify the structure of HCN channels, which could modify their functional properties. Here we predict that membrane bound metalloendopeptidases, by assuring selective proteolysis, can contribute to regulation of HCN channels. Endothelin-converting enzyme 1 (EC 3.4.24.71) is a membrane bound metalloendopeptidase, ubiquitously distributed in mammalian tissues, which contains PROSITE PS00142 (Fig. III.1). This metalloendopeptidase is highly expressed in the analysed tissues (Turner and Tanzawa, 1997). The metalloendopeptidases nardilysin convertase isoform 1 (EC 3.4.24.61) attenuates mK44-dependent current in mouse fibroblasts and modifies the plasma membrane expression of mK44 and its response to intracellular Ca^{2+} in human myometrial smooth muscle cells (Korovkina *et al.,* 2009). The regulation of ion channel activity, targeting and expression by membrane bound endopeptidases is poorly understood. Our results prompt further studies to clarify the role of these enzymes in the regulatory mechanisms of ion channel function.

In conclusion, differential expression of HCN isoforms in different tissues was shown, contributing to understanding the expression pattern of the HCN isoforms in mammalian tissues. Moreover, we postulate that proteolysis may regulate the function of HCN channels. The widespread expression of HCN channels with heterogeneous isoform distribution and eventually proteolytic regulation are particularly relevant for future strategies exploring the potential of HCN channels for therapeutic intervention (Postea and Biel, 2011). Therefore, it is important to generate antibodies with epitopes scattered throughout the entire sequence of HCN isoforms in order to determine the physiological relevance of *in vivo* proteolytic processing for HCN function.

6 References

Accili EA, Proenza C, Baruscotti M, DiFrancesco D (2002). From funny current to HCN channels: 20 years of excitation. *News Physiol Sci* 17:32-37.

Altomare C, Terragnim B, Brioschi C, Milanesi R, Pagliuca C, Viscomi C, Moroni A, Baruscotti M, DiFrancesco D (2003). Heteromeric HCN1-HCN4 channels: a comparison with native pacemaker channels from the rabbit sinoatrial node. *J Physiol* 549:347-359.

Aponte Y, Lien CC, Reisinger E, Jonas P (2006). Hyperpolarization-activated cation channels in fast-spiking interneurons of rat hippocampus. *J Physiol* 574:229-243.

Biel M, Wahl-Schott C, Michalakis S, Zong X (2009). Hyperpolarization-activated cation channels: from genes to function. *Physiol Rev* 89:847-885.

Brown HF, DiFrancesco D, Noble SJ (1979). How does adrenaline accelerate the heart? *Nature* 280:235-236.

Cho HJ, Furness JB, Jennings EA (2011). Postnatal maturation of the hyperpolarization-activated cation current, I(h), in trigeminal sensory neurons. *J Neurophysiol* 106:2045-2056.

El-Kholy W, MacDonald PE, Fox JM, Bhattacharjee A, Xue T, Gao X, Zhang Y, Stieber J, Li RA, Tsushima RG, Wheeler MB (2007). Hyperpolarization-activated cyclic nucleotide-gated channels in pancreatic beta-cells. *Mol Endocrinol* 21:753-764.

Greener ID, Monfredi O, Inada S, Chandler NJ, Tellez JO, Atkinson A, Taube MA, Billeter R, Anderson RH, Efimov IR, Molenaar P, Sigg DC, Sharma V, Boyett MR,

Dobrzynski H (2011). Molecular architecture of the human specialised atrioventricular conduction axis. *J Mol Cell Cardiol* 50:642-651.

He P, Deng J, Zhong X, Zhou Z, Song B, Li L (2012). Identification of a hyperpolarization-activated cyclic nucleotide-gated channel and its subtypes in the urinary bladder of the rat. *Urology* 79:1411e7-13.

Hegle AP, Nazzari H, Roth A, Angoli D, Accili EA (2010). Evolutionary emergence of N-glycosylation as a variable promoter of HCN channel surface expression. *Am J Physiol Cell Physiol* 298:C1066-C1076.

Herrmann S, Stieber J, Ludwig A (2007). Pathophysiology of HCN channels. *Pflugers Arch* 454:517-522.

Horton P, Nakai K (1997). Better prediction of protein cellular localization sites with the k nearest neighbors classifier. *Proc Int Conf Intell Syst Mol Biol* 5:147-152.

Horwitz GC, Lelli A, Géléoc GS, Holt JR (2010). HCN channels are not required for mechanotransduction in sensory hair cells of the mouse inner ear. *PLoS One* 5:e8627.

Hurtado R, Bub G, Herzlinger D (2010). The pelvis-kidney junction contains HCN3, a hyperpolarization-activated cation channel that triggers ureter peristalsis. *Kidney Int* 77:500-508.

Kaupp UB, Seifert R (2001). Molecular diversity of pacemaker ion channels. *Annu Rev Physiol* 63:235-257.

Kretschmannova K, Kucka M, Gonzalez-Iglesias AE, Stojilkovic SS (2012). The expression and role of hyperpolarization-activated and cyclic nucleotide-gated channels in endocrine anterior pituitary cells. *Mol Endocrinol* 26:153-164.

Korovkina VP, Stamnes SJ, Brainard AM, England SK (2009). Nardilysin convertase regulates the function of the maxi-K channel isoform mK44 in human myometrium. *Am J Physiol Cell Physiol* 296:C433-C440.

Lewis AS, Estep CM, Chetkovich DM (2010). The fast and slow ups and downs of HCN channel regulation. *Channels* 4:215-31.

Marionneau C, Couette B, Liu J, Li H, Mangoni ME, Nargeot J, Lei M, Escande D, Demolombe S (2005). Specific pattern of ionic channel gene expression associated with pacemaker activity in the mouse heart. *J Physiol* 562:223-234.

Michels G, Er F, Khan I, Südkamp M, Herzig S, Hoppe UC (2005). Single-channel properties support a potential contribution of hyperpolarization-activated cyclic nucleotide-gated channels and If to cardiac arrhythmias. *Circulation* 111:399-404.

Monteggia LM, Eisch AJ, Tang MD, Kaczmarek LK, Nestler EJ (2000). Cloning and localization of the hyperpolarization-activated cyclic nucleotide-gated channel family in rat brain. *Brain Res Mol Brain Res* 81:129-139.

Much B, Wahl-Schott C, Zong X, Schneider A, Baumann L, Moosmang S, Ludwig A, Biel M (2003). Role of subunit heteromerization and N-linked glycosylation in the formation of functional hyperpolarization-activated cyclic nucleotide-gated channels. *J Biol Chem* 278:43781-43786.

Poller WC, Bernard R, Derst C, Weiss T, Madai VI, Veh RW (2011). Lateral habenular neurons projecting to reward-processing monoaminergic nuclei express hyperpolarization-activated cyclic nucleotid-gated cation channels*. Neuroscience* 193:205-216.

Postea O, Biel M (2011). Exploring HCN channels as novel drug targets. *Nat Rev Drug Discov* 10:903-914.

Proenza C, Tran N, Angoli D, Zahynacz K, Balcar P, Accili EA (2002). Different roles for the cyclic nucleotide binding domain and amino terminus in assembly and expression of hyperpolarization-activated, cyclic nucleotide-gated channels. *J Biol Chem* 277:29634-29642.

Robinson RB, Siegelbaum SA (2003). Hyperpolarization-activated cation currents: from molecules to physiological function. *Annu Rev Physiol* 65:453-480.

Santoro B, Liu DT, Yao H, Bartsch D, Kandel ER, Siegelbaum SA, Tibbs GR (1998). Identification of a gene encoding a hyperpolarization-activated pacemaker channel of brain. *Cell* 93:717-729.

Schechter I, Berger A (1968). On the active site of proteases. 3. Mapping the active site of papain; specific peptide inhibitors of papain. *Biochem Biophys Res Commun* 32:898-902.

Turner AJ, Tanzawa K (1997). Mammalian membrane metallopeptidases: NEP, ECE, KELL, and PEX. *FASEB J* 11:355-364.

Ulens C, Tytgat J (2001). Functional heteromerization of HCN1 and HCN2 pacemaker channels. *J Biol Chem* 276:6069-6072.

Varghese A, Tenbroek EM, Coles JJr, Sigg DC (2006). Endogenous channels in HEK cells and potential roles in HCN ionic current measurements. *Prog Biophys Mol Biol* 90:26-37.

Whitaker GM, Angoli D, Nazzari H, Shigemoto R, Accili EA (2007). HCN2 and HCN4 isoforms self-assemble and co-assemble with equal preference to form functional pacemaker channels. *J Biol Chem* 282:22900-22909.

Xue L, Li Y, Han X, Yao L, Yuan J, Qin W, Liu F, Wang H (2012). Investigation of hyperpolarization-activated cyclic nucleotide-gated channels in interstitial cells of Cajal of human bladder. *Urology* 224:e13-18.

Ye B, Nerbonne JM (2009). Proteolytic processing of HCN2 and co-assembly with HCN4 in the generation of cardiac pacemaker channels. *J Biol Chem* 284:25553-25559.

Zhong N, Beaumont V, Zucker RS (2004). Calcium influx through HCN channels does not contribute to cAMP-enhanced transmission. *J Neurophysiol* 92:644-647.

Chapter IV - HCN channels and cAMP-dependent modulation of fusion pore diameter in cultured pituitary lactotrophs

NOTE: The results in this chapter are in preparation for publication as: Calejo A.I., Jorgačevski J, Pereira P.M., Santos M.A.S., Potokar M., Vardjan N., Kreft M., Gonçalves P.P., Zorec R. HCN channels and cAMP-dependent modulation of fusion pore diameter in cultured pituitary lactotrophs.

1 Abstract

Hormones and neurotransmitters are released from vesicles by passing through a fusion pore that forms upon the merger between the vesicle and the plasma membranes. Once formed the fusion pore can either fully expand leading to the release of the entire vesicle content (full-fusion exocytosis), or reversibly close, retaining vesicle integrity and at least to a certain extent also the residual cargo (transient exocytosis). It was shown recently that the second messenger cAMP stimulates exocytosis by increasing the occurrence of transient exocytotic events and by promoting wider fusion pores with longer dwell-times. However the mechanism by which these effects occur are not yet clear. Since cAMP also modulates ion channels, including the hyperpolarization-activated cyclic nucleotide-gated channels (HCN), by facilitating their activation and that these channels have been considered to be present in pituitary lactotrophs, we here asked whether these channels may play a role in the properties of exocytosis directly. By using immunocytochemistry in combination with confocal microscopy we show here the presence of HCN channels in the plasma membrane and in the secretory vesicles containing prolactin (PRL). Moreover, we recorded unitary transient and full-fusion exocytic events by monitoring discrete increases in membrane capacitance (C_m) in cell-attached patches of lactotrophs with overexpressed HCN channels or incubated with ZD7288, a HCN channel blocker and in the presence/absence of dbcAMP, a membrane permeable analogue of cAMP. These treatments affected the occurrence of both transient and full fusions exocytic events. Moreover, the results show that HCN channels modulate the fusion pore properties directly. Therefore, we propose that the modulation of fusion pore by HCN channels indicates a role of the cation flux as a regulator of exocytosis.

Key words: lactotrophs, HCN channels, exocytosis, fusion pore, patch-clamp, cAMP

2 Introduction

Communication between cells is of key importance for multicellular organisms and secretory vesicles, which contain signalling molecules, play a vital role in this process (Jorgačevski *et al.,* 2012). When vesicles are formed, they are trafficked to the plasma membrane (Potokar *et al*., 2011), where they dock, get primed and finally their membrane merges with the plasma membrane. The transition from non-fused vesicle to fully fused vesicle proceeds through several stages; first the outer membrane leaflets merge (hemi-fusion), then the merger of inner membrane leaflets gives rise to a narrow channel, which connects the vesicle lumen and the cell exterior (i.e. the fusion pore) and finally the expansion of the fusion pore results in the complete collapse of the vesicle membrane with the plasma membrane (full-fusion) (Chernomordik and Kozlov, 2008). However, not all vesicles complete all these transitions at once. Some vesicles are engaged in the so called transient exocytosis stage, where a fusion pore opens and closes for minutes before completely merging with the plasma membrane (Vardjan *et al*., 2007; Jorgačevski *et al*., 2008, 2010). Fusion pore formation is promoted by membrane associated soluble N-ethylmaleimide-sensitive factor attachment protein receptors (SNAREs), that besides interacting with each other also bind to other proteins (e.g. Munc18-1) (reviewed in Vardjan *et al.,* 2013). The fusion pore conductance (diameter) of the same vesicle engaged in repetitive transient exocytic events is relatively constant (Jorgačevski *et al.,* 2010). This led to the conclusion that the fusion pore formed during transient exocytosis represents a relatively stable state with a preferred narrow equilibrium diameter, which depends on the vesicle diameter (Jorgačevski *et al*., 2010). Recent findings indicated, that the relationship between fusion pore diameter and vesicle diameter in transient exocytic events can be affected by introducing specific mutants of the proteins which have been shown to play a role in exocytosis (Jorgačevski *et al*., 2011), by electrostatic interactions (p.119) and possibly by changing lipid composition (Rituper *et al*., 2012). In addition, Miklavc *et al*. (2011) showed another intriguing possibility for the fusion pore regulation in pneumocytes by Ca^{2+} entry into the

vesicle through the fusion pore and then through vesicular channels into the cytoplasm.

We have recently shown that cAMP has a biphasic modulatory role on the release of PRL from anterior pituitary lactotrophs. (pp. 21). However, the exact mechanism(s) of how cAMP elicits changes on PRL release, has not yet been determined. It is well documented that cAMP can affect exocytosis by acting through: i) protein kinase A (PKA) dependent mechanism, ii) via the exchange protein directly activated by cAMP (Epac) and iii) by activating hyperpolarization-activated and cyclic nucleotide-gated (HCN) channels (Seino and Shibasaki, 2005). Cyclic AMP directly facilitates HCN channels activation by shifting activation curve to more positive voltages and thus speeds up channel opening, which results in a flux of Na^+, K^+ and Ca^{2+}. HCN channel specific current (hyperpolarization-activated cation current) is present in most neuroendocrine cells, including lactotrophs (Gonzalez-Iglesias *et al*., 2006b; Stojilkovic *et al*., 2010). HCN channels are arranged in a homo- or hetero-tetrameric configuration, depending on the presence of four known isoforms (HCN1, 2, 3 and 4) in a single channel. HCN channels were first reported in the rabbit cardiac sinoatrial node (Brown *et al.,* 1979), but are not confined to the heart. They are present in different cell types throughout the body and were found also in the brain where HCN2 isoform is the most ubiquitous (Kretschmannova *et al.,* 2012). Most HCN channel isoforms are expressed also in pituitary gland cell populations, and among them HCN2 mRNA transcript is the most abundantly expressed (Kretschmannova *et al.,* 2012). There are at least six different cell types in the pituitary gland (reviewed in Stojilkovic *et al.,* 2010), but we focused our attention to the presence of HCN channels in lactotrophs, and more specifically in PRL-containing vesicles.

To address the question whether HCN channels regulate exocytosis of neuroendocrine cells, we used rat pituitary lactotrophs, which have proved to be an excellent model to study exocytosis (Vardjan *et al*., 2007; Jorgačevski *et al*., 2008, 2010). We report here that HCN2 isoform is localized in the plasma membrane and in PRL-containing vesicles in single isolated pituitary lactotrophs. By using cell-attached patch clamp technique to monitor unitary exocytic events we demonstrate that HCN2 channels directly modulate exocytosis.

3 Materials and Methods

3.1 Cell cultures

Male Wistar rats were euthanized according to the International Guiding Principles for Biomedical Research Involving Animals developed by the Council for International Organizations of Medical Sciences and the Directive on Conditions for Issue of License for Animal Experiments for Scientific Research Purposes (Official Gazette of the Republic of Slovenia 40/85 and 22/87). The procedures using animals were approved by the Veterinary Administration of the Republic of Slovenia. Lactotrophs were isolated according to the previously described method (Ben-Tabou *et al.,* 1994). After isolation, lactotrophs were platted on poly-L-lysine coated glass coverslips and kept in high-glucose Dulbecco's modified Eagle's medium (Invitrogen) with 10% newborn calf serum and L-glutamine at 37 ºC with 95% humidity and 5% CO2.

3.2 Western-blot

Total lysates of pituitary were collected by using RIPA buffer supplemented with protease inhibitor cocktail (Roche). Proteins were loaded in 4–15% SDS-PAGE gel and transferred to a polyvinylidene fluoride membrane (PVDF, Amersham Biosciences, UK) for 1 hour at 100 V and 4 °C. Membranes were incubated with polyclonal rabbit anti-HCN2 antibodies (1:200, Alamone, Israel) in 5% non-fat milk/TBS-T 0.1% overnight at 4 ºC with constant agitation. Afterwards they were washed and incubated with secondary antibodies Irdye680 Red anti-rabbit IgG (1:10 000, Odyssey) in 5% non-fat milk/TBS-T 0.1% and washed again in TBS. Tubulin was used as control, membranes were incubated in 5% non-fat milk/TBS-T 0.1% with monoclonal rabbit anti-tubulin (1:500, Abcam) overnight at 4 ° C. Membranes were scanned for fluorescence emission at 700 nm, by using an Odyssey infrared imaging system (Li-Cor Biosciences, Lincoln, NE) and analyzed with the software of the afore mentioned system.

3.3 Real-time PCR

Freshly isolated lactotrophs were incubated at 37 ºC for 12 h, frozen in liquid N_2 and stored at -80 ºC. Total RNA and genomic DNA (gDNA) were extracted from lactotroph cultures using AllPrep DNA/RNA/Protein Mini Kit (QIAGEN), according to the manufacture's protocol. By using SuperScript IITM RT enzyme (Invitrogen), 2 µg of total RNA was reversely transcribed to complementary DNA (cDNA). We used Platinum®SYBR®Green qPCR Super-Mix-UDG (Invitrogen), according to the manufacturer's instructions. Primers were chosen according to previously published data (El-Kholy *et al*., 2007; p. 59): HCN2 the forward primer was GGGAATCGACTCCGAGGTCTAC and reverse primer AGACTGAGGATCTTGGTGAAACG, while for β-actin the forward primer was TAGCCATCCAGGCTGTGTTG and reverse primer GGAGCGCGTAACCCTCATAG. We used the detection system, ABI Prism® 7000 Sequence Detection System (Applied Biosystems) running Sequence Detection System, software Version 1.1 (Applied Biosystems) cycling condition were set according to the manufacturer instructions: 1 cycle at 50 ºC for 2 min, 1 cycle at 95 ºC for 2 min and 40 cycles at 95 ºC for 15 seconds plus 60 ºC for 30 seconds. Quantity of HCN2 and β-actin was calculated based on standard curves produced from gDNA and relative HCN2 channel transcript abundance was determined for a specific amount of total RNA using β-actin as normalization control.

3.4 Immunocytochemistry and confocal microscopy

For immunocytochemistry cells were fixed (4% formaldehyde, 15 min, RT) and permeabilized (0.1% Triton X-100, 10 min, RT). To reduce non-specific binding of antibodies, cells were incubated in 3% bovine serum albumin (BSA) and 10% goat serum in PBS (1 h, 37 °C). Afterwards, cells were labelled first with primary mouse polyclonal anti-HCN2 or rabbit polyclonal anti-PRL antibodies (1:50, Abcam and 1:40, Chemicon, respectively) and then with secondary antibodies conjugated to Alexa Fluor® 488 or Alexa Fluor® 546 (1:600, 45 min, 37 °C, Invitrogen). The plasma membrane was labelled prior fixation (2% formaldehyde, 10 min, RT) with 5% Vybrant® DiD (4 min, 37 °C, Invitrogen).

Immunolabeled cells were recorded with the inverted confocal microscope (Zeiss LSM 510, Jena, Germany) equipped with an oil-immersion Plan-Apochromatic objective (63×, numerical aperture 1.4). For excitation of Alexa Fluor® 488 Ar-ion laser were used in combination with band-pass emission filter (505–530 nm) and for excitation of Alexa Fluor®543 He-Ne laser was used in combination with long-pass emission filter (cutoff below 560 nm). He-Ne laser with 633 nm was used for excitation of Vybrant DiD in combination with long-pass emission filter with the cutoff below 650 nm. The colocalization was analyzed by using ColocAna software (Celica, Slovenia) by taking into account colocalized pixels above the threshold of 25% of maximum green and red fluorescence intensities. The mean fluorescence was determined for the whole cell and for the plasma membrane and cell interior separately, by using custom software written for MATLAB (Math Works, Natick, MA, USA). Images of cells were separated into the cell interior and the cell periphery (plasma membrane) by manually delimiting the perimeter of the cells. The mean fluorescence intensity was then automatically calculated for the rim (plasma membrane ± 0.35 µm, which is the average diameter of PRL-containing vesicles, Zorec *et al*., 1991; Angleson *et al*., 1999) and in the region positioned centrally to the rim (see Fig. IV.2).

3.5 Transfection

24h after the isolation, lactotrophs were co-transfected with plasmids DNA encoding HCN2 channel isoform (Vacarri *et al*., 1999) and plasmid DNA encoding enhanced green florescence protein (EGFP). Transfection reagent Lipofectamine® (Invitrogen) was applied, according to the manufacturer's guidelines. Electrophysiological recordings were performed on EGFP-positive cells only.

3.6 Electrophysiology

Cell-attached capacitance measurements were performed with a dual-phase lock-in patch-clamp amplifier (1591 Hz; SWAM IIC, Celica, Ljubljana, Slovenia). A sine wave (111 mV r.m.s voltage) was applied to the pipette, the pipette potential was held at 0 mV and the glass micropipettes constructed as

described previously (Vardjan *et al.,* 2007, Jorgačevski *et al.,* 2010). We used fire polished pipettes, heavily coated with Sylgard and with resistance of 3–6 MΩ. The bath and pipettes contained extracellular solution, which consisted of 10 mM HEPES/NaOH (pH 7.2), 10 mM D-glucose, 130 mM NaCl, 8 mM $CaCl_2$, 1 mM $MgCl_2$, and 5 mM KCl with or without 100 µM 4-Ethylphenylamino-1,2-dimethyl-6-methylaminopyrimidinium chloride (ZD7288). After recording for several minutes cells were stimulated with 10 mM N^6,2'-O-dibutyryl adenosine-3′,5′-cyclic monophosphate (cAMP). During experiments phase angle was adjusted to nullify the changes in the real (Re) trace in response to the manually generated 10 fF calibration pulses. Vesicle capacitance (C_v) and fusion pore conductance (G_p) were calculated from the imaginary (Im) and real (Re) part of the admittance traces as reported previously (Lollike and Lindau, 1999): $C_v=[(Re^2 + Im^2)/Im]/\omega$, where ω is the angular frequency ($\omega=2\pi f$, f is the sine-wave frequency, 1591 Hz) and $G_p=(Re^2 + Im^2)/Re$. Fusion pore radius was estimated by using the equation $G_p=(\pi r^2)/(\rho\lambda)$, where r represents fusion pore radius, ρ the estimated resistivity of the saline (100 Ωcm), and λ the estimated length of a gap junction channel (15 nm) (Spruce *et al*., 1990). Vesicle diameter was calculated by using specific membrane capacitance (c_m) of 8 fF/µm^{-2}. We used custom-made software (CellAn, Celica, Slovenia) written for MATLAB (Math Works, Natick, MA, USA) to analyse unitary exocytic events.

3.7 Data Analysis

All statistics were performed with Sigma Plot. All results are presented as mean ± standard error of the mean (s.e.m.). Statistical significance was evaluated by using Student's t-test for normally distributed data and Man-Whitney test for non-normally distributed data, considering $P < 0.05$ (*), $P < 0.01$ (**) and $P < 0.001$ (***).

3.8 Chemicals

ZD7288 was obtained from Tocris (Ellisville, MO). All other chemicals were purchased from Sigma-Aldrich, unless stated otherwise.

4 Results

Our previous results show that increased intracellular cAMP significantly affects exocytosis in cultured pituitary lactotrophs by increasing the occurrence of transient exocytic events and by stabilizing the transient fusion pore with increased diameter and prolonged dwell-time (p. 21). In different cell types cAMP affects exocytosis by utilizing different signalling pathways (reviewed in Seino and Shibasaki, 2005). One of these pathways involves activation of the hyperpolarization cyclic nucleotide activated (HCN) channels. The presence of HCN channel specific currents indicates that these channels reside in lactotrophs (Gonzalez-Iglesias *et al.,* 2006b; reviewed in Stojilkovic *et al.,* 2012), though this has not been confirmed. Therefore, our goal was first to study the presence and sub-cellular localization of HCN channels in pituitary lactotrophs and then to determine the possible effects of HCN channels on exocytosis. The latter was achieved by monitoring the properties of unitary exocytic events in lactotrophs where the presence of HCN channels was either enhanced by overexpression or blocked by pharmacological agents.

4.1 HCN2 isoform is present in lactotrophs

To assess if HCN2 isoform is expressed in anterior pituitary lactotrophs we used three different techniques. First, we used the Western blot technique to confirm the presence of HCN2 in the pituitary gland (Fig. IV.1a). In pituitary gland lysate we detected a weak, but distinctive band with previously described molecular weight of 95 kDa (pp. 59). Because of the weakly present HCN2 band on Western blot gel, we next performed quantitative real time PCR (qRT-PCR) specifically from lactotroph lysates (Fig. IV.1b). We collected cell lysates from >95% pure primary lactotroph culture, as determined by labelling the cells with antibodies against PRL (Fig. IV.1ci) and counting the fluorescent cells in three different isolations. For qRT-PCR we used specific primers (see Materials and Methods). We confirmed the presence of HCN2 mRNA in lactotrophs.

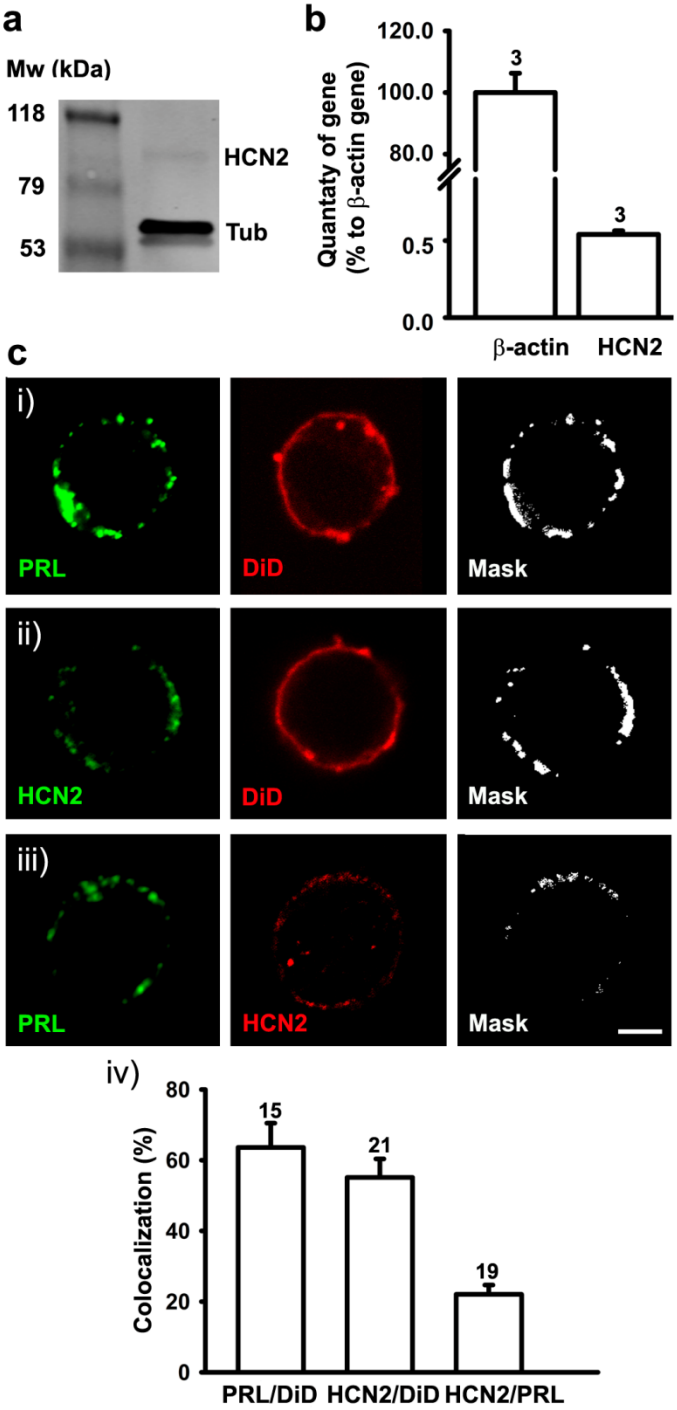

Figure IV.1: HCN2 isoform is present in the plasma membrane and in vesicles of pituitary lactotrophs.

(a) Western Blot of the lysate of the whole pituitary gland showing a weak band corresponding to HCN2 isoform and a stronger band corresponding to tubulin. **(b)** In isolated lactotrophs, quantitative real time PCR (qRT-PCR) revealed that the relative expression of HCN2 mRNA in comparison to β-actin mRNA is 0.54 ± 0.02%. **(c) (i)** Representative confocal image of a lactotroph, which was exposed to the plasma membrane marker Vybrant® DiD (DiD), fixed and labelled with anti-prolactin antibodies

(PRL). The mask shows the co-localization between PRL and DiD. **(ii)** Representative confocal image of a lactotroph, which was exposed to DiD, fixed and labelled with anti-HCN2 antibodies (HCN2). The mask shows the co-localization between HCN2 and DiD. **(iii)** Representative confocal image of a fixed lactotroph, labelled with anti-HCN2 antibodies (HCN2) and with anti-prolactin antibodies (PRL). The mask shows the co-localization between HCN2 and PRL. Scale bar = 3 µm. **(iv)** The average co-localization of DiD and PRL was 64 ± 7% (co-localized pixels vs. PRL fluorescence pixels), the co-localization of DiD and HCN2 fluorescence was 55 ± 5% (co-localized pixels vs. HCN2 fluorescence pixels) and the co-localization of PRL and HCN2 fluorescence was 22 ± 3% (co-localized pixels vs. HCN2 fluorescence pixels). Values are means ± s.e.m.

HCN2 mRNA transcripts in pituitary lactotrophs were 0.5% when compared to the quantity of mRNA of the housekeeping gene, β-actin (Fig. IV.1b). Since the amount of mRNA transcripts of HCN2 does not necessarily reflect the amount of HCN2 expressed proteins and the purity of the primary lactotroph culture is never 100%, we used immunocytochemical labelling of cultured lactotrophs in combination with confocal microscopy. This technique is suitable to quantify the amount HCN2 isoform in single lactotrophs and, due to its resolution, also the sub-cellular localization of HCN2 isoform (Fig. IV.1c). By using specific primary antibodies against PRL in combination with fluorescent secondary antibodies we first assessed the proportion of PRL containing vesicles near the plasma membrane (Fig. IV.1ci). The co-localization of PRL with the plasma membrane dye Vybrant® DID (DiD) fluorescent signals was 61 ± 5%, suggesting that a large proportion of PRL-containing vesicles are located near the plasma membrane (Fig. IV.1civ), consistent with previous report (Jorgačevski *et al*., 2010). Our next step was to determine the distribution of HCN2 isoform. Since HCN channels are normally expressed in the plasma membrane, we immunolabeled HCN2 in combination with the plasma membrane (Vybrant® DID; Fig. IV.1cii). The co-localization of HCN2 with the plasma membrane fluorescent signals was 55 ± 5%, suggesting that only half of the channels containing HCN2 isoform are located in the plasma membrane. One of the possible locations for the remaining HCN channels in the cytoplasm (p. 59) are vesicular membranes, as in neurons (Noam *et al*., 2010). To check whether HCN2 channels are co-localized with PRL-containing vesicles, we immunolabeled lactotrophs with antibodies against HCN2 and PRL (Fig. IV.1ciii). The average co-localization of the fluorescence signals of

these two markers was 22 ± 3% (Fig. IV.1civ). This confirms that HCN2 isoforms are also localized in the membrane of PRL-containing vesicles. To summarize, our results show that HCN channels containing isoform 2 are expressed in anterior pituitary lactotrophs and are localized both, in the vesicle and in the plasma membranes.

4.2 The expression of HCN2 channels in lactotrophs can be augmented

We next explored the possibility to augment the expression of HCN2 isoform in lactotrophs. To accomplish this we transfected lactotrophs with plasmid DNA (pDNA) encoding HCN channels isoform 2. This approach has been successfully applied to lactotrophs with other plasmids (Jorgačevski *et al.,* 2011). Co-transfection was performed using equal amounts of pDNA encoding HCN2 and pEGFP (see Materials and Methods). Expression of EGFP was used to identify successfully transfected cells. To determine the rate of augmentation of the HCN2 expression, we immunolabeled non-transfected (control) lactotrophs and lactotrophs 24 h, 48 h and 72 h after transfection, with antibodies against HCN2 isoform (Fig. IV.2a).

The average fluorescence intensity of HCN2, determined in the region of the whole cell, was 0.0026 ± 0.0003 a.u. (n = 11 cells) in controls and significantly increased 24 h after the transfection to 0.0043 ± 0.0003 a.u. (n = 13 cells; P <0.001; Fig. IV.2b). This augmentation was still observed 48 h after transfection, 0.0043 ± 0.0004 a.u. (n = 11 cells; P <0.001, Fig. IV.2b), while 72 h after transfection the average fluorescence decreased below control conditions, to 0.0016 ± 0.0004 a.u. (n = 5 cells; P = 0.1). In order to determine if the observed augmentation of fluorescent signals (after 24 h and 48 h) is occurring proportionally in the plasma membrane and in the cell interior, we performed separate analysis of the fluorescence intensity of the plasma membrane region and of the cell interior region, as shown in the scheme in Fig. IV.2a (below). The results show that the augmentation of HCN2 isoform was similar in both regions, at the plasma membrane and at the PRL-positive structures (P<0.01, compared to

non-transfected lactotrophs). These results confirm that the expression of HCN2 isoforms may be augmented both in the vesicle and in the plasma membranes of single transfected lactotrophs.

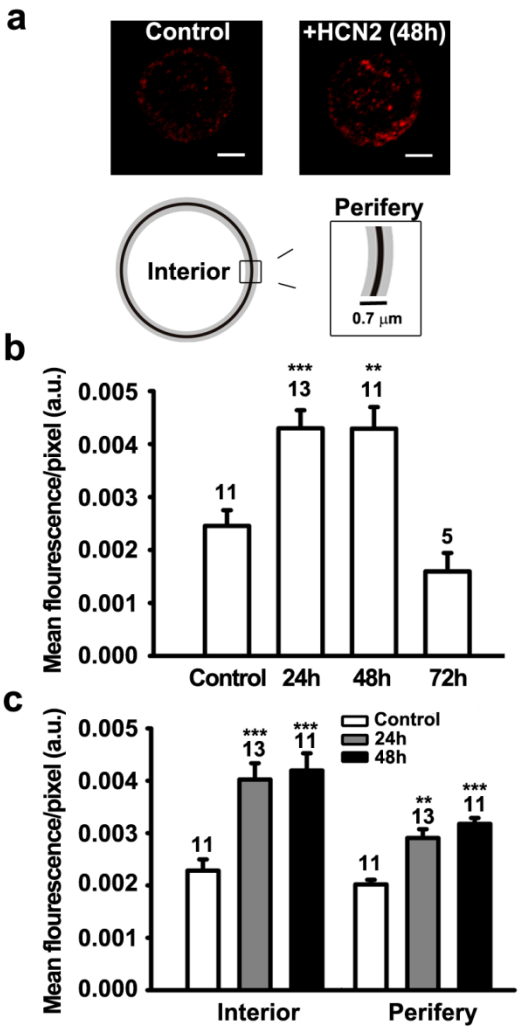

Figure IV.2: Over-expression of HCN2 isoform augments the presence of HCN2 in vesicles and on the plasma membrane of lactotrophs.

(a) Representative confocal images of a non-transfected lactotroph and of a lactotroph 48 h after transfection with pDNA encoding HCN2. Both lactotrophs were fixed and immuno-labelled with anti-HCN2 antibodies. Scale bars = 3 µm. We analysed the intensity of fluorescence, as depicted on the diagram in the lower part of the panel. The fluorescence intensity was separated into two areas; the rim representing the plasma membrane (depicted in grey) and the cell interior, which is located centrally to the afore mentioned rim. The thickness of the rim representing the plasma membrane was 0.7 µm, which corresponds to the average diameter of two lactotroph vesicles (Zorec *et al.,* 1991; Angleson *et al.,* 1999). **(b)** The mean fluorescence, measured in confocal micrographs of fixed HCN2 labelled lactotrophs. The mean fluorescence of HCN2 labelled of lactotrophs transfected with HCN2 plasmids increased from 0.0026 ± 0.0003 a.u. (non-transfected

lactotrophs) to 0.0043 ± 0.0003 a.u (24 h post transfection; P<0.001) and to 0.0043 ± 0.0004 a.u (48 h post transfection; P<0.01), respectively. 72 h post transfection, the mean fluorescence of HCN2 transfected cells decreased to 0.0016 ± 0.0004 a.u. (P=0.1 versus control). **(c)** Separate analysis of the mean fluorescence in the cell interior region and in the plasma membrane region showed that both regions follow similar trend as the average fluorescence of whole cells, analysed in panel b. The mean fluorescence of both regions significantly increased (P<0.01) 24h and 48 h post transfection. Numbers above error bars indicate the number of analysed cells. Values are means ± s.e.m.

4.3 Transient and full fusion exocytic events are present in lactotrophs with augmented HCN2 isoform

We have previously shown that the increase in intracellular cAMP affects exocytosis by stabilizing transient fusion pores with relatively wide fusion pore diameters and with prolonged fusion pore dwell-times (p. 21). To this end, we have demonstrated that HCN channels containing isoform 2 are present in both the vesicle and the plasma membranes and that we can augment the isoform 2. Our next goal was to assess the possible influence of HCN channels on unitary exocytic events. We used cell-attached patch-clamp technique to monitor discrete changes in membrane capacitance (C_m), with sufficient resolution to detect unitary fusions of vesicles with the plasma membrane in HCN2 over-expressed lactotrophs. C_m measurements were performed on EGFP positive (fluorescent) lactotrophs as depicted in Fig. IV.3a. We observed discrete reversible steps in C_m, which are usually attributed to reversible exocytotic events (Vardjan *et al.,* 2007; Jorgačevski *et al.,* 2008; 2010; Fig. IV.3b, marked with 1 and 2) and irreversible upward steps in C_m, most likely representing full-fusion exocytotic events (Vardjan *et al.,* 2007; Jorgačevski *et al.,* 2008; 2010; Fig. IV.3d, marked with 3). Transient exocytotic events, observed in the imaginary trace of admittance signal (Im), were often projected to the real part of the admittance signal (Re). These events indicate the presence of a narrow fusion pore (Lollike and Lindau, 1999; Fig. IV.3b marked with 1) and were used to calculate fusion pore conductance (G_p), which is proportional to the fusion pore diameter (Fig. IV.3c, Lollike and Lindau, 1999, see Materials and Methods). Additionally, we calculated vesicle capacitance (C_v),

which was used to calculate the surface area of vesicles and, by considering that vesicles are spheres, their diameters (see Materials and Methods).

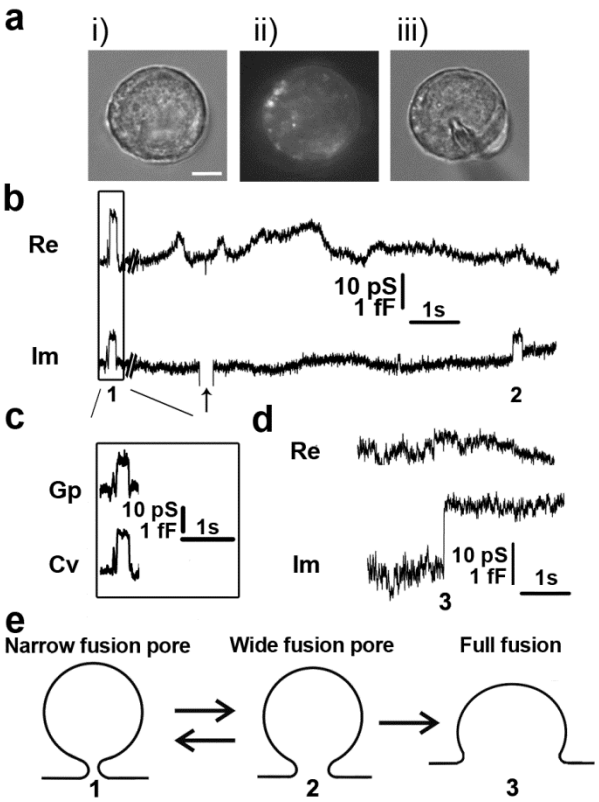

Figure IV.3: Cell-attached C_m measurements on transfected lactotrophs confirm the presence of transient and full-fusion exocytic events.

(a) Lactotrophs co-transfected with HCN2 pDNA and EGFP pDNA were used for the C_m measurements in the cell-attached configuration. All measurements were performed only on lactotrophs exhibiting EGFP fluorescence, as shown for the same cell under transmitted light **(i)**, under epi-fluorescence **(ii)** and during the measurement **(iii)**. Scale bar = 3 µm. **(b)** An epoch from the representative recording, showing reversible steps in the imaginary part of the admittance trace (Im). Reversible events in Im, which likely represent transient exocytic events, either exhibited projections (1) to the real part of the admittance trace (Re) or not (2). Arrows point to the calibration pulse in Im, which were triggered manually to assure the correct phase angle settings. **(c)** We calculated vesicle capacitance (C_v) and fusion pore conductance (G_p) for all reversible events with projections (See Materials and Methods for details). **(d)** A representative examples of irreversible up-ward steps in Im trace and the corresponding Re trace (3), which likely denotes full-fusion exocytic event. **(e)** A scheme of the stages a vesicle must pass in order to completely fuse with the plasma membrane; from narrow fusion pore formation (1), to widening of the fusion pore (2) and finally to full-fusion of the vesicle membrane and the plasma membrane (3).

4.4 HCN channels modulate the frequency of exocytic events in lactotrophs

To see whether altered expression of HCN channels modulate the extent of exocytosis, we performed several sets of experiments where we monitored changes in C_m. In the first set of experiments, we performed measurements on lactotrophs expressing only native HCN2 isoform (control), in the second set we performed measurements on lactotrophs expressing native HCN2 isoform and transfected with pEGFP (EGFP), in the third set we performed measurements on lactotrophs co-transfected with pDNA of HCN2 and pEGFP (HCN2) and in the last set we performed measurements on lactotrophs where the activity of HCN channels was blocked with specific inhibitor, 4-Ethylphenylamino-1,2-dimethyl-6-methylaminopyrimidinium chloride (ZD7288). Additionally, the recordings of the latter two conditions were divided into two parts, where in the first part we monitored changes in C_m in normal extracellular solution for ~600 s and then changes in C_m under stimulated conditions, where we added 10 mM N6,2'-O-dibutyryl adenosine-3′,5′-cyclic monophosphate (dbcAMP) for additional ~600 s.

We analysed the occurrence of transient and full-fusion exocytic events by determining the frequency of reversible (Fig. IV.4a) and irreversible (Fig. IV.4b) events. The frequency of reversible and irreversible events in pEGFP transfected lactotrophs was identical to controls, 0.05 ± 0.01 events/s (n = 8) and 0.06 ± 0.01 events/s (n = 16) for reversible events and 0.005 ± 0.001 events/s (n = 8) and 0.005 ± 0.001 events/s (n = 16) for irreversible events, respectively. These results confirm that the expression of EGFP does not affect to a great extent the frequency of unitary exocytic events in lactotrophs. On the other hand, the over-expression of HCN2 isoform significantly decreased the frequency of transient fusion events to 0.02 ± 0.01 events/s (n = 16; $P<0.01$), while after stimulation with cAMP, the frequency of transient fusion events increased and was similar to non-transfected (and non-stimulated) lactotrophs (0.04 ± 0.001 events/s; n = 16 cells; $P<0.05$) (Fig. IV.4c).

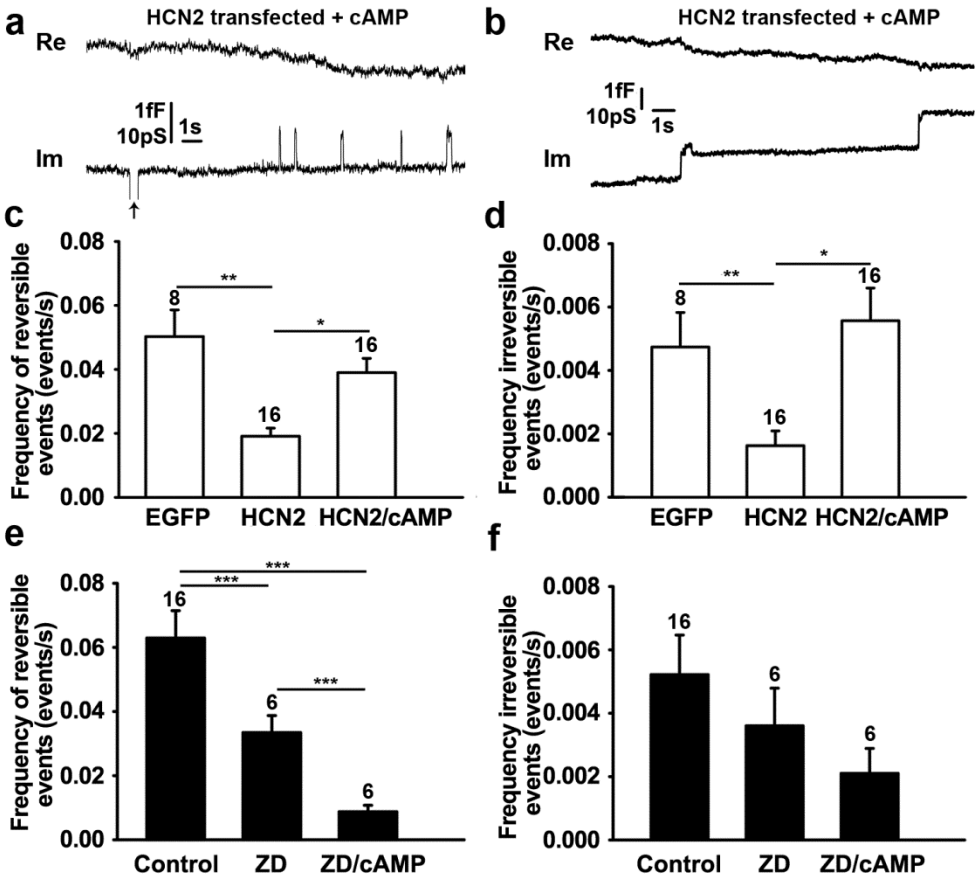

Figure IV.4: HCN2 channel isoform modulates the frequency of exocytotic events in pituitary lactotrophs.

Two epochs of the representative electrophysiological recording, which was made on a lactotroph transfected with pDNA of HCN2 and stimulated with dbcAMP, show reversible **(a)** and irreversible **(b)** events in the imaginary part of the admittance trace (Im). Arrow marks calibration pulse in Im trace, used to adjust the phase of the lock-in amplifier. **(c)** The average frequency of reversible events was 0.05 ± 0.01 events/s in EGFP transfected cells, significantly higher than in HCN2 transfected cells (0.02 ± 0.01 events/s. After the stimulation of HCN2 transfected cells with dbcAMP the average frequency of reversible events increased to 0.04 ± 0.01 events/s. **(d)** The average frequency of irreversible up-ward events in EGFP transfected cells was 0.005 ± 0.001 events/s, significantly more than in HCN2 transfected cells (0.002 ± 0.001 events/s). However, the addition of dbcAMP to the HCN2 transfected cells increased the frequency of irreversible up-ward events to 0.006 ± 0.001 events/s. **(e)** The addition of ZD7288 (blocker of HCN2 channels) decreased the average frequency of reversible events from 0.06 ± 0.01 events/s (controls) to 0.04 ± 0.01 events/s (ZD7288) to 0.01 ± 0.01 events/s (with ZD7288 and cAMP). **(f)** Similar trend was observed in the frequencies of irreversible up-ward events, which were 0.005 ± 0.001 events/s (controls), 0.004 ± 0.001 events/s (ZD7288 treated cells) and 0.002 ± 0.001 events/s (with ZD7288 and cAMP). Values are means ± s.e.m. Numbers above error bars indicate the number of patches. P*<0.05, P**<0.01, P***<0.001.

The increase of frequency of transient exocytic events after stimulation with cAMP in HCN2 transfected lactotrophs is in line with the cAMP-stimulated effects recorded in non-transfected lactotrophs (p. 21). However, in the afore-mentioned study (p. 21), we observed a decrease of full-fusion exocytic events in non-transfected lactotrophs after the addition of cAMP. This was not the case in HCN2-transfected lactotrophs, where the addition of cAMP significantly increased the frequency of full-fusion exocytotic events, from 0.002 ± 0.001 events/s prior cAMP stimulation to 0.006 ± 0.001 events/s (n = 16; P<0.01; Fig. IV.4d) after stimulation. To pursue the question of how HCN channels affect exocytosis further, we inhibited these channels and monitored the changes in C_m. The inhibition was performed by incubating lactotrophs with ZD7288 (ZD), which has been shown to successfully inhibit HCN current in neuroendocrine cells (Gonzalez-Iglesias *et al.,* 2006b). In our experiments the treatment of lactotrophs with ZD resulted in a significantly reduced frequency of transient exocytotic events (0.04 ± 0.01 events/s; n = 6 cells; P<0.001) compared to controls (Fig. IV.4e). The addition of cAMP further decreased the frequency of transient exocytotic events to 0.01 ± 0.01 events/s (n = 6 cells; P<0.001; Fig. IV.4e). The same tendency was observed in the frequency of full-fusion events, which decreased to 0.004 ± 0.001 events/s (n = 6 cells; ZD) and to 0.002 ± 0.001 events/s (n = 6 cells; after the addition of cAMP; Fig. IV.4f).

Taken together these data shows that HCN channels have a very pronounced effect on the occurrence of unitary exocytic events. Our next aim was to analyse transient fusion events in detail, to see if HCN channels also affect the transient exocytic states that lead to full-fusion.

4.5 HCN2 isoform modulates fusion pore properties in lactotrophs

Previously, we have observed that vesicles, which are engaged in transient exocytosis, exhibit fusion pore diameters that are related to the vesicle diameter (Jorgačevski *et al.,* 2010). The relationship between the fusion pore diameter and the vesicle diameter is, however, sensitive to involved proteins (Jorgačevski *et al.,* 2011), electrostatic interactions (p. 119) and also to the increase in cAMP (p. 21).

To assess if HCN channels affect the afore mentioned relationship, we used transient fusion events, which appear in the Im trace and exhibit a projection to the Re trace to calculate G_p and C_v (Fig. IV.3c; Lollike and Lindau, 1999). We first compared how the overexpression of HCN2 and the pharmacologic inhibition of HCN channels (ZD) in cAMP-stimulated conditions affect the relationship between G_p and C_v (Fig. IV.5a). Respective data points were best fitted with linear regressions lines, which had the following slopes: 20.0 ± 6.0 for HCN2 transfected lactotrophs and 5.6 ± 1.0 for lactotrophs treated with the ZD (Fig. IV.5a). These results indicate that HCN channels are important for the regulation of transitions from narrow to wider fusion pore states. However, the relationship between G_p and C_v can only be determined for the fusion events which exhibit narrow fusion pores (with a projection between the Im to the Re trace), which corresponds to 25% of all events in controls (Fig. IV.5b). Treatment with ZD increased the proportion of narrow fusion pores to 38% and the addition of cAMP further increased it further to 55%. On the other hand, the overexpression of HCN2 isoform decreased the proportion of narrow fusion pores to 17%, which decreased further to 8% after the addition of cAMP.

These results confirm that HCN channels modulate the fusion pore diameter.

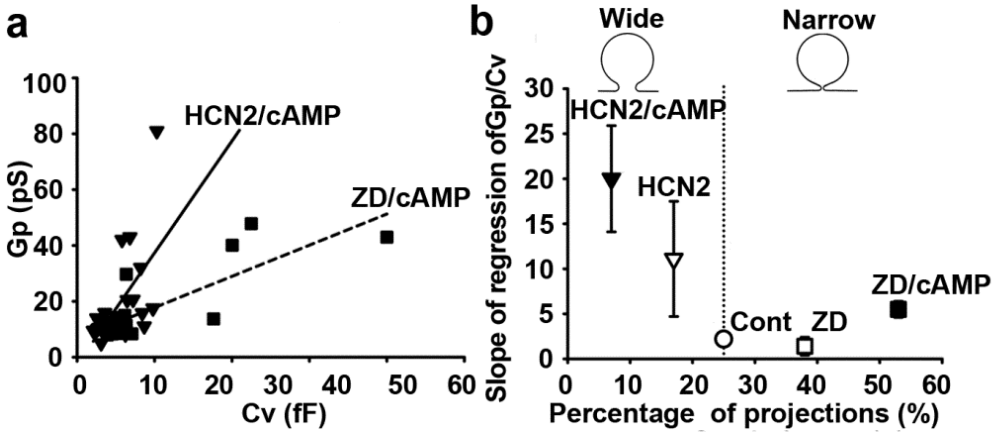

Figure IV.5: HCN channel isoform increases the fusion pore conductance.

(a) Scatter plot diagram of fusion pore conductance (G_p) *vs.* vesicle capacitance (C_v) of reversible events in cells transfected with pDNA of HCN2 isoform and stimulated with cAMP (full triangles) and of reversible events in cells treated with ZD7288 and stimulated with cAMP (full squares). Respective data points were best fitted with two linear

regressions of the form: y (G_p) = (20 ± 6) × x (C_v) + (3 ± 7) (HCN2/cAMP, solid line, r = 0.6) and y (G_p) = (6 ± 1) × x (C_v) + (7 ± 3) (ZD7288/cAMP, dashed line, r=0.8, P<0.05). Significance was tested using one-way ANCOVA for two independent samples. **(b)** The relationship between the percentage of projected reversible events and the slope of the regression line between G_p and C_v, for each of the tested conditions. Dotted vertical line denotes the percentage of transient exocytic events, which exhibited measurable fusion pores of transient events at spontaneous conditions (25%, see Fig. IV.3 and Materials and Methods). Transfection with pDNA of HCN2 resulted in the decreased percentage of measurable fusion pores of transient events (wider fusion pores). On the other hand, treatment with ZD7288 resulted in increased percentage of measurable fusion pores (narrower fusion pores).

5 Discussion

We propose that fusion pore properties can be regulated by HCN channels, which are activated by cAMP. The flow of cations through the channels located either in the vesicle membrane or in the plasma membrane next to the fused vesicle likely determines the local cation concentration and thus likely induces changes in local membrane curvature, which in turn may modulate fusion pore diameter (Fig. IV.6; see Kabaso *et al.,* 2012).

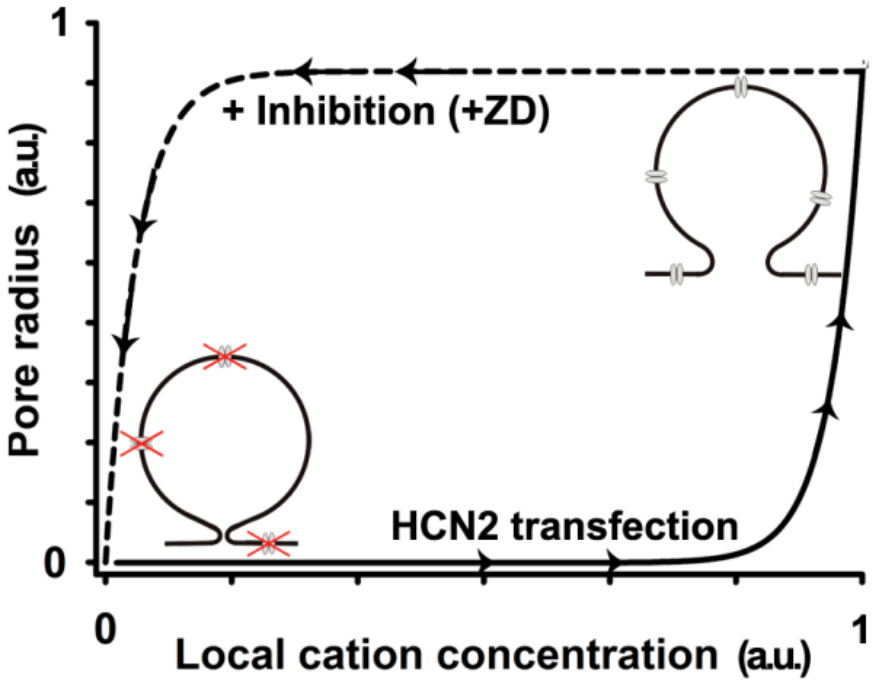

Figure IV.6: HCN channel isoform modulate the fusion pore properties.

Model describing the possible effect of HCN channels in the fusion pore diameter due to fluctuations in local cation concentration. Augmentation of HCN channels in the vesicle and plasma membrane creates influx of cation current which increases local cation concentration nearby the vesicles leading to changes in the spontaneous curvature of the membrane resulting in wider fusion pores. On the contrary, when HCN channels current is blocked, the influx of cations is reduced and the local cation concentration decreased reflecting narrower fusion pores (adapted from Kabaso *et al*., 2012).

Hyperpolarization activated and cyclic nucleotide-gated (HCN) channels have four isoforms, HCN1-4, which are arranged in tetrameric complexes consisting of either

identical (homomeric) or different (heteromeric) types of subunits. cAMP directly binds and actives them by shifting the voltage dependence to more depolarized values (facilitates activation), which increases the probability of an open channel state. It has been shown that mRNA transcripts of HCN channels and their expression can be detected in the pituitary gland (Kretschmannova *et al.,* 2012; p. 59; see also Fig. IV.1a and b) and that specific HCN currents are present in lactotrophs (Gonzalez-Iglesias *et al.,* 2006b). Our results unambiguously confirm that HCN channels, and HCN2 isoform specifically, are present in isolated rat lactotrophs (Fig. IV.1). We focused on HCN2 isoform for three reasons: i) this isoform is the most ubiquitously distributed isoform of all HCN isoforms in the brain, ii) mRNA transcripts of this isoform are the most abundant in the pituitary gland (Kretschmannova *et al.,* 2012; p. 59) and iii) HCN2 isoform is the most sensitive to cAMP. By using Western blot we confirmed the native expression of HCN2 isoform in the pituitary gland, which was detected as a band with molecular weight similar to those previously published for this isoform (Fig. IV.1a; p. 59). Relatively weak bands, obtained with Western blot of the whole pituitary led us to use qRT-PCR to detect the presence of mRNA in lactotrophs, which comprise only a fraction (10-25%) of the anterior pituitary. The overall amount of HCN2 mRNA transcript in lactotrophs, which was less than 1% of the mRNA transcript of β-actin (Fig. IV.1b), is in agreement with previous studies on secretory cells, where very low amount of transcripts were detected in rat islets and MIN6 β-cell lines (El-Kholy *et al.,* 2007). Expression of HCN channels in lactotrophs was attested by immunocytochemistry (Fig. IV.1c). Sub-cellular localization of HCN channels in lactotrophs is consistent with findings on other cell types. Noam *et al.* (2010) showed that these channels are also located in vesicle-like organelles that moved along dendrites in hippocampal neurons. It is therefore not surprising that in our experiments 55% of HCN2 isoform is located in the plasma membrane of lactotrophs, while 22% are confined to PRL-containing vesicles (Fig. IV.1iv). The remaining ~20% that are not accounted for, are most likely localized in other subcellular organelles, like constitutive vesicles, endoplasmic reticulum and Golgi apparatus.

The surface expression of HCN2 and HCN4 isoforms is maintained by recycling endosomes, which store HCN channels (Hardel *et al.,* 2008). The abundance of HCN channels on the cell surface is critically dependent on secretory and endocytic pathways. Is the opposite true as well? Do HCN channels affect secretory pathway, more specifically, do they affect stages of vesicular fusion with the plasma membrane, which involve the fusion pore? In order to understand the effect of HCN channels on the fusion of secretory vesicles in pituitary lactotrophs, we transfected cells with the plasmid encoding HCN2 isoform (Fig. IV.2a). Over-expression of the HCN2 isoform was successfully confirmed 24–48 h post transfection, in the cell interior and in the plasma membrane (Fig. IV.2c). The fact that we observed equivalent increase of HCN2 isoform in the plasma membrane and in the cell interior indicates that the afore mentioned time window was sufficient for the balance between synthesis, traffic to and internalization into the plasma membrane of over-expressing HCN2 to be restored. Here we can ask, whether the increase of HCN2 fluorescence reflects the augmentation of channels, or just an increase in the proportion of HCN2 isoform units in the unaltered number of HCN channels. Visual inspection of all immunolabeled lactotrophs, before and after transfection with pDNA of HCN2, indicates that the overall number of distinct fluorescent puncta (which indicate either single channels or a group of channels where the distance between them is smaller than the resolution limit of confocal microscope, i.e. ~200 nm) as well as the fluorescence of individual puncta increased. Therefore, we suggest that the number of individual channels with isoform 2, as well as the proportion of this isoforms in individual channels have increased in HCN2 transfected lactotrophs.

cAMP has been shown to affect the release of PRL from lactotrophs, facilitating pacemaking and facilitating voltage gated calcium influx (Gonzalez-Iglesias *et al.,* 2006; p. 21), whereas PKA- and Epac-dependent mechanisms were bypassed (Gonzalez-Iglesias *et al.,* 2006). This makes HCN channels very likely candidates to be involved in the regulation of exocytosis. Our results support this notion, since the frequency of transient and full-fusion events significantly decreased in lactotrophs over-expressing HCN2 isoform (Fig. IV.4c and d). This effect was rather surprising, since previous studies on lactotrophs confirmed that

there is a strong correlation between an increase in intracellular Ca^{2+} ($[Ca^{2+}]_i$) concentration and an increase in transient fusion exocytosis (Vardjan *et al.,* 2007, Jorgačevski *et al.,* 2008). Full-fusion exocytosis, on the other hand, is apparently unaffected by the increase in $[Ca^{2+}]_i$ (Vardjan *et al.,* 2007, Jorgačevski *et al.,* 2008), yet over-expression of HCN2 isoform decreased also this type of exocytosis. The conclusion can be drawn that over-expression of HCN2 results in local increase in $[Ca^{2+}]_i$, which is so minute that it is not sufficient to affect calcium dependent fusion of vesicles or that there are additional mechanisms with negative effect on the rate of exocytosis, which masks the positive effect of the $[Ca^{2+}]_i$ increase. To stress the first option it has been recently shown that vesicular calcium channels regulate exocytosis by facilitating calcium entry trough the fusion pore. This generates microdomains of increased $[Ca^{2+}]_i$ around the fused vesicles, which leads to the fusion pore expansion (Miklavc *et al.,* 2011). HCN channels are permeable for Ca^{2+} (Yu *et al.,* 2004; Michels *et al*., 2008), though major physiological implications of Ca^{2+} signalling through these channels remain unclear. In neurons Ca^{2+} current through HCN channels can contribute to activity-evoked neuronal secretion (Yu *et al.,* 2004; Zhong *et al.,* 2004). Resting concentrations of intracellular cAMP are sufficient to activate HCN channels in lactotrophs (Kretschmannova *et al*., 2006). However, in lactotrophs over-expressing HCN channels, resting cAMP might be insufficient to activate all channels. Increasing the intracellular cAMP would activate all HCN channels, which could thus enhance the rate of exocytosis. We observed this when we added cAMP to lactotrophs over-expressing HCN2, as an increase in frequency of exocytic events (Fig. IV.4c and d) and as the fusion pore expansion (Fig. IV.5). Nonetheless, the frequency of exocytosis was merely rescued to the basal level, which suggests that additional mechanism of HCN action with negative effect on the rate of exocytosis must be present. One of many may be related to the rate of change in cAMP. Recent experiments of measuring the dynamics of cAMP in single cells by the FRET technique, revealed that different mechanisms of adenylate cyclase activation result in different kinetics of cAMP concentration change, i.e. the activation via membrane receptors results in a more rapid increase in cAMP in comparison to the addition of dbcAMP (unpublished). If the

rate of change determines the activation of HCN2 channels, then this may play an important factor in regulating exocytosis.

One possibility is that HCN directly affects the exocytotic machinery, by interactions between HCN related proteins and proteins involved in the exocytic process. In AtT20 neuroendocrine cell line accessory subunit for HCN channels, TRIP8b (tetratricopetide repeat containing Rab8b interacting protein) interacts with Rab8b and both proteins are involved in regulated exocytosis, promoting cAMP induced release of adrenocorticotropic hormone (Chen *et al.,* 2001). Also Mint2 has been shown to bind to HCN channels due to interaction between munc18-interacting domain of Mint2 (Kimura *et al.,* 2004), Mint has been proposed to have a role in insulin granule exocytosis (Zhang *et al.,* 2004) and lactotrophs transfected with Munc18 mutant with a deficiency in Mint binding exhibited different fusion pore properties (Jorgačevski *et al.,* 2011).

Even though proteins interaction is likely to occur, we do not exclude other options. Kabaso and co-workers (2012) have proposed that rhythmic opening and closing of the fusion pore is related with the influx of cations into the vesicles. Even though HCN channels have a permeability ratio of 3-5 K^+ to 1 Na^+, under physiological conditions when they open, this results in a cation inward current of Na^+. Cation influx through HCN channels, into the cell in the close proximity of fusing vesicles (through the fusion pore and vesicular HCN channels or/and through the channels in the plasma membrane), would increase local cation concentration. Local increase in cations could affect membrane fluidity and local membrane lipid composition by means of altered electrostatic interactions. Inhibition of cation current with ZD7288 (specific blocker of the HCN current), should then have the opposite effect. Similar effect on the rate of exocytosis was observed when we studied the effects of extracellular addition of sub-lethal dose of aluminium on PRL secretion in isolated rat pituitary lactotrophs (p. 119). Moreover, it has been previously proposed that in lactotrophs ZD7288 action is downstream of Ca^{2+}-dependent initiation step for exocytosis, since PRL release is inhibited by ZD7288 while it increases pacemaking activity and intracellular Ca^{2+}. Surprisingly, exocytotic inhibition occurred in ZD7288 incubated cells even after adding cAMP, which was not expected since cAMP is a channel activator. A possible explanation

is that this is still the effect of ZD7288 rather that of cAMP. ZD7288 has a slow time of action since it works in the intracellular side of the channel pore and at the time that cAMP was added not all HCN channels were yet inhibited. None the less, El-Kholy and co-workers propose that ZD7288 directly blocks exocytosis, in addition to inhibiting HCN channels, likely via a direct interaction with the exocytic machinery in β-cells (El-Kholy *et al.,* 2007). We propose that HCN channels modulate the fusion pore in a cAMP dependent manner mainly via the modulation of cation flux.

6 References

Angleson J, Cochilla A, Kilic G, Nussinovitch I, Betz W (1999). Regulation of dense core release from neuroendocrine cells revealed by imaging single exocytotic events. *Nat Neurosci* 2:440-446.

Ben-Tabou S, Keller E, Nussinovitch I (1994). Mechanosensitivity of voltage-gated calcium currents in rat anterior pituitary cells. *J Physiol* 476:29–39.

Brown HF, DiFrancesco D, Noble SJ (1979). How does adrenaline accelerate the heart? *Nature* 280:235-236.

Chen S, Liang MC, Chia JN, Ngsee JK, Ting AE (2001). Rab8b and its interacting partner TRIP8b are involved in regulated secretion in AtT20 cells. *J Biol Chem* 276:13209-13216.

Chernomordik LV, Kozlov MM (2008). Mechanics of membrane fusion. *Nat Struct Mol Biol* 15: 675–683.

El-Kholy W, MacDonald PE, Fox JM, Bhattacharjee A, Xue T, Gao X, Zhang Y, Stieber J, Li RA, Tsushima RG, Wheeler MB (2007). Hyperpolarization-activated cyclic nucleotide-gated channels in pancreatic beta-cells. *Mol Endocrinol* 21:753-764.

Gonzalez-Iglesias AE, Jiang Y, Tomic M, Kretschmannova K, Andric SA, Zemkova H, Stojilkovic SS (2006). Dependence of electrical activity and calcium influx-controlled prolactin release on adenylyl cyclase signalling pathway in pituitary lactotrophs. *Mol Endocrinol* 20:2231-2246.

Gonzalez-Iglesias AE, Kretschmannova K, Tomic M., Stojilkovic SS (2006b). ZD7288 inhibits exocytosis in an HCN-independent manner and downsstream of

voltage-gated calcium influx in pituitary lactotrophs. *Biochem Biophys Res Commun* 346:845-850.

Hanna ST, Pigeau GM, Galvanovskis J, Clark A, Rorsman P, MacDonald PE (2009). Kiss-and-run exocytosis and fusion pores of secretory vesicles in human β-cells. *Pflugers Arch - Eur J Physiol* 457:1343–1350.

Hardel N, Harmel N, Zolles G, Fakler B, Klöcker N (2008). Recycling endosomes supply cardiac pacemaker channels for regulated surface expression. *Cardiovasc Res* 79:52-60.

Jorgacevski J, Stenovec M, Kreft M, Bajić A, Rituper B, Vardjan N, Stojilkovic S, Zorec R (2008). Hypotonicity and peptide discharge from a single vesicle. *Am J Physiol Cell Physiol* 295:624-631.

Jorgačevski J, Fošnarič M, Vardjan N, Stenovec M, Potokar M, Kreft M, Kralj-Iglič V, Iglič A, Zorec R (2010). Fusion pore stability of peptidergic vesicles. *Mol Membr Biol* 27:65-80.

Jorgačevski J, Potokar M, Grilc S, Kreft M, Liu W, Barclay WF, Buckers J, Medda R, Hell SH, Parpura V, Burgoyne RD, Zorec R (2011). Munc18-1 Tuning of Vesicle Merger and Fusion Pore Properties. *J Neurosci* 31:9055–9066.

Jorgačevski J, Kreft M, Vardjan N, Zorec R (2012). Fusion pore regulation in peptidergic vesicles.*Cell Calcium* 52:270-276.

Kabaso D, Calejo AI, Jorgačevski J, Kreft M, Zorec R, Iglič A (2012). Fusion pore diameter regulation by cations modulating local membrane anisotropy. *Scientific World Journal*, Article ID 983138, 7 pages doi:10.1100/2012/983138

Kimura K, Kitano J, Nakajima Y, Nakanishi S (2004). Hyperpolarization-activated, cyclic nucleotide-gated HCN2 cation channel forms a protein assembly with

multiple neuronal scaffold proteins in distinct modes of protein-protein interaction. *Genes Cells* 9:631-640.

Kretschmannova K, Kucka M, Gonzalez-Iglesias AE, Stojilkovic SS (2012). The expression and role of hyperpolarization-activated and cyclic nucleotide-gated channels in endocrine anterior pituitary cells. *Mol Endocrinol* 26:153-164.

Lollike K, Lindau M (1999). Membrane capacitance techniques to monitor granule exocytosis in neutrophils. *J Immunol Methods* 232:111–120.

Michels G, Brandt MC, Zagidullin N, Khan IF, Larbig R, van Aaken S, Wippermann J, Hoppe UC (2008). Direct evidence for calcium conductance of hyperpolarization-activated cyclic nucleotide-gated channels and human native If at physiological calcium concentrations. *Cardiovasc Res* 78:466-475.

Miklavc P, N Mair, OH Wittekindt, T. Hallerb, P. Dietla, E. Feldera, M. Timmlera, M. Fricka (2011). Fusion-activated Ca^{2+} entry via vesicular P2X4 receptors promotes fusion pore opening and exocytotic content release in pneumocytes. *PNAS* 108:14503-14508.

Noam Y, Zha Q, Phan L, Wu RL, Chetkovich DM, Wadman WJ, Baram TZ (2010). Trafficking and surface expression of hyperpolarization-activated cyclic nucleotide-gated channels in hippocampal neurons. *J Biol Chem* 285:14724-14736.

Okamoto M, Sudhof TC (1997). Mints, Munc18-interacting proteins in synaptic vesicle exocytosis. *J Biol Chem* 272:31459–31464.

Potokar M, Stenovec M, Kreft M, Gabrijel M, Zorec R(2011). Physiopathologic dynamics of vesicle traffic in astrocytes. *Histol Histopathol* 26:277-284.

Rituper B, Flašker A, Guček A, Chowdhury HH, Zorec R (2012). Cholesterol and regulated exocytosis: a requirement for unitary exocytotic events. *Cell Calcium* 52:250-258.

Santoro B, Wainger BJ, Siegelbaum SA (2004). Regulation of HCN channel surface expression by a novel C-terminal protein-protein interaction. *J Neurosci* 24:10750-10762.

Seino S, Shibasaki T (2005). PKA-dependent and PKA-independent pathways for cAMP-regulated exocyosis. *Physiol Rev* 85:1303-1342.

Stojilkovic SS, Tabak J, Bertram R (2010). Ion channels and signaling in the pituitary gland. *Endocr Rev* 31:845-915.

Stojilkovic SS, Kretschmannova K, Tomic M, Stratakis CA (2012). Dependence of excitability of pituitary cells on cyclic nucleotides. *J Neuroendocrinol* 24:1183-1200.

Vaccari T, Moroni A, Rocchi M, Gorza L, Bianchi ME, Beltrame M, DiFrancesco D (1999) The human gene coding for HCN2, a pacemaker channel of the heart1. *Biochim Biophys Acta* 1446:419-425.

Vardjan N, Stenovec M, Jorgačevski J, Kreft M, Zorec R (2007). Subnanometer fusion pores in spontaneous exocytosis of peptidergic vesicles. *J Neurosci* 27:4737–4746.

Vardjan N, Jorgacevski J, Zorec R (2013). Fusion Pores, SNAREs, and Exocytosis. *Neuroscientist* 19:160-174.

Yu X, Duan KL, Shang CF, Yu HG, Zhou Z (2004). Calcium influx through hyperpolarization-activated cation channels (I(h) channels) contributes to activity-evoked neuronal secretion. *Proc Natl Acad Sci USA* 101:1051-1056.

Zhang W, Lilja L, Bark C, Berggren PO, Meister B (2004). Mint1, a Munc-18-interacting protein, is expressed in insulin-secreting beta-cells. *Biochem Biophys Res Commun* 320:717-721.

Zhong N, Beaumont V, Zucker RS (2004). Calcium influx through HCN channels does not contribute to cAMP-enhanced transmission. *J Neurophysiol* 92:644-647.

Zorec R, Sikdar SK, Mason WT (1991). Increased Cytosolic Calcium Stimulates Exocytosis in Bovine Lactotrophs. *J Gen Physiol* 97:473-497.

Chapter V - Aluminium-induced changes of fusion pore properties attenuate prolactin secretion in rat pituitary lactotrophs

NOTE: The results in this chapter were published as: Calejo A.I., Jorgačevski J, Silva V.S., Stenovec M., Kreft M., Gonçalves P.P., Zorec R. Aluminium-induced changes of fusion pore properties attenuate prolactin secretion in rat pituitary lactotrophs (2012). Neuroscience 201:57-66.

1 Abstract

Hormone secretion is mediated by Ca^{2+}-regulated exocytosis. The key step of this process consists of the merger of the vesicle and the plasma membranes, leading to the formation of a fusion pore. This is an aqueous channel through which molecules stored in the vesicle lumen exit into the extracellular space on stimulation. Here we studied the effect of sub-lethal dose of aluminium on prolactin secretion in isolated rat pituitary lactotrophs with an enzyme immunoassay and by monitoring electrophysiologically the interaction of a single vesicle with the plasma membrane in real time, by monitoring membrane capacitance. After 24 h exposure to sub-lethal $AlCl_3$ (30 μM), the secretion of prolactin was reduced by 14±8% and 46±11% under spontaneous and K^+-stimulated conditions, respectively. The frequency of unitary exocytotic events, recorded by the high-resolution patch-clamp monitoring of membrane capacitance, a parameter linearly related to the membrane area, under spontaneous and stimulated conditions, was decreased in aluminium-treated cells. Moreover, while the fusion pore dwell-time was increased in the presence of aluminium, the fusion pore conductance, a measure of fusion pore diameter, was reduced, both under spontaneous and stimulated conditions. These results suggest that sub-lethal aluminium concentrations reduce prolactin secretion downstream of stimulus secretion coupling by decreasing the frequency of unitary exocytotic events and by stabilizing the fusion pore diameter to a value smaller than prolactin molecule, thus preventing its discharge into the extracellular space.

Keywords: Membrane fusion, fusion pore properties, prolactin, aluminium toxicity, lactotrophs.

2 Introduction

Prolactin (PRL) is a stress hormone that regulates reproduction, metabolism, osmoregulation, immunoregulation and behaviour (Freeman *et al*., 2000). The main source of serum PRL is pituitary lactotrophs, which comprise 10–25% of the entire anterior pituitary cell population (Stojilkovic *et al*., 2010). The secretory activity of the lactotrophs mirrors the action of a complex network of local and distant regulators, orchestrated by the hypothalamus, which tonically suppresses pituitary PRL secretion (Freeman *et al*., 2000). Thereby, alterations of mammalian plasma PRL levels are often interpreted as a result of an impaired hypothalamic modulation of pituitary secretion, given that hypothalamic dopamine released into the pituitary portal systems is the major PRL-inhibiting factor (Ben-Jonathan and Hnasko, 2001).

Considerable progress has been made in understanding the toxicological actions of aluminium since Alfrey *et al.* (1976) described dialysis encephalopathy as aluminium intoxication in patients undergoing long-term dialysis. Besides other adverse effects, especially at the level of blood and osseous tissues, the nervous system appears to be the most sensitive target of aluminium toxicity (ATSDR, 2008). Presently, neurotoxicity, neurodevelopmental toxicity, and delays in maturation are considered as the most critical deleterious effects of exposure to aluminium (Golub *et al.,* 1989).

Several investigators suggested that PRL depletion might occur during aluminium intoxication both in humans and in animal models. Decreased PRL serum concentrations have been reported in a study involving 227 subjects with occupational exposure to aluminium (Alessio *et al*., 1989). PRL depletion in male mice correlated with aluminium intoxication (Galoyan *et al*., 2004). One week after a single s.c. injection of 0.2 ml of 3% solution of $AlCl_3$, the PRL content decreased in serum and brain (more than threefold and sixfold, respectively) and dropped close to undetectable levels in liver and thymus. At a first glance, the reported decrease of serum PRL levels after exposure to aluminium suggests exacerbated hypothalamic delivery of dopamine, which seems not to be the case. *In vivo* exposure to aluminium produces a diminishment of the levels of dopamine,

dihydroxyphenylacetic acid, and homovanillic acid in mice hypothalamus consistent with aluminium-induced inhibition of dopamine synthesis (Tsunoda and Sharma, 1999). In contrast, intracytoplasmic aluminium containing inclusions in the pituitary gland was observed in dialysis encephalopathy cases at autopsy (Reusche *et al*., 1994). Aluminium accumulation in the cytoplasm of rat anterior pituitary cells has been histologically documented by Walton (2004). Allen *et al*., (1991) reported that the enhancement of aluminium concentration in the pituitary gland of wether lambs dosed with aluminium citrate was more pronounced than in brain, suggesting aluminium might impair the PRL secretion even before aluminium-induced impairment of hypothalamic dopaminergic neuronal systems (Ben-Jonathan and Hnasko, 2001).

Lactotrophs have a high constitutive production and large storage capacity for PRL and release of hormone by the calcium-dependent exocytosis (Stojilkovic *et al*., 2010). Cultured lactotrophs exhibit spontaneous and stimulated release of secretory peptides (Zorec *et al.,* 1991; Stenovec *et al*., 2004; Gonçalves *et al*., 2008), which enables studying PRL secretion in the absence of regulation by the hypothalamic dopaminergic neuronal systems.

This study was undertaken to determine whether exposure of lactotrophs to sub-lethal $AlCl_3$ concentration (Calejo *et al*., 2010) directly reduces PRL secretion by affecting Ca^{2+}-regulated exocytosis from cultured rat pituitary lactotrophs. The inhibitory effect of aluminium on PRL secretion from lactotrophs was experimentally demonstrated by combining the biochemical and electrophysiological methods. An immunoassay assuring specific detection of PRL was used to quantify the PRL secretion by cell cultures. In electrophysiological experiments discrete changes in membrane capacitance (C_m) were monitored to examine the effects of aluminium at the level of elementary exocytotic events (Kreft and Zorec, 1997).

3 Experimental Procedures

3.1 Cell cultures and the aluminium exposure

Male Wistar rats were handled in accordance with EU regulation of the accommodation and care of animals used for experimental and other scientific purposes (86/609/EEC and 2007/526/EC). All efforts were made to minimize the number of animals used and their suffering. Primary lactotroph cultures were prepared from the anterior pituitaries as described previously (Ben-Tabou *et al*., 1994). The rat pituitary lactotroph-enriched cultures, plated on poly-L-lysine coated glass coverslips, were maintained at 37 ºC (89-92% humidity and 5% CO_2) in high-glucose Dulbecco's Modified Eagle's Medium buffered with HEPES-Tricine and supplemented with 1.5 µM bovine serum albumin, 2 mM L-glutamine and 10% newborn calf serum (DMEM medium). Incubation medium was changed every second day and experiments were carried out at room temperature 1-4 days after the isolation. The aluminium exposure was initiated by addition of $AlCl_3$ (final concentration of 30 µM) to the incubation medium and the cell cultures were maintained under the previously mentioned conditions for 24 h (aluminium treatment). To determine the viable cell density in lactotroph-enriched cultures, the cells were detached from the coverslips by applying a trypsin-EDTA solution and then a viability analyzer (Vi-CELL^{TM} XR 2.03, Beckman, Indianapolis, USA) was used to count cells by the Trypan Blue dye exclusion method. Fifty real-time images were collected per sample and the number of living and dead cells was recorded per frame to calculate the viable cell concentration.

3.2 Prolactin quantification

The amount of secreted PRL by cell cultures was measured by means of a competitive enzyme immunoassay with a double antibody procedure using the Rat Prolactin EIA Kit (SPI-bio) according to the manufacturer instructions.

Cells-loaded coverslips were incubated for 24 h in the absence and in the presence of 30 µM of $AlCl_3$. The incubation media were collected and cleared by

centrifugation (5000×g for 5 min) to determine the basal level of PRL secretion. Then cell cultures were incubated for 10 min either with extracellular solution (130 mM NaCl, 5 mM KCl, 8 mM $CaCl_2$, 1 mM $MgCl_2$, 10 mM D-glucose and 10 mM HEPES/NaOH, at pH 7.2) or K^+-enriched solution (100 mM KCl, 35 mM NaCl, 8 mM $CaCl_2$, 1 mM $MgCl_2$, 10 mM D-glucose and 10 mM HEPES/NaOH, at pH 7.2). The incubation media were collected and cleared by centrifugation to determine the PRL secretion under spontaneous and stimulated conditions, respectively. The PRL quantification assays were performed in 96-well microtiter plates coated with a mouse monoclonal anti-rabbit immunoglobulin antibody. The specific immunoreaction was carried out in the presence of rat PRL labelled with acetylcholinesterase as tracer and rabbit antiserum raised against rat PRL, as the primary antibody. After incubation with Ellman's Reagent, the concentration of PRL in supernatants and in rat PRL standard solutions was determined spectrophotometrically at 405 nm using a spectrophotometer plate reader (Original Multiskan Ex, Thermo Electron Corporation). The results were expressed in ng of PRL per 10^5 viable cells per minute.

3.3 Electrophysiology

Cell-loaded coverslips were maintained in the recording chamber on the inverted microscope (Zeiss Axio Observer, Jena, Germany) filled up with extracellular solution. Cell stimulation was performed by partial replacement of the extracellular solution with 130 mM KCl, 5 mM NaCl, 8 mM $CaCl_2$, 1 mM $MgCl_2$, 10 mM D-glucose and 10 mM HEPES/NaOH (pH 7.2) to reach the final concentration of 100 mM KCl.

Cell-attached capacitance measurements were performed with a dual-phase lock-in patch-clamp amplifier (sine-wave frequency (f) 1591 Hz; 111 mV root mean square; SWAM IIC, Celica, Ljubljana, Slovenia) as previously described (Zorec *et al.,* 1991; Kreft and Zorec, 1997; Jorgačevski *et al.,* 2011). A sine wave voltage was applied to the pipette and the pipette potential was set to 0 mV. The patch pipette resistance ranged from 2 to 6 MΩ. Phase angle was adjusted to nullify the changes in the real (Re) part of the admittance signal. To guarantee

correct phase angle settings, 10 fF calibration pulses in the imaginary part (Im) of the admittance signal were manually triggered every 10 s. For transient fusion events, vesicle capacitance (C_v) and fusion pore conductance (G_p) [$G_p = (Re^2 + Im^2)/Re$; $C_v = [(Re^2 + Im^2)/Im]/\omega$ were calculated from the Im and Re part of admittance signals (Lollike and Lindau, 1999), where ω is the angular frequency ($\omega = 2\pi f$). Fusion pore radius was estimated by using the equation $G_p = (\pi r^2)/(\rho\lambda)$; where r denotes fusion pore radius, ρ the estimated resistivity of the saline (100 Ω cm), and λ the estimated length of a gap junction channel (15 nm) (Spruce *et al.,* 1990). Vesicle diameter was calculated by using specific membrane capacitance of 8 f*F*/μm^2.

Events were analysed by the custom software CellAn (Celica, Slovenia) written for MATLAB. (Math Works, Natick, MA, USA). The appearance of events was ascertained by progressive filtering and taking into consideration the absence of a projection in the current trace. Events were considered reversible if an on-step in Im was followed by an off-step within 5 s.

3.4 Data analysis

Statistical analysis was performed using Student's t-test, unless otherwise stated in the figure legend. Data are reported as mean ± standard error of the mean (s.e.m.) of the number of experiments indicated in each legend to figures and $P<0.05$ was considered significant.

4 Results

4.1 Aluminium inhibits prolactin secretion from cultured lactotrophs

The level of spontaneous PRL secretion from cultured lactotrophs is relatively high and depends on the extracellular calcium and the spontaneous electrical activity (Stojilkovic, 2005). In addition to spontaneous secretion, secretory activity can be increased by K^+-depolarization, which triggers voltage-gated calcium influx, mediating enhanced PRL secretion (Zorec *et al.,* 1991; Gonçalves *et al.,* 2008). In this study we explored both types of secretion to examine the effect of a sub-lethal $AlCl_3$ concentration (30 µM) on PRL release.

To investigate the abiding effect of aluminium on the spontaneous secretion of PRL, lactotrophs, plated on poly-L-lysine coated glass coverslips, were incubated for 24 h in high-glucose DMEM Medium (see Materials and Methods) and the amount of released PRL normalized to account for the differences in cell density and viability. The data obtained were compared with the control values (Fig. V.1a).

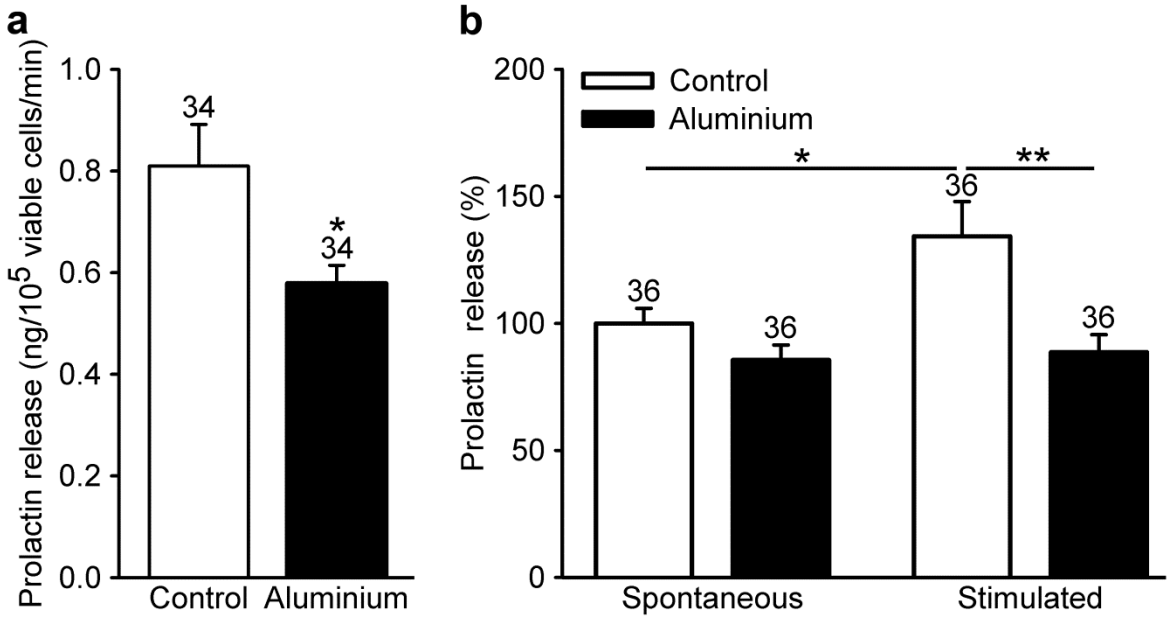

Figure V.1: The exposure of cultured lactotrophs to aluminium inhibits spontaneous and K^+-stimulated prolactin (PRL) release.

Secreted PRL was determined in the supernatants obtained by harvesting cell cultures

after 24 h incubation in the absence (white bars) and in the presence of 30 μM $AlCl_3$ (black bars). **(a)** Spontaneous release of PRL was significantly diminished in aluminium-treated cells (24 h in DMEM at 37º C) compared with controls (obtained in the absence of added aluminium). **(b)** Comparison of stimulated PRL release from controls and cells previously exposed to aluminium. PRL release was stimulated by 10 min incubation of cells either in extracellular solution (Spontaneous) or K^+-enriched solution (Stimulated). Stimulation significantly increased PRL release in controls, whereas in cells previously exposed to aluminium the hormone release remained unchanged compared with spontaneous release. Values are expressed as mean ± s.e.m., numbers adjacent to bars show the number of experiments. **P*<0.05 and ***P*<0.01.

We neither detect significant differences (*P*>0.05) in cell viability nor in density in cultures, which were incubated in the absence (95±1%; 2.9±0.3×10^4 cells/ml) and in the presence of 30 μM $AlCl_3$ (95±1%; 3.8±0.3×10^4 cells/ml). The level of PRL release in $AlCl_3$-treated cells controls was lower than in controls (Fig. V.1a). To test whether regulated exocytosis accounts for the aluminium-induced reduction of PRL release, lactotrophs were briefly (10 min) incubated in the extracellular solution containing 8 mM $CaCl_2$ and in the K^+-depolarising solution with the same calcium concentration (Fig. V.1b). Lactotrophs that were not exposed to $AlCl_3$ responded to the elevation of extracellular calcium concentration by increasing the amount of released PRL (3.25±0.40 ng/10^5 viable cells/minute; n=36) compared with the basal release values obtained in DMEM (0.81±0.08 ng/10^5 viable cells/minute; n=34; P<0.001). Stimulation of lactotrophs with K^+-depolarising solution increased PRL release 1.3-folds, compared to the spontaneous release (extracellular solution containing 8 mM $CaCl_2$) (Fig. V.1b). However, K^+-stimulation did not affect the amount of released PRL from lactotrophs previously exposed to $AlCl_3$ (2.47±0.24 ng/10^5 viable cells/minute vs. 2.31±0.12 ng/10^5 viable cells/minute; n=36 and 36 respectively; Fig. V.1b).

These results demonstrate that aluminium most likely inhibits the release of PRL by affecting Ca^{2+}-regulated exocytosis from cultured lactotrophs. Therefore, we focused on the mechanism underlying the inhibitory action of aluminium on Ca^{2+} regulated exocytosis by using the high-resolution membrane capacitance measurements (Neher and Marty, 1982) to resolve unitary fusion events (Kreft and Zorec, 1997; Stenovec *et al.,* 2004; Jorgačevski *et al.,* 2011).

4.2 Full and transient fusion events are present in $AlCl_3$-treated and non-treated lactotrophs

Lactotrophs contain large dense-core vesicles containing PRL (the mean diameter of 250 nm), which undergo Ca^{2+}-regulated exocytosis followed by endocytosis (Smets *et al.,* 1987; Stojilkovic, 2005). In contrast, constitutive endo- and exocytosis are thought to involve much smaller vesicles (the mean diameter under 100 nm) (Pow and Morris, 1991).

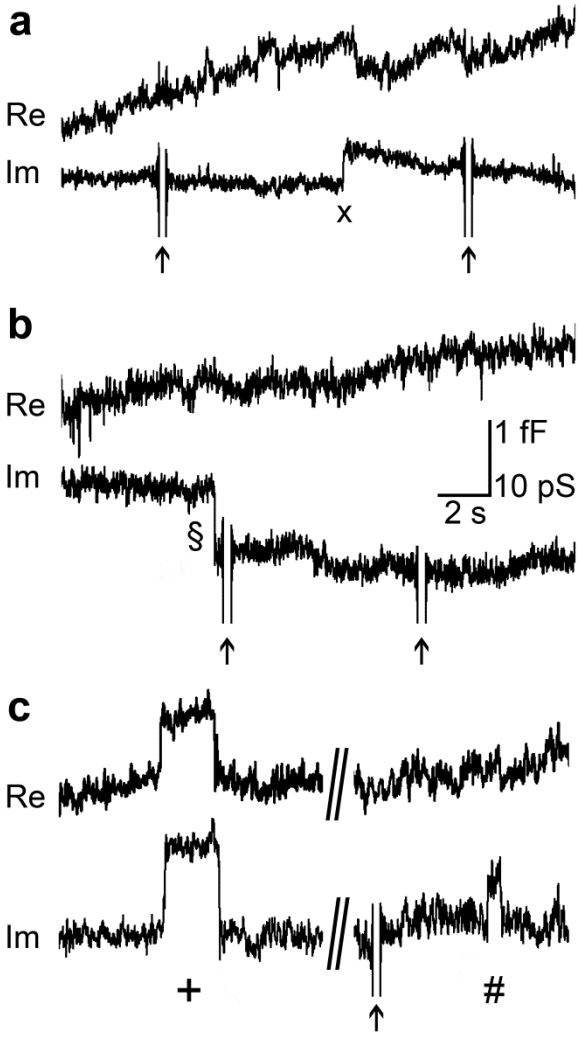

Figure V.2: Representative discrete steps in membrane capacitance (Cm) obtained in cell-attached configuration in cultured lactotrophs in aluminium treated and non-treated cells.

Discrete steps in the imaginary part (Im, proportional to the membrane capacitance C_m) and in the real part (Re) of admittance signals show representative exocytotic events in lactotrophs after the incubation with 30 μM $AlCl_3$ for 24 h. The steps in Im that lasted for more than 5 s were considered irreversible, and most likely reflect **(a)** full vesicle

fusion/exocytosis (x, upward step) and **(b)** vesicle fission/endocytosis (§, downward step). **(c)** Reversible discrete steps in membrane capacitance were also observed; they consisted of discrete increase followed by a discrete decrease in C_m. These events most likely correspond to individual transient fusion pore openings and closings (Jorgačevski *et al*., 2008). The reversible Im steps either exhibited (+) or not (#) a measurable cross-talk with the *Re* signal. The events with a measurable cross-talk reflect the establishment of a narrow fusion pore, whereas those without the cross-talk reflect the establishment of fusion pores with relatively wide diameter (Jorgačevski *et al.,* 2008). Arrows denote calibration pulses (10 fF) that do not project to the Re signal, indicating the correct phase angle setting of the lock-in amplifier. The signals were acquired at 500 Hz and filtered at 10 Hz -3 dB, low pass, Bessel 4^{th} order.

Changes in the cell surface area due to exo- and endocytosis can be monitored by measurements of C_m, a parameter related to the surface area (Neher and Marty, 1982; Jorgačevski *et al.,* 2008). To study sub-lethal effects of $AlCl_3$ on fusion/fission of large dense-core vesicle with the lactotroph plasma membrane we performed electrophysiological C_m measurements in cell-attached patch-clamp configuration (Kreft and Zorec, 1997).

We observed discrete step changes in membrane capacitance, reflecting secretory activity in ~34% of patched lactotrophs. Fig. V.2 shows epochs of representative traces of the Im and the Re part of the admittance signals. Detectable discrete steps in Im (proportional to the changes in C_m; C_m=Im/2πf) most likely resulted from fusion (upward steps) and fission (downward steps) events reflecting exocytosis and endocytosis of single large dense-core vesicles, respectively. Simultaneously, we also monitored Re traces, which, together with Im traces, were used to calculate the conductance of the fusion pore, an aqueous channel connecting the lumen of the vesicles with the external space (for calculations see Materials and methods). Occasionally, we observed the rapid onset of long-lasting (>5 s) changes of the Im signal (with the amplitude of 0.5–9 fF), either up-ward or down-ward, which were not accompanied by changes in the *Re* signal (Fig. V.2a, b). These types of discrete steps in Im were interpreted as either full fusion exocytosis (irreversible up-ward steps, Fig. V.2a), or as endocytosis (irreversible down-ward steps, Fig. V.2b) of large dense-core vesicles (Neher and Marty, 1982; Vardjan *et al.,* 2007). We have also observed up-ward steps in Im trace, followed by a down-ward step of similar amplitude within a few seconds (Fig. V.2c). These events most likely represent transient fusion of large

dense-core vesicles (Smets *et al.,* 1987; Vardjan *et al.,* 2007). For some of the reversible events in the Im trace, we also observed the crosstalk to the Re trace (Fig. V.2c, marked with +), which most likely mirrors the electrical resistance of the relatively narrow fusion pore (Spruce *et al.,* 1990; Vardjan *et al.,* 2007).

In conclusion, both reversible and irreversible fusion and fission elementary events were observed in lactotrophs previously exposed or not to $AlCl_3$, consistent with previous reports (Vardjan *et al*., 2007).

4.3 Aluminium reduces the frequency of stimulation-induced exocytotic events

We recorded spontaneous exocytotic activity for 8 min and then replaced the bath solution by an equivalent amount of saline solution containing 100 mM K^+ (K^+-stimulation). We recorded stimulated exocytotic activity for 8 more minutes in controls and in cells treated with aluminium.

First we focused on the occurrence of events, to see how aluminium exposure affects the appearance of fusion events. K^+-stimulation increased the frequency of reversible events 5-folds, from 0.08±0.01 events/s (n=7 patches) to 0.45±0.05 events/s (n=7 patches; P<0.001) (Fig. V.3a), as previously reported for similar conditions (Vardjan *et al*., 2007; Jorgačevski *et al*., 2008). In contrast, $AlCl_3$ treatment resulted in a reduction rather than an increase of the occurrence of transient events in response to K^+-stimulation (0.016±0.003 events/s *vs.* 0.004±0.001 events/s; n=10 and 10 patches, respectively; *P*<0.001) (Fig. V.3a). These results demonstrate that aluminium pre-treatment of cultured lactotrophs inhibits the K^+-stimulated secretory activity monitored at the elementary exocytotic event.

Next we separately analyzed the occurrence of irreversible events, which accounted for 1% of all fusion events observed in control conditions and 20% of all fusion events in cells treated with aluminium. The occurrence of irreversible upward C_m steps in controls (Fig. V.3b) was 0.004±0.002 events/s before K^+-stimulation and 0.002±0.001 events/s (*P*=0.14) after the K^+-stimulation.

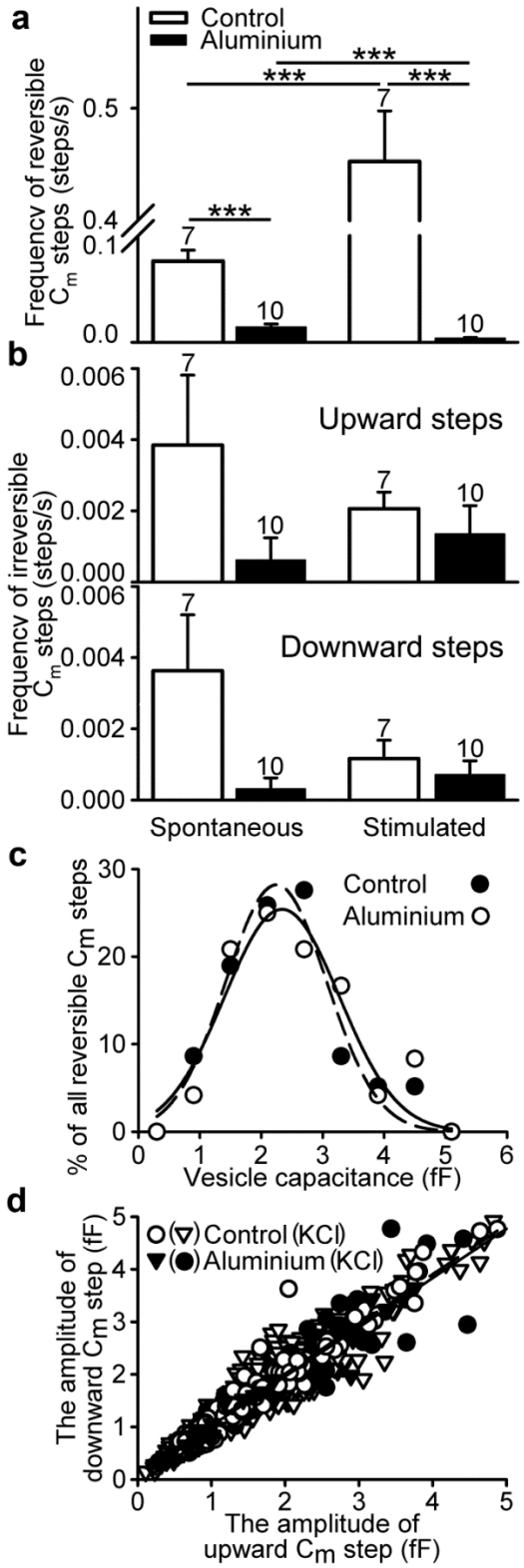

Figure V.3: Aluminium treatment of lactotrophs decreases the frequency of discrete steps in C_m.

The incubation of cultured lactotrophs with 30 µM $AlCl_3$ for 24 h decreases the frequency of capacitance steps measured in cell-attached configuration while the amplitude of the

steps remains unchanged. **(a)** The aluminium treatment significantly decreased the frequency of reversible capacitance steps in spontaneous (10 min incubation with the extracellular solution) and stimulated (10 min incubation with the K^+-enriched solution) conditions. Values are expressed as mean ± s.e.m; the number of cells is indicated above bars. ***P<0.001. **(b)** The aluminium treatment had no significant effect on the average frequency of upward and downward irreversible capacitance steps. **(c)** The distribution of the vesicle capacitance amplitudes of transient capacitance steps in controls (n=58 events; empty symbols) and in aluminium-treated cells (n=24 events; full symbols) was similar. These distributions, which are shown for a representative recording, were best-fitted with Gaussian curves with the mean values of 2.24±0.08 fF (controls; r^2=0.94; dashed line) and 2.34±0.12 fF (+$AlCl_3$; r^2=0.88; solid line) and were not statistically different (*P*=0.82). **(d)** The relationship between the amplitudes of upward and ensuing downward steps in short-lasting (<5 s) C_m changes was best-fitted with the linear regression lines of the form: y = (0.94±0.03) × x + (0.08±0.06) (r^2=0.90; solid line; aluminium-treated cells) and y= (0.95±0.01) × x + (0.12±0.02) (r^2=0.91; dashed line; controls) (P=0.99). Empty symbols denote control conditions and full symbols denote aluminium treatment. Circles mark spontaneous events and triangles mark stimulated events.

There was also no significant difference in cells treated with aluminium before and after K^+-stimulation (0.001±0.001 events/s *vs.* 0.001±0.001 events/s; *P*=0.45), respectively. The frequency of downward irreversible C_m steps in controls did not change significantly after K^+-stimulation (0.004±0.002 events/s before K^+-stimulation and 0.001±0.001 events/s after K^+-stimulation; *P*=0.06). The frequency of irreversible downward C_m steps remained similar in cells treated with aluminium (0.001±0.001 events/s before K^+-stimulation and 0.001±0.001 events/s after K^+-stimulation; P=0.49). As mentioned previously in the text, the irreversible events accounted for only a minor fraction of the total of 1580 events observed. These results are in line with those reported by Vardjan *et al.* (2007) and Jorgačevski *et al.* (2008) showing that the predominant elementary exocytotic events exhibit transient fusion pore openings before and after K^+-stimulation of lactotrophs.

4.4 Aluminium does not affect the diameter of fusing vesicles

We then measured C_v amplitudes to calculate the vesicles diameter (for calculations see Materials and Methods), which ranged from 67 to 414 nm, matching the diameters of PRL containing vesicles (Smets *et al*., 1987; Angleson

et al., 1999). To evaluate the putative effect of $AlCl_3$ treatment on the average diameters of the fusing vesicles, we analyzed C_v amplitudes in controls (1.74±0.09 fF; n=102) and in cells treated with aluminium (1.91±0.10 fF; n=99; P=0.21). Recalculated vesicle diameters in controls (239±6 nm) and in cells previously exposed to $AlCl_3$ (253±7 nm) did not differ significantly (*P*=0.15). Fig. V.3c shows the distribution of the amplitudes of C_v, with the modal peak of 2.2±0.1 fF for representative control cell and 2.3±0.1 fF for representative cell treated with aluminium. Therefore, aluminium treatment did not affect the size of fusing vesicles.

To further clarify that the observed transient events represent reopening of the single vesicle fusion pores and not consecutive full fusion exocytosis followed by endocytosis, we plotted C_v amplitudes of upward steps *versus* the ensuing C_v amplitudes of downward steps (Fig. V.3d). Slopes of fitted linear regression lines of controls and aluminium treated cells were close to 1. Moreover, correlation coefficients were high (r^2=0.94 and r^2=0.88, respectively), which means that each of the reported transient C_m events most likely represents transient exocytosis of a single vesicle.

4.5 Aluminium-induced changes of the fusion pore properties

PRL secretion in transient exocytosis might be limited not only by the frequency of transient fusion pore openings, but also by the fusion pore dwell-time and its diameter (Vardjan *et al*., 2007; Jorgačevski *et al*., 2008, 2010, 2011). To determine whether aluminium treatment changes the elementary properties of fusion pores, we analyzed the transient fusion pore events (Fig. V.3d). In these events, fusion pores establish stable diameters for several tens of milliseconds, which render them appropriate for the detailed analysis (Neher and Marty, 1982; Vardjan *et al*., 2007).

Surprisingly, aluminium treatment prolonged the average fusion pore dwell-time of transient fusion pore events (Fig. V.4a).

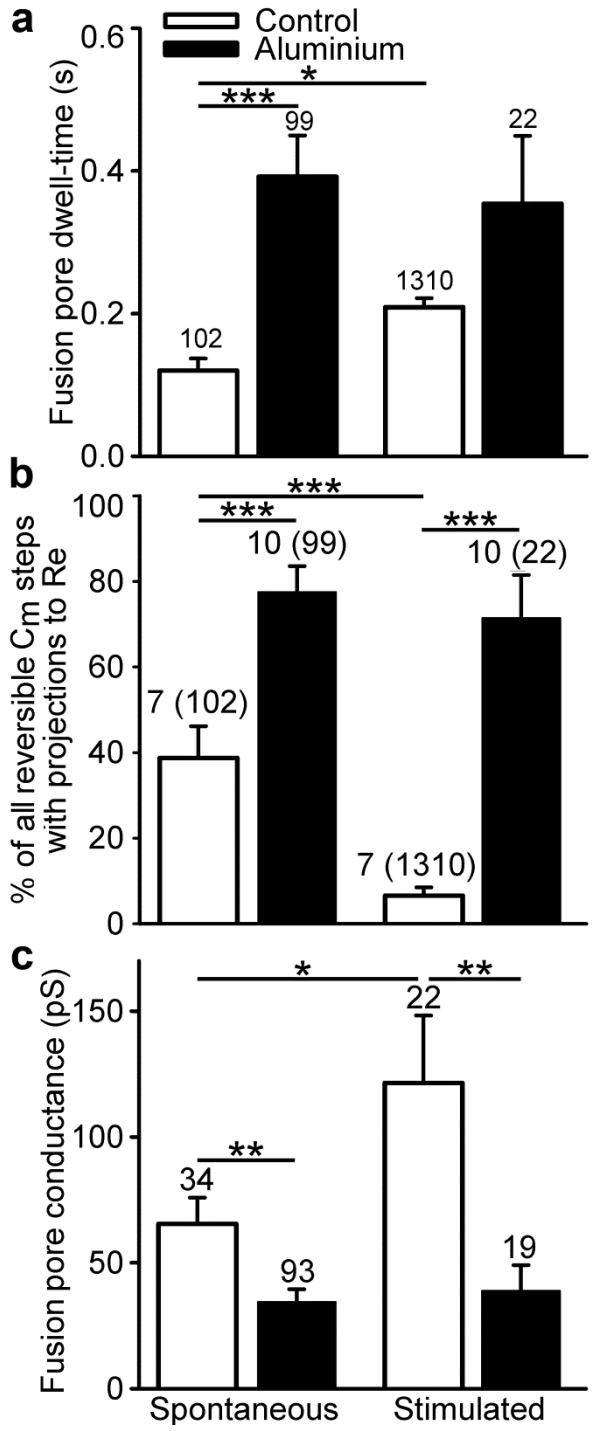

Figure V.4: Aluminium treatment prolongs the average fusion pore dwell-time and decreases the effective width of the fusion pores.

(a) The average fusion pore dwell-time of transient events increased in aluminium-treated cells (black bars), compared to the average fusion pore dwell-time of transient events in controls (white bars) in spontaneous conditions (Spontaneous). Similar effect, though less pronounced, was observed also in K^+-stimulated conditions (Stimulated). **(b)** The average percentage of transient events exhibiting crosstalk between Im and Re traces (narrow fusion pores, see Materials and Methods for details) calculated in 10 s epochs

was significantly higher in aluminium-treated cells (black bars), compared to the controls (white bars) in spontaneous and K^+-stimulated conditions. Numbers above bars correspond to the number of analysed patches and numbers in brackets to the total number of events. **(c)** On the same note, the average fusion pore conductance was significantly lower in aluminium-treated cells (black bars), compared to the controls (white bars). Values are expressed as mean ± s.e.m. of the number of events indicated above bars. *P<0.05, **P<0.01 and ***P<0.001.

The average fusion pore dwell-time of transient fusion events in non-stimulated (spontaneous) cells treated with aluminium was 0.39±0.06 s (range 0.02–4.48 s; n=99 events), which is significantly higher (P<0.001) than the average fusion pore dwell-time of transient events in controls (0.12±0.02 s; range 0.02–1.40 s; n=102 events). Controls responded to K^+-stimulation by significantly increasing the fusion pore dwell-time (0.21±0.01 s; range 0.01–3.85 s; n=1310 events, P<0.05), as previously reported (Vardjan *et al.,* 2007; Jorgačevski *et al.,* 2008). Remarkably, the average fusion pore dwell-time of cells which were treated with aluminium and stimulated with high K^+, was 0.35±0.10 s (range from 0.04–1.78 s, 22 events). These results show that cells that were treated with aluminium failed to respond to K^+-stimulation by increasing the average fusion pore dwell-time (0.39±0.06 s; n=99; spontaneous conditions vs. 0.35±0.10 s; n=22; simulated conditions, P=0.77).

In our experiments transient fusion pore events observed in the Im trace were often projected to the Re trace. These events most likely denoted fusion pore openings to a narrow pore diameter, which act as a resistor, and were therefore used to calculate fusion pore conductance (G_p) (Spruce *et al.,* 1990; Vardjan *et al*., 2007, Fig. V.2c). If the transient event in the Im trace is devoid of the projection to the *Re* trace, the conductance of the fusion pore is higher than the upper limit of the resolution of the experimental setup, which depends on the diameter of the fusing vesicle and the sine wave frequency of the lock-in amplifier (Debus and Lindau, 2000; Vardjan *et al*., 2007). Therefore, we next addressed the question whether aluminium treatment affects the diameter of fusion pores.

To assess the effect of aluminium on the average G_p, we first compared the occurrence of cross talks between Im and Re traces (Fig. V.4b). Under spontaneous conditions, we observed the occurrence of projections to the *Re*

trace in 39±7% of the total recorded events. The percentage of cross talks between Im and Re traces doubled after aluminium exposure (78±6%; P<0.001). These results are in line with those presented in Fig. V.1, where the inhibitory effect of aluminium on PRL release from cultured lactotrophs was observed in spontaneous and stimulated conditions. Likely, the reduced aluminium PRL release (Fig. V.1) is mediated in part also by the narrowing of the open fusion pores as determined from the reduced fusion pore conductance. Accordingly, K^+-stimulation significantly (*P*<0.001) decreased the percentage of cross talks between Im and Re traces to 7±2% in controls, whereas the percentage remained almost unchanged (P=0.59) in lactotrophs treated with aluminium (78±6% and 71±10% before and after K^+-stimulation, respectively).

These results suggest that aluminium prevents the stimulation-mediated fusion pore expansion. To further test the effect of aluminium on fusion pore expansion, we analyzed the G_p of the measurable fusion pores (Fig. V.4c). Measurable G_p values ranged from 7 to 536 pS, corresponding to fusion pore diameters of 0.37–3.20 nm. As can be observed in Fig. V.4c, the average G_p increased two-fold after K^+-stimulation in controls, from 65±10 pS to 121±27 pS (P<0.05), which is in agreement with previous study (Vardjan *et al*., 2007). Conversely, no significant difference (P>0.05) could be observed in aluminium-treated cells (35±5 pS and 39±10 pS) before and after K^+-stimulation, respectively. Compared to the controls under spontaneous conditions, aluminium treatment significantly (P<0.01) decreased the average G_p of the measurable fusion pores, in spontaneous and K^+-stimulated conditions.

Finally, we compared G_p of measurable fusion pores with similar diameters in controls and in cells treated with aluminium (Fig. V.5). Fig. 5a shows the frequency histogram of G_p of controls and of cells treated with aluminium. The G_p distribution appears Gaussian, however the peak parameters in controls and in cells treated with aluminium differ, which reflects the effect of aluminium on the relative heterogeneity of G_p values. We observed an aluminium-induced shift of the peak position toward lower G_p values (17.91±0.27 pS *vs*. 32.14±1.74 pS), which was also accompanied by the increase of the amplitude of the peak (relative

percentage of transient events) (47±1% versus 17±2% of the total events with measurable fusion pore conductance).

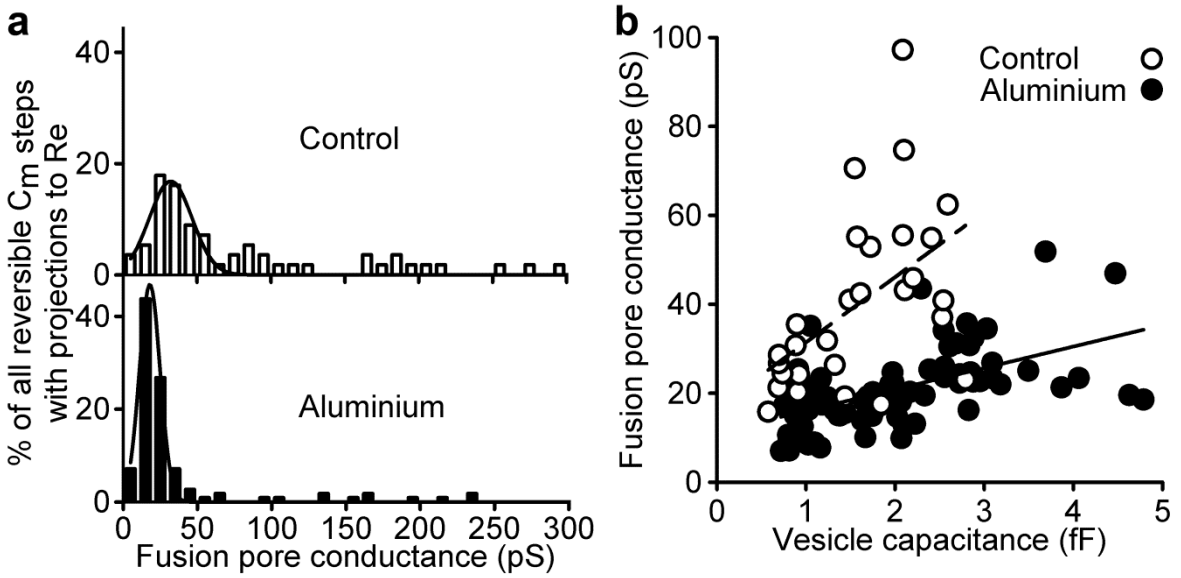

Figure V.5: Aluminium-treated lactotrophs exhibit reduced fusion pore conductance. We analysed reversible C_m steps with cross-talk between Im and Re traces in cultured lactotrophs, which were aluminium treated (black symbols) or not (white symbols). **(a)** The frequency histograms, where the ordinate represents the percentage of all reversible C_m steps and the abscissa the fusion pore conductance (G_p), were fitted with Gaussian functions with the following parameters: 32.14±1.74 pS (top, open columns, n=56 events) for controls and 17.91±0.27 pS (bottom, filled columns, n=112 events) for aluminium-treated cells. **(b)** The relationship between the vesicle capacitance (C_v) and G_p of spontaneous transient fusion events in controls (white symbols) and in aluminium-treated cells (black symbols). The lines represent best-fits of aluminium treated cells: G_p = (4.82±0.81) × x + (11.23±1.78) (r^2=0.30, r=0.55, P<0.0001, solid line) and of controls: G_p = (14.67±4.87) × x + (16.78±8.37) (r^2=0.26, r=0.51, P<0.01, dashed lines). Statistical analysis was performed using Pearson test for correlation coefficient, P<0.05 was considered significantly different from zero. Values are expressed as mean ± s.e.m..

A positive correlation between G_p and C_v of elementary fusion events under control conditions reflects the tendency of smaller vesicles to exhibit stable fusion pores with a narrower diameter (Jorgačevski *et al.,* 2010). However, aluminium treatment did not affect the average diameter of the fusing vesicles significantly, as shown in Fig. V.3c. These results, which are in line with those presented in Fig. V.4c, suggest that aluminium reduces G_p of elementary fusion events. Yet it could be argued that the aluminium induced decrease of G_p mirrors the engagement of

large dense-core vesicles with different C_v. Data displayed in Fig. V.5b argue against this hypothesis because events of the same amplitude of C_v displayed lower G_p values after the aluminium treatment than controls under spontaneous conditions. This constitutes unequivocal evidence that aluminium consistently reduced G_p values of transient fusion events of vesicles with similar diameters.

5 Discussion

The results show that the exposure of lactotrophs to sub-lethal concentrations (30 µM) of $AlCl_3$ reduces PRL release (Fig. V.1). This is likely due to aluminium-mediated changes in the fusion pore properties, summarized in Fig. V.6, which suggests that vesicles are entrapped in the unproductive exocytosis (Vardjan *et al.,* 2007).

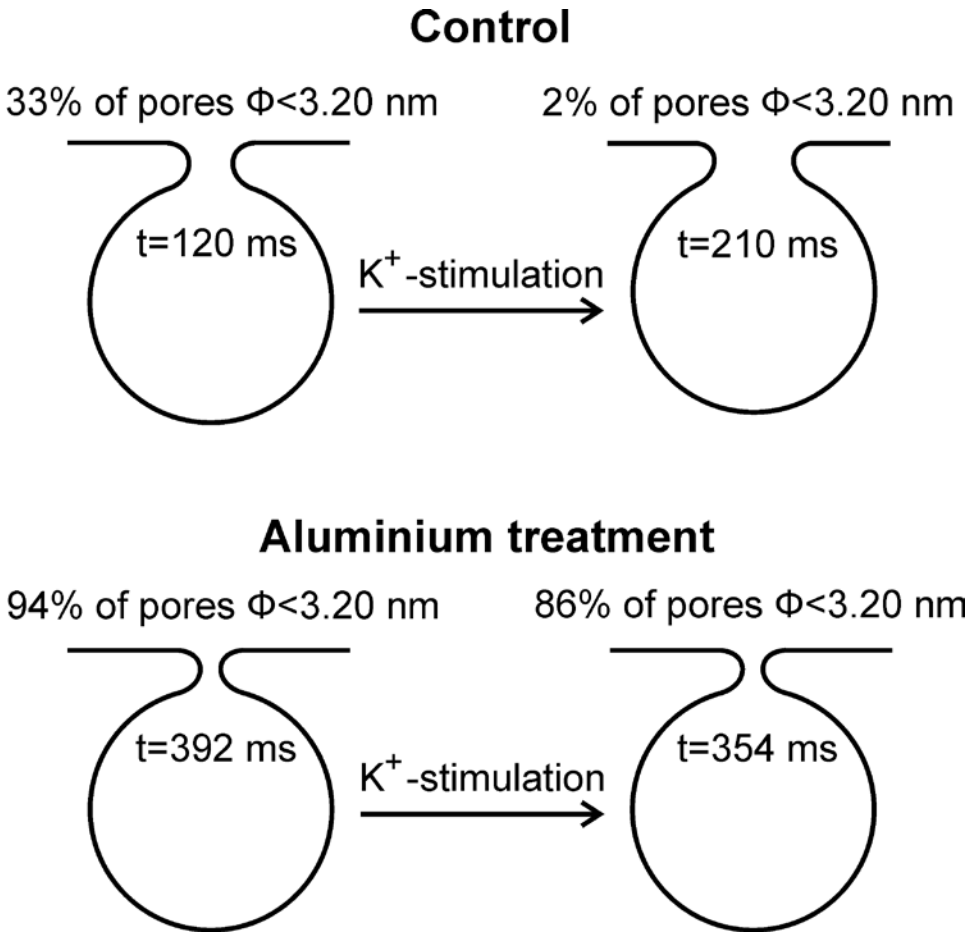

Figure V.6: Summarized effects of aluminium on transient exocytotic events in cultured lactotrophs.

Aluminium treatment increased the average fusion pore dwell-time of transient events (t) of non-stimulated cells, compared to controls (392 ms *vs.* 120 ms, respectively). In contrast, aluminium treatment decreased the average diameter (Ø) of measurable fusion pores of non-stimulated conditions: 33% of fusion pores were narrower than 3.20 nm (value represents the largest measured diameter, while larger diameters could not be measured due to the limitations of the experimental setup (Debus and Lindau, 2000) in controls, and 94% of fusion pores were narrower than 3.20 nm in aluminium-treated cells.

K^+-stimulation increased the average fusion pore dwell-time of controls to 210 ms, but decreased the average fusion pore dwell-time of aluminium-treated cells to 354 ms. K^+-stimulation decreased the percentage of fusion pores narrower than 3.20 nm to 2% in controls and to 86% in aluminium-treated cells.

One of the most discernible effects of aluminium was the reduced depolarization-evoked frequency of unitary exocytotic events in lactotrophs (Fig. V.3a). Interestingly, the average fusion pore dwell-time of transient exocytotic events was significantly prolonged after the addition of aluminium (Figs. V. 4a and V.6), whereas the fusion pore conductance was significantly decreased, compared with controls (Figs. V.4b, V.4c, V.5a, V.5b, V.6). Therefore, the aluminium-induced decrease of PRL release can be largely attributed to the entrapment of vesicles in a mode in which the release is hindered: unproductive exocytosis (Vardjan *et al*., 2007). Unproductive exocytosis denotes exocytosis, where a fusion pore transiently opens to the diameter of a specific molecule, which is stored in the vesicle (e.g. prolactin) (Vardjan *et al*., 2007). It is estimated that ~5 nm is the minimal diameter of the fusion pore which would allow the release of PRL from vesicular lumen to the extracellular space (Vardjan *et al*., 2007). Our data (Figs. V.1, V.3 and V.4) suggest that aluminium treatment diminishes secretion of PRL in part due to the large fraction (~94% and 86%; before and after the depolarization, respectively) of fusion pores that exhibited diameters below 3.2 nm (this value represents the largest measured fusion pore diameter, whereas the diameters of wider fusion pore could not be precisely determined due to the limitations of the experimental setup (Debus and Lindau, 2000)). Additionally, the addition of aluminium decreased the average Gp (Figs. V.4c and V.5b), while the size of the vesicles remained virtually unchanged (Fig. V.5b).

These results are in line with the previously reported serum PRL depletion in aluminium intoxication (Alessio *et al*., 1989; Galoyan *et al.* 2004), but provide a novel mechanistic explanation. Moreover, the results reported here are consistent with the previous studies revealing the inhibitory action of aluminium on the release of acetylcholine (Yokel *et al.,* 1994; Bielarczyk *et al*. 1998) and glutamate (Provan and Yokel, 1992), despite the differences of the models of aluminium neurotoxicosis. In mammalian brain aluminium reduces stimulated, Ca^{2+}-regulated

exocytosis of acetylcholine in synaptosomes (Bielarczyk *et al.*, 1998; Silva *et al.,* 2007) and in hippocampus (Yokel *et al.*, 1994). The inhibitory effect was partially attributed to the diminution of the quantal transmitter pool because the choline acetyltransferase is inhibited either by *in vivo* or *in vitro* exposure to aluminium (Bilkei-Gorzó, 1994). The effect was also tightly linked to the availability of acetyl-CoA and choline for the synthesis of acetylcholine during intensive firing (Bielarczyk *et al*., 1998).

Similar as in neurons, voltage-gated calcium influx triggers PRL secretion in lactotrophs (Stojilkovic *et al*., 2005). In contrast to neuronal active zones, where the pool of readily releasable vesicles is in close proximity to Ca^{2+} channels, in lactotrophs global Ca^{2+} oscillations are required to trigger secretion (Ben-Jonathan and Hnasko, 2001). Although pacemaking channels appear to be key determinants of excitability and its association with voltage-gated Ca^{2+} influx assures PRL secretion in lactotrophs, the regulatory mechanism of stimulation – secretion coupling remains one of the most poorly understood processes. Several lines of evidence strongly support a facilitating role of cAMP on PRL secretion predominantly in a protein kinase A- and Epac cAMP receptor-independent manner (Gonzalez-Iglesias *et al*., 2006). The results presented in this work do not exclude the possibility that aluminium interferes indirectly with PRL secretion in cultured lactotrophs: through aluminium-induced impairment of intracellular signal transduction pathways, binding to G proteins and alteration of the GTPase activity (G protein-mediated second messenger systems) (Matzel *et al.,* 1996), or modification of the adenylyl cyclase and phosphodiesterase activities (cyclic AMP second messenger system) and competitive inhibition of phosphatidylinositol 4,5-bisphosphate (PIP_2) hydrolysis by PIP_2-specific phospholipase C (phosphoinositide second messenger-producing system) (Shafer and Mundy, 1995). The inhibition of PIP_2-specific phospholipase C by aluminium (Shafer and Mundy, 1995) could, through CAPS (Ca^{2+}-dependent activator protein for secretion), affect the kinetics of regulated exocytosis (Grishanin *et al*., 2004). Experimental evidence supports the interference of aluminium with signaling cascades involving G proteins (Provan and Yokel, 1992; Rupnik and Zorec, 1995), cyclic AMP (Ebstein *et al.,* 1986), and calcium (Provan and Yokel, 1992), which

have been often implicated in the mechanisms of regulated exocytosis (Seino and Shibasaki, 2005). Moreover, distinct mechanisms appear to be involved in coupling of PRL secretion with different stimuli. For instances, the Na^+-Ca^{2+} and Na^+-H^+ antiporters were implicated in the regulation of PRL secretion elicited by inhibition of the Na^+/K^+-ATPase and by thyrotropin releasing hormone, respectively (Di Renzo *et al.,* 1995). However, following aluminium treatment of lactotrophs, a consistent suppression of the secretion was observed, which was independent of the conditions (resting, spontaneous or stimulating conditions). These observations strongly suggest that aluminium inhibits PRL secretion downstream of the stimulation – secretion coupling, as demonstrated in this work.

In spite of being intrinsically related processes, secretion (the release of cargo from secretory vesicles to the extracellular space) and the formation of an aqueous fusion pore between the vesicle and the plasma membrane can be considered separately. PRL secretion only occurs when the fusion pore expansion is sufficient to allow PRL diffusion into the cell exterior. Otherwise release-unproductive exocytosis takes place - the fusion of vesicle with the plasma membrane is not followed by secretion of PRL (Vardjan *et al.,* 2007). The presented data clearly show that aluminium exposure prevented fusion pore dilation (Figs. 4b, 4c and 5b) that significantly diminished PRL secretion (Fig. V.1). These results constitute evidence that aluminium may also compromise the secretory activity of other cells, accounting for a more broad impairment of neurotransmission during intoxication by aluminium (Gonçalves and Silva, 2007).

The potency and efficacy of vesicle cargo discharge through fusion pores depends on the perfect match of the curvature of the opposing membranes, since it was demonstrated that the size of the t-/v-SNARE complex is directly proportional to the diameter of the discharging vesicle (Cho *et al.*, 2005). Recently, the occurrence of repetitive, transient fusion pore events with energetically stable narrow pore diameters in lactotrophs was interpreted as a new intermediate state in the sequence of reactions between the vesicle and the plasma membrane that take place after the establishment of hemi-fusion stalk and the formation of a fusion pore (Jorgačevski *et al.,* 2010). We speculate that aluminium favors the stabilization of this intermediate state. Aluminium-induced alterations of membrane

properties, like modification of membrane fluidity and local membrane lipid composition, have been reported (Silva *et al.,* 2002). According to the stalk-pore model of membrane fusion, which emphasizes the role of hydrophobic attractions and curvature stress in lipid packing/mixing and the transient formation of intermediate membrane structures, the intrinsic negative curvature of cholesterol contributes to a critical local negative curvature that supports formation of lipidic fusion intermediates (Furber *et al.,* 2009). Exposure to the dietary aluminium leads to a significant reduction of the cholesterol/phospholipid molar ratio in rat brain synaptosomes (Silva *et al.,* 2002) and could thus be responsible for the observed change in the G_p/C_v ratio (Fig. V.5b).

5.1 Conclusion

Overall, the present study demonstrates that aluminium affects the vesicle membrane fusion process, which not only chiefly supports the intercellular communication in the nervous and endocrine systems but also functions as a well-conserved apparatus for membrane fusion from yeast to mammalian cells (Chen and Scheller, 2001). In contrast to the previous studies of aluminium effect on neurotransmitter secretion (Banin and Meiri, 1987; Provan and Yokel, 1992; Yokel *et al*., 1994; Bielarczyk *et al*., 1998; Silva *et al*., 2007), the present results highlight prominent differences in the characteristics of elementary Ca^{2+} regulated exocytotic events after exposure to aluminium, which motivate additional mechanistic studies yielding a more precise determination of the sequence of events which lead to aluminium-induced alterations of fusion pore properties.

6 References

Alessio L, Apostoli P, Ferioli A, Di Sipio I, Mussi I, Rigosa C (1989). Behaviour of biological indicators of internal dose and some neuro-endocrine tests in aluminium workers. *Med Lav* 80:290-300.

Alfrey AC, LeGendre GR, Kaehny WD (1976). The dialysis encephalopathy syndrome - Possible aluminum intoxication. *N Engl J Med* 294:184-188.

Allen VG, Fontenot JP, Rahnema SH (1991). Influence of aluminum-citrate and citric acid on tissue mineral composition in wether sheep. *J Anim Sci* 69:792-800.

Angleson J, Cochilla A, Kilic G, Nussinovitch I, Betz W (1999). Regulation of dense core release from neuroendocrine cells revealed by imaging single exocytotic events. *Nat Neurosci* 2:440-446.

Agency for Toxic Substances and Disease Registry (ATSDR) (2008). *Toxicological Profile for Aluminium*, U.S. Department of Health and Human Services, Division of Toxicology and Environmental Medicine/Applied Toxicology Branch, Atlanta.

Banin E, Meiri H (1987). Impaired control of information transfer at an isolated synapse treated by aluminum: is it related to dementia? *Brain Res* 423:359-363.

Ben-Jonathan N, Hnasko R (2001). Dopamine as a prolactin (PRL) inhibitor. *Endocr Rev* 22:724-763.

Ben-Tabou S, Keller E, Nussinovitch I (1994). Mechanosensitivity of voltage-gated calcium currents in rat anterior pituitary cells. *J Physiol* 476:29-39.

Bielarczyk H, Tomaszewicz M, Szutowicz A (1998). Effect of aluminum on acetyl-CoA and acetylcholine metabolism in nerve terminals. *J Neurochem* 70:1175-1181.

Bilkei-Gorzó A (1994). Effect of chronic treatment with aluminum compound on rat brain choline acetyltransferase activity. *Pharmacol Toxicol* 74:359-360.

Calejo AI, Rodriguez E, Silva VS, Jorgačevski J, Stenovec M, Kreft M, Santos C, Zorec R, Gonçalves PP (2010). Life and death in aluminium-exposed cultures of rat lactotrophs studied by flow cytometry. *Cell Biol Toxicol* 26:341-353.

Chen YA, Scheller RH (2001). SNARE-mediated membrane fusion. *Nat Rev Mol Cell Biol* 2:98-106.

Cho WJ, Jeremic A, Jena BP (2005). Size of supramolecular SNARE complex: membrane-directed self-assembly. *J Am Chem Soc* 127:10156-10157.

Debus K, Lindau M (2000). Resolution of patch capacitance recordings and of fusion pore conductances in small vesicles. *Biophys J* 78:2983-2997.

Di Renzo G, Amoroso S, Bassi A, Fatatis A, Cataldi M, Colao AM, Lombardi G, Annunziato L (1995). Role of the Na^{+}-Ca^{2+} and Na^{+}-H^{+} antiporters in prolactin release from anterior pituitary cells in primary culture. *Eur J Pharmacol* 294:11-15.

Ebstein RP, Oppenheim G, Ebstein BS, Amiri, Z, Stessman J (1986). The cyclic AMP second messenger system in man: the effects of heredity, hormones, drugs, aluminum, age and disease on signal amplification. *Prog Neuropsychopharmacol Biol Psychiatry* 10:323-353.

Freeman ME, Kanyicska B, Lerant A, Nagy G (2000). Prolactin: structure, function, and regulation of secretion. *Physiol Rev* 80:1523-1631.

Furber KL, Churchward MA, Rogasevskaia TP, Coorssen JR (2009). Identifying critical components of native Ca^{2+}-triggered membrane fusion. Integrating studies of proteins and lipids. *Ann N Y Acad Sci* 1152:121-134.

Galoyan AA, Shakhlamov VA, Aghajanov MI, Vahradyan HG (2004). Hypothalamic proline-rich polypeptide protects brain neurons in aluminum neurotoxicosis. *Neurochem Res* 29:1349-1357.

Golub MS, Donald JM, Gershwin ME, Keen CL (1989). Effects of aluminum ingestion on spontaneous motor activity of mice. *Neurotoxicol Teratol* 11:231-235.

Gonçalves PP, Silva VS (2007). Does neurotransmission impairment accompany aluminium neurotoxicity? *J Inorg Biochem* 101:1291-1338.

Gonçalves PP, Stenovec M, Chowdhury HH, Grilc S, Kreft M, Zorec R (2008). Prolactin secretion sites contain syntaxin-1 and differ from ganglioside monosialic acid rafts in rat lactotrophs. *Endocrinology* 149:4948-4957.

Gonzalez-Iglesias AE, Jiang Y, Tomić M, Kretschmannova K, Andric SA, Zemkova H, Stojilkovic SS (2006). Dependence of electrical activity and calcium influx-controlled prolactin release on adenylyl cyclase signaling pathway in pituitary lactotrophs. *Mol Endocrinol* 20:2231-2246.

Grishanin R, Kowalchyk J, Klenchin V, Ann K, Earles C, Chapman E, Gerona R, Martin T (2004). CAPS Acts at a Prefusion Step in Dense-Core Vesicle Exocytosis as a PIP2 Binding Protein. *Neuron* 43:551-562.

Jorgačevski J, Stenovec M, Kreft M, Bajić A, Rituper B, Vardjan N, Stojilkovic SS, Zorec R (2008). Hypotonicity and peptide discharge from a single vesicle. *Am J Physiol Cell Physiol* 295:C624-C631.

Jorgačevski J, Fosnaric M, Vardjan N, Stenovec M, Potokar M, Kreft M, Kralj-Iglic V, Iglic A, Zorec R (2010). Fusion pore stability of peptidergic vesicles. *Mol Membr Biol* 27:65-80.

Jorgačevski J, Potokar M, Grilc S, Kreft M, Liu W, Barclay JW, Bückers J, Medda R, Hell SW, Parpura V, Burgoyne RD, Zorec R (2011). Munc18-1 tuning of vesicle merger and fusion pore properties. *J Neurosci* 31:9055-9066.

Kreft M, Zorec R (1997). Cell-attached measurements of attofarad capacitance steps in rat melanotrophs. *Pflugers Arch* 434:212-214.

Lollike K, Lindau M (1999). Membrane capacitance techniques to monitor granule exocytosis in neutrophils. *J Immunol Methods* 232:111-120.

Matzel LD, Rogers RF, Talk AC (1996). Bidirectional regulation of neuronal potassium currents by the G-protein activator aluminium fluoride as a function of intracellular calcium concentration. *Neuroscience* 74:1175–1185.

Neher E, Marty A (1982). Discrete changes of cell membrane capacitance observed under conditions of enhanced secretion in bovine adrenal chromaffin cells. *Proc Natl Acad Sci USA* 79:6712-6716.

Pow DV, Morris JF (1991). Membrane routing during exocytosis and endocytosis in neuroendocrine neurones and endocrine cells: use of colloidal gold particles and immunocytochemical discrimination of membrane compartments. *Cell Tissue Res* 264:299-316.

Provan SD, Yokel RA (1992). Aluminum inhibits glutamate release from transverse rat hippocampal slices: role of G proteins, Ca^{2+} channels and protein kinase C. *Neurotoxicology* 13:413-420.

Reusche E, Lindner B, Arnholdt H (1994). Widespread aluminium deposition in extracerebral organ systems of patients with dialysis-associated encephalopathy. *Virchows Arch* 424:105-112.

Rupnik M, Zorec R (1995). Intracellular Cl^- modulates Ca^{2+}-induced exocytosis from rat melanotrophs through GTP-binding proteins. *Pflugers Arch* 431:76-83.

Seino S, Shibasaki T (2005). PKA-dependent and PKA-independent pathways for cAMP-regulated exocytosis. *Physiol Ver* 85:1303-1342.

Shafer TJ, Mundy WR (1995). Effects of aluminum on neuronal signal transduction: mechanisms underlying disruption of phosphoinositide hydrolysis. *Gen Pharmacol* 26:889-895.

Silva VS, Cordeiro JM, Matos MJ, Oliveira CR, Gonçalves PP (2002). Aluminium accumulation and membrane fluidity alteration in synaptosomes isolated from brain cortex following aluminium ingestion: effect of cholesterol. *Neurosci Res* 44:181-193.

Silva VS, Nunes MA, Cordeiro JM, Calejo AI, Santos S, Neves P, Sykes A, Morgado F, Dunant Y, Gonçalves PP (2007). Comparative effects of aluminum and ouabain on synaptosomal choline uptake, acetylcholine release and (Na^+/K^+)ATPase. *Toxicology* 236:158-177.

Smets G, Velkeniers B, Finne E, Baldys A, Gepts W, Vanhaelst L (1987). Postnatal development of growth hormone and prolactin cells in male and female rat pituitary. An immunocytochemical light and electron microscopic study. *J Histochem Cytochem* 35:335-341.

Spruce A, Breckenridge L, Lee A, Almers W (1990). Properties of the fusion pore that forms during exocytosis of a mast cell secretory vesicle. *Neuron* 4:643-654.

Stenovec M, Kreft M, Poberaj I, Betz WJ, Zorec R (2004). Slow spontaneous secretion from single large dense-core vesicles monitored in neuroendocrine cells. *FASEB J* 18:1270-1272.

Stojilkovic SS (2005). Ca^{2+}-regulated exocytosis and SNARE function. *Trends Endocrinol Metab* 16:81-83.

Stojilkovic SS, Tabak J, Bertram R (2010). Ion channels and signalling in the pituitary gland. *Endocr Rev* 31:845–915.

Tsunoda M, Sharma RP (1999). Altered dopamine turnover in murine hypothalamus after low-dose continuous oral administration of aluminum. *J Trace Elem Med Bio* 13:224-231.

Vardjan N, Stenovec M, Jorgačevski J, Kreft M, Zorec R (2007). Subnanometer fusion pore in spontaneous exocytosis of peptidergic vesicles. *J Neurosci* 27:4737-4746.

Walton JR (2004). A bright field/fluorescent stain for aluminum: its specificity, validation, and staining characteristics. *Biotech Histochem* 79:169-176.

Yokel RA, Allen DD, Meyer JJ (1994). Studies of aluminum neurobehavioral toxicity in the intact mammal. *Cell Mol Neurobiol* 14:791-808.

Zorec R, Sikdar S, Mason W (1991). Increased cytosolic calcium stimulates exocytosis in bovine lactotrophs. Direct evidence from changes in membrane capacitance. *J Gen Physiol* 97:473-497.

Chapter VI - Conclusions

In this work the results show that an increase in cAMP affects the fusion pore properties studied in single hormone-secreting cell. By elevating the concentration of a cAMP analog, dbcAMP, a biphasic effect on prolactin (PRL) secretion from pituitary lactotrophs was observed. Moreover, at high cAMP concentrations vesicles exhibiting a wide diameter fusion pore state were recorded, however too narrow to permit hormone discharge from the vesicle lumen. These effects likely involve contributions by hyperpolarization cyclic nucleotide activated (HCN) channels, as key effectors, since at least some of these were found present on secretory vesicles and also factors that modulated HCN expression/function modulated cAMP-induced exocytotic activity and fusion pore properties. Furthermore, by using a common neurotoxic agent, such as aluminium at sub-lethal concentrations, we recorded an inhibition of PRL release which was associated with unitary exocytic activity exhibiting stabilized fusion pores to a relatively narrow diameter.

Cyclic AMP regulates PRL secretion from pituitary lactotrophs by modulating fusion pore properties. We propose that relatively high cAMP levels stabilizes an intermediate exocytic stage, where fusion is transient and pores are wider and with longer dwell-times, which consequently reduces the probability of the secretory vesicles to enter into fully fused state. This represents a post-fusion rate-limiting step which likely leads to a reduction on PRL secretion (Chapter II).

● Increasing concentrations of forskolin (adenylyl cyclases activator) enhance cAMP concentration in a concentration dependent way (Fig. II.1a).

● PRL secretion reveals a biphasic dose-dependent response to increasing intracellular cAMP levels, low concentration of cAMP-increasing agents (2-10 µM forskolin and 2.5-5 mM dbcAMP) stimulated PRL release, while higher concentration (50 µM forskolin and >10 mM dbcAMP) reduced PRL release (Fig. II.1b and c).

● All cAMP- increasing agents tested enhance transient exocytotic activity, namely, IBMX or forskolin doubled and dbcAMP tripled its incidence (Fig. II.2d). On the contrary, no changes were observed in full-fusion events incidence (Fig. II.2d). dbcAMP mainly modified frequency of small transient vesicles (147 ± 17 nm), while in controls we observed two populations of vesicles with different diameters (143 ± 17 nm and 226 ± 26 nm; Fig. II.3c).

● Fusion pore widening is significantly enhanced by dbcAMP. The percentage of fusion pores with relatively wider diameters (without projections to the Re) enhanced from 67% to 99% (Table II.1). Simultaneously, the average fusion pore conductance (G_p) of measurable pores increased from 23 ± 2 pS to 32 ± 6 pS (Fig. II.4a) and the G_p of vesicles with a given vesicle capacitance (C_v) increased threefold (Fig. II.6a).

● The probability of open fusion pore state and its dwell-time were also significantly enhanced (three- and twofold, respectively) after incubation with dbcAMP (Fig. II.4c).

● The elevation of dbcAMP changed transient fusion events nature by turning them into periodic bursts (Fig. II.5), with time between consecutive events relatively constant (Fig. II.5d and e). Additionally, dbcAMP increased the probability of periodicity from 0.1% to 15% (Fig. II.5h and i).

Heterogeneous expression of HCN channels with different patterns in rat tissues attests to the complexity of cAMP–HCN channel signaling (Chapter III).

● The expression of the four HCN isoforms was confirmed at mRNA and proteins levels in heart, pituitary, kidney and brain (Fig. III.2 and 3; Table 1), although with different expression patterns. The mRNA transcript encoding HCN2 was the most abundant in kidney, heart and pituitary (Fig. III.2 left panel), while the predominant transcript isoform in brain was HCN1 (Fig. III.3b; right panel). HCN4 isoform was the most abundant protein for all the analyzed tissues (Fig. III.2 and 3b). The

specific antibodies against HCN isoforms detected not only full-length chains but also fragments with lower molecular weights (Fig. III.1, 2 and 3; Table 1).

In cAMP-induced exocytic events of rat pituitary lactotrophs, the fusion pore diameter is modulated by HCN channels. Most likely, HCN channels present in vesicle and plasma membrane affect local cation flux, which induces changes in membrane curvature modulating fusion pore diameter (Chapter IV).

● The most abundant mRNA transcript encodes HCN2 isoform (0.54%, compared to β-actin). HCN2 protein is expressed 22 ± 3% in PRL-containing vesicle and 55 ± 5% in lactotrophs plasma membranes (Fig. IV.1c).

● 24h transfected lactotrophs with plasmids DNA encoding HCN2, over-expressed HCN2 in both vesicle and plasma membranes (Fig. IV.2) and exhibited transient and full-fusion exocytotic events (Fig. IV.3e).

● In HCN2 over-expressing lactotrophs, dbcAMP significantly increased not only the occurrence of transient events but also of full-fusion events (Fig. IV.4c and d). Accordingly, in non-transfected lactotrophs HCN channels blocker, ZD7288, decreased to less than half the occurrence of transient and full-fusion events (Fig. IV.4e and f).

● In the presence of dbcAMP, HCN2 over-expression and ZD7288 incubation changed the relation between G_p and C_v (Fig. IV.5a). Moreover, HCN2 over-expression induced a decrease of the percentage of transient events with narrow pores from 25% to 17% and to 7% after incubation with dbcAMP (Fig. IV.5b). In lactotrophs incubated with ZD7288 the percentage of transient events with narrow pores increased from 25% to 38% under non-stimulated conditions and up to 55% after dbcAMP stimulation (Fig. IV.5b).

The 24h exposure of pituitary lactotrophs cultures to micromolar concentration of aluminium chloride prevents fusion pore expansion in response to K^+-depolarizing stimulus, downstream of stimulus and likely

directly interfering with the fusion pore, resulting in inhibition of PRL secretion (Chapter V).

● In cultured lactotrophs, K^+-stimulation enhanced 1.3-fold PRL release, while PRL release remained unchanged with 30 µM $AlCl_3$ pre-treatment (Fig. V.1).

● In control cells a fivefold increase in the occurrence of transient fusion events was observed after stimulation with depolarizing K^+ concentration, while in lactotrophs pre-treated with $AlCl_3$ it was reduced by 75% (Fig. V.3a). Apparently, $AlCl_3$ pre-treatment had no major impact on full-fusion and endocytic events (Fig. V.3b).

● The average vesicle diameter and the C_v distribution of transient events remained unchanged after pre-treatment of cell cultures with $AlCl_3$ (239 ± 6 nm; 2.2 ± 0.1 fF *vs.* 253 ± 7 nm; 2.3 ± 0.1 fF) (Fig. V.3c).

● In $AlCl_3$ pre-treated lactotrophs, the fusion pore dwell-time remained unchanged after K^+-stimulation (0.39 ± 0.06 s to 0.35 ± 0.10 s), while in control cells K^+-stimulation elicited a 1.75-fold increase of the fusion pore dwell-time (Fig. V.4a).

● Pre-treatment of lactotrophs with $AlCl_3$ prevents widening of fusion pore in response to K^+-stimulation. The percentage of narrow pores increased from 39 ± 7% to 78 ± 6%, while in control cells reduced to 7±2% (Fig. V.4b). Additionally, $AlCl_3$ reduced the average Gp (35 ± 5 pS in spontaneous and 39 ± 10 pS after K+-depolarizing conditions), when compared to control cells (65 ± 10 pS in spontaneous and 121 ± 27 pS after stimulation; Fig. V.4c). Moreover, vesicles with similar C_v exhibit lower G_p values after pre-treatment with $AlCl_3$ (Fig. V.5).

Future perspectives

Since it was discovered, cAMP has been extensively studied and implicated in several physiological roles. Studies regarding cAMP in the context of regulated exocytosis are increasing and what was initially believed to be PKA-dependent, is currently being revised in light of the new effectors involved, namely Epac and HCN channels. Nowadays, it is important to understand the role of each of the cAMP signaling pathways on exocytotic activity and vesicular release.

To pursue this it is imperative to: understand the molecular mechanism involving cAMP-induced and HCN-dependent effect on the fusion pore; assess possible interactions between cAMP effectors (PKA, Epac and HCN channels) and several proteins and/or lipids implicated in exocytotic apparatus; and evaluate these effectors role in the pre- and post-fusion stages of vesicular content release. Furthermore, clarify HCN signaling pathway, which might lead to the discovery of secretion targeting new drugs.

Chapter VII - References

Accili EA, Proenza C, Baruscotti M, DiFrancesco D (2002). From funny current to HCN channels: 20 years of excitation. *News Physiol Sci* 17:32-37.

Agency for Toxic Substances and Disease Registry (ATSDR) (2008). *Toxicological Profile for Aluminium*, U.S. Department of Health and Human Services, Division of Toxicology and Environmental Medicine/Applied Toxicology Branch, Atlanta.

Alessio L, Apostoli P, Ferioli A, Di Sipio I, Mussi I, Rigosa C (1989). Behaviour of biological indicators of internal dose and some neuro-endocrine tests in aluminium workers. *Med Lav* 80:290-300.

Alés E, Tabares L, Poyato JM, Valero V, Lindau M, Alvarez de Toledo G (1999). High calcium concentrations shift the mode of exocytosis to the kiss-and-run mechanism. *Nat Cell Biol* 1:40–44.

Alfrey AC, LeGendre GR, Kaehny WD (1976). The dialysis encephalopathy syndrome - Possible aluminum intoxication. *N Engl J Med* 294:184-188.

Allen VG, Fontenot JP, Rahnema SH (1991). Influence of aluminum-citrate and citric acid on tissue mineral composition in wether sheep. *J Anim Sci* 69:792-800.

Altomare C, Terragnim B, Brioschi C, Milanesi R, Pagliuca C, Viscomi C, Moroni A, Baruscotti M, DiFrancesco D (2003). Heteromeric HCN1-HCN4 channels: a comparison with native pacemaker channels from the rabbit sinoatrial node. *J Physiol* 549:347-359.

Alvarez de Toledo G, Fernández-Chacón R, Fernández J (1993). Release of secretory products during transient vesicle fusion. *Nature* 363:554–558.

Angleson J, Cochilla A, Kilic G, Nussinovitch I, Betz W (1999). Regulation of dense core release from neuroendocrine cells revealed by imaging single exocytotic events. *Nat Neurosci* 2:440–446.

Aponte Y, Lien CC, Reisinger E, Jonas P (2006). Hyperpolarization-activated cation channels in fast-spiking interneurons of rat hippocampus. *J Physiol* 574:229-243.

Banin E, Meiri H (1987). Impaired control of information transfer at an isolated synapse treated by aluminum: is it related to dementia? *Brain Res* 423:359-363.

Barbuti A, Gravante B, Riolfo M, Milanesi R, Terragni B, DiFrancesco D (2004). Localization of pacemaker channels in lipid rafts regulates channel kinetics. *Circ Res* 94:1325-1331.

Barg S, Olofsson C, Schriever-Abeln J, Wendt A, Gebre-Medhin S, Renstrom E, Rorsman P (2002). Delay between fusion pore opening and peptide release from large-dense-core vesicles from neuroendocrine cells. *Neuron* 33:287–299.

Battey NH, James NC, Greenland AJ, Brownleec C (1999). Exocytosis and Endocytosis. *The Plant Cell* 11:643-659.

Beaumont V, Zucker RS (2000). Enhancement of synaptic transmission by cyclic AMP modulation of presynaptic Ih channels. *Nat Neurosci* 3:133-141.

Ben-Jonathan N, Hnasko R (2001). Dopamine as a prolactin (PRL) inhibitor. *Endocr Rev* 22:724-763.

Ben-Tabou S, Keller E, Nussinovitch I (1994). Mechanosensitivity of voltage-gated calcium currents in rat anterior pituitary cells. *J Physiol* 476:29–39.

Berridge MJ, Bootman MD, Roderick HL (2003). Calcium signalling: dynamics, homeostasis and remodelling. *Nat Rev Mol Cell Biol* 4:517-529.

Betz W, Bewick G (1992). Optical analysis of synaptic vesicle recycling at the frog neuromuscular junction. *Science* 255:200–203.

Biel M, Wahl-Schott C, Michalakis S, Zong X (2009). Hyperpolarization-activated cation channels: from genes to function. *Physiol Rev* 89:847-885.

Bielarczyk H, Tomaszewicz M, Szutowicz A (1998). Effect of aluminum on acetyl-CoA and acetylcholine metabolism in nerve terminals. *J Neurochem* 70:1175-1181.

Bilkei-Gorzó A (1994). Effect of chronic treatment with aluminum compound on rat brain choline acetyltransferase activity. *Pharmacol Toxicol* 74:359-360.

Bole-Feysot C, Goffin V, Edery M, Binart N, Kelly P (1998). Prolactin (PRL) and its receptor: actions, signal transduction pathways and phenotypes observed in PRL receptor knockout mice. *Endocr Rev* 19:225–268.

Branham MT, Mayorga LS, Tomes CN (2006). Calcium-induced acrosomal exocytosis requires cAMP acting through a PKA-independent, EPAC-mediated pathway. *J Biol Chem* 281:8656-8666.

Braun M, Ramracheya R, Johnson PR, Rorsman P (2009). Exocytotic properties of human pancreatic beta-cells. *Ann N Y Acad Sci* 1152:187-193.

Breckenridge LJ, Almers W (1987). Currents through the fusion pore that forms during exocytosis of a secretory vesicle. *Nature* 328:814–817.

Brown HF, DiFrancesco D, Noble SJ (1979). How does adrenaline accelerate the heart? *Nature* 280:235-236.

Burgess TL, Kelly RB (1987). Constitutive and regulated secretion of proteins. *Annu Rev Cell Biol* 3:243-293.

Calejo AI, Rodriguez E, Silva VS, Jorgačevski J, Stenovec M, Kreft M, Santos C, Zorec R, Gonçalves PP (2010). Life and death in aluminium-exposed cultures of rat lactotrophs studied by flow cytometry. *Cell Biol Toxicol* 26:341-353.

Ceccarelli B, Hurlbut W, Mauro A (1973). Turnover of transmitter and synaptic vesicles at the frog neuromuscular junction. *J Cell Biol* 57:499–524.

Chang YC, Ma JF, Matsumoto H (1998). Mechanism of Al-induced iron chlorosis in wheat (*Triticum aestivum*). Al-inhibited biosynthesis and secretion of phytosiderophore. *Physiol Plant* 102:9–15.

Chen EC, Javors MA, Norris C, Siler-Khodr T, Schenken RS, King TS (2004). Dependence of 3',5'-cyclic adenosine monophosphate--stimulated gonadotropin-releasing hormone release on intracellular calcium levels and L-type calcium channels in superfused GT1-7 neurons. *J Soc Gynecol Investig* 11:393-398.

Chen G, Gutman DA, Zerby SE, Ewing AG (1996). Electrochemical monitoring of bursting exocytotic events from the giant dopamine neuron of Planorbis corneus. *Brain Res* 733:119–124.

Chen S, Liang MC, Chia JN, Ngsee JK, Ting AE (2001). Rab8b and its interacting partner TRIP8b are involved in regulated secretion in AtT20 cells. *J Biol Chem* 276:13209-13216.

Chen X, Wang L, Zhou Y, Zheng LH, Zhou Z (2005). "Kiss-and-run" glutamate secretion in cultured and freshly isolated rat hippocampal astrocytes. *J Neurosci* 25:9236-9243.

Chen YA, Scheller RH (2001). SNARE-mediated membrane fusion. *Nat Rev Mol Cell Biol* 2:98-106.

Chernomordik LV, Kozlov MM (2008). Mechanics of membrane fusion. *Nat Struct Mol Biol* 15:675–683.

Cho HJ, Furness JB, Jennings EA (2011). Postnatal maturation of the hyperpolarization-activated cation current, I(h), in trigeminal sensory neurons. *J Neurophysiol* 106:2045-2056.

Cho WJ, Jeremic A, Jena BP (2005). Size of supramolecular SNARE complex: membrane-directed self-assembly. *J Am Chem Soc* 127:10156-10157.

Chow R, von Rüden L, Neher E (1992). Delay in vesicle fusion revealed by electrochemical monitoring of single secretory events in adrenal chromaffin cells. *Nature* 356:60–63.

Churchward MA, Rogasevskaia T, Hofgen J, Bau J, Coorssen JR (2005). Cholesterol facilitates the native mechanism of Ca^{2+}-triggered membrane fusion. *J Cell Sci* 118:4833–4848.

Cochilla AJ, Angleson JK, Betz WJ (2000). Differential regulation of granule-to-granule and granule-to-plasma membrane fusion during secretion from rat pituitary lactotrophs. *J Cell Biol* 150:839–848.

Coorssen JR, Zorec R (2012). Regulated exocytosis per partes. *Cell Calcium* 52:191–195.

Dannies P (2003). Manipulating the reversible aggregation of protein hormones in secretory granules: potential impact on biopharmaceutical development. *BioDrugs* 17:315–324.

Darios F, Wasser C, Shakirzyanova A, Giniatullin A, Goodman K, Munoz-Bravo JL, Raingo J, Jorgačevski J, Kreft M, Zorec R, Rosa JM, Gandia L, Gutiérrez LM, Binz T, Giniatullin R, Kavalali ET, Davletov B (2009). Sphingosine facilitates

SNARE complex assembly and activates synaptic vesicle exocytosis. *Neuron* 62:683–694.

de Rooij J, Zwartkruis FJT, Verheijen MHG, Cool RH, Nijman SMB, Wittinghofer A, Bos JL (1998). Epac is a Rap1 guanine-nucleotide-exchange factor directly activated by cyclic AMP. *Nature* 396:474–477.

Deák F, Shin OH, Kavalali ET, Südhof T (2006). Structural determinants of synaptobrevin 2 function in synaptic vesicle fusion. *J Neurosci* 26:6668–6676.

Debus K, Lindau M (2000). Resolution of patch capacitance recordings and of fusion pore conductances in small vesicles. *Biophys J* 78:2983–2997.

Di Renzo G, Amoroso S, Bassi A, Fatatis A, Cataldi M, Colao AM, Lombardi G, Annunziato L (1995). Role of the Na^{+}-Ca^{2+} and Na^{+}-H^{+} antiporters in prolactin release from anterior pituitary cells in primary culture. *Eur J Pharmacol* 294:11-15.

Eberhard DA, Cooper CL, Low MG, Holz RW (1990). Evidence that the inositol phospholipids are necessary for exocytosis. Loss of inositol phospholipids and inhibition of secretion in permeabilized cells caused by a bacterial phospholipase C and removal of ATP. *Biochem J* 268:15–25.

Ebstein RP, Oppenheim G, Ebstein BS, Amiri Z, Stessman J (1986). The cyclic AMP second messenger system in man: the effects of heredity, hormones, drugs, aluminum, age and disease on signal amplification. *Prog Neuropsychopharmacol Biol Psychiatry* 10:323-353.

Elhamdani A, Azizi F, Artalejo C (2006). Double patch clamp reveals that transient fusion (kiss-and run) is a major mechanism of secretion in calf adrenal chromaffin cells: high calcium shifts the mechanism from kiss-and-run to complete fusion. *J Neurosci* 26:3030–3036.

El-Kholy W, MacDonald PE, Fox JM, Bhattacharjee A, Xue T, Gao X, Zhang Y, Stieber J, Li RA, Tsushima RG, Wheeler MB (2007). Hyperpolarization-activated cyclic nucleotide-gated channels in pancreatic beta-cells. *Mol Endocrinol* 21:753-764.

Exley C, Birchall JD (1992). The cellular toxicity of aluminium. *J Theor Biol* 159:83-98.

Fatt P, Katz B (1952). Spontaneous subthreshold activity at motor nerve endings. *J Physiol* 117:109–128.

Fernandez J, Neher E, Gomperts B (1984). Capacitance measurements reveal stepwise fusion events in degranulating mast cells. *Nature* 312:453–455.

Fesce R, Grohovaz F, Valtorta F, Meldolesi J (1994). Neurotransmitter release: fusion or “kiss-and-run”? *Trends Cell Biol* 4:1–4.

Freeman ME, Kanyicska B, Lerant A, Nagy G (2000). Prolactin: structure, function, and regulation of secretion. *Physiol Rev* 80:1523-1631.

Fulop T, Radabaugh S, Smith C (2005). Activity-dependent differential transmitter release in mouse adrenal chromaffin cells. *J Neurosci* 25:7324-7332.

Furber KL, Churchward MA, Rogasevskaia TP, Coorssen JR (2009). Identifying critical components of native Ca^{2+}-triggered membrane fusion. Integrating studies of proteins and lipids. *Ann N Y Acad Sci* 1152:121-134.

Galoyan AA, Shakhlamov VA, Aghajanov MI, Vahradyan HG (2004). Hypothalamic proline-rich polypeptide protects brain neurons in aluminum neurotoxicosis. *Neurochem Res* 29:1349-1357.

Gandhi S, Stevens C (2003). Three modes of synaptic vesicular recycling revealed by single-vesicle imaging. *Nature* 423:607–613.

Golub MS, Donald JM, Gershwin ME, Keen CL (1989). Effects of aluminum ingestion on spontaneous motor activity of mice. *Neurotoxicol Teratol* 11:231-235.

Gonçalves PP, Silva VS (2007). Does neurotransmission impairment accompany aluminium neurotoxicity? *J Inorg Biochem* 101:1291-1338.

Gonçalves PP, Stenovec M, Chowdhury HH, Grilc S, Kreft M, Zorec R (2008). Prolactin secretion sites contain syntaxin-1 and differ from ganglioside monosialic acid rafts in rat lactotrophs. *Endocrinology* 149:4948-4957.

Gonzalez-Iglesias AE, Jiang Y, Tomic M, Kretschmannova K, Andric SA, Zemkova H, Stojilkovic SS (2006). Dependence of electrical activity and calcium influx-controlled prolactin release on adenylyl cyclase signalling pathway in pituitary lactotrophs. *Mol Endocrinol* 20:2231–2246.

Gonzalez-Iglesias AE, Kretschmannova K, Tomic M., Stojilkovic SS (2006b). ZD7288 inhibits exocytosis in an HCN-independent manner and downsstream of voltage-gated calcium influx in pituitary lactotrophs. *Biochem Biophys Res Commun* 346:845-850.

Gonzalez-Iglesias AE, Murano T, Li S, Tomic M, Stojilkovic SS (2008). Dopamine inhibits prolactin release in pituitary lactotrophs through pertussis toxin-sensitive and -insensitive signaling pathways. *Endocrinology* 149:1470–1479.

Greener ID, Monfredi O, Inada S, Chandler NJ, Tellez JO, Atkinson A, Taube MA, Billeter R, Anderson RH, Efimov IR, Molenaar P, Sigg DC, Sharma V, Boyett MR, Dobrzynski H (2011). Molecular architecture of the human specialised atrioventricular conduction axis. *J Mol Cell Cardiol* 50:642-651.

Grishanin R, Kowalchyk J, Klenchin V, Ann K, Earles C, Chapman E, Gerona R, Martin T (2004). CAPS Acts at a Prefusion Step in Dense-Core Vesicle Exocytosis as a PIP2 Binding Protein. *Neuron* 43:551-562.

Grünberger C, Obermayer B, Klar J, Kurtz A, Schweda F (2006). The calcium paradoxon of renin release: calcium suppresses renin exocytosis by inhibition of calcium-dependent adenylate cyclases AC5 and AC6. *Circ Res* 99:1197-206.

Han X, Wang C-T, Bai J, Chapman ER, Jackson MB (2004). Transmembrane segments of syntaxin line the fusion pore of Ca^{2+}-triggered exocytosis*. Science* 304:289–292.

Hanna ST, Pigeau GM, Galvanovskis J, Clark A, Rorsman P, MacDonald PE (2009). Kiss-and-run exocytosis and fusion pores of secretory vesicles in human β-cells. *Pflugers Arch - Eur J Physiol* 457:1343–1350.

Harata N, Aravanis A, Tsien R (2006). Kiss and- run and full-collapse fusion as modes of exoendocytosis in neurosecretion. *J Neurochem* 97:1546–1570.

Hardel N, Harmel N, Zolles G, Fakler B, Klöcker N (2008). Recycling endosomes supply cardiac pacemaker channels for regulated surface expression. *Cardiovasc Res* 79:52-60.

Hatakeyama H, Kishimoto T, Nemoto T, Kasai H, Takahashi N (2006). Rapid glucose sensing by protein kinase A for insulin exocytosis in mouse pancreatic islets*. J Physiol* 570:271–282.

He P, Deng J, Zhong X, Zhou Z, Song B, Li L (2012). Identification of a hyperpolarization-activated cyclic nucleotide-gated channel and its subtypes in the urinary bladder of the rat. *Urology* 79:1411e7-13.

Hegle AP, Nazzari H, Roth A, Angoli D, Accili EA (2010). Evolutionary emergence of N-glycosylation as a variable promoter of HCN channel surface expression. *Am J Physiol Cell Physiol* 298:C1066-C1076.

Henkel AW, Meiri H, Horstmann H, Lindau M, Almers W (2000). Rhythmic opening and closing of vesicles during constitutive exo- and endocytosis in chromaffin cells. *EMBO J* 19:84–93.

Herrmann S, Stieber J, Ludwig A (2007). Pathophysiology of HCN channels. *Pflugers Arch* 454:517-522.

Heuser J, Reese T (1973). Evidence for recycling of synaptic vesicle membrane during transmitter release at the frog neuromuscular junction. *J Cell Biol* 57:315–344.

Horst WJ, Wang Y, Eticha D (2010). The role of the root apoplast in aluminium-induced inhibition of root elongation and in aluminium resistance of plants: a review. *Ann Bot* 106:185-197.

Horton P, Nakai K (1997). Better prediction of protein cellular localization sites with the k nearest neighbors classifier. *Proc Int Conf Intell Syst Mol Biol* 5:147-152.

Horwitz GC, Lelli A, Géléoc GS, Holt JR (2010). HCN channels are not required for mechanotransduction in sensory hair cells of the mouse inner ear. *PLoS One* 5:e8627.

Hua S, Raciborska D, Trimble W, Charlton M (1998). Different VAMP/synaptobrevin complexes for spontaneous and evoked transmitter release at the crayfish neuromuscular junction. *J Neurophysiol* 80:3233–3246.

Huerta-Ocampo I, Christian H, Thompson N, El-Kasti M, Wells T (2005). The Intermediate lactotroph: a morphologically distinct, ghrelin-responsive pituitary cell in the dwarf (dw/dw) rat. *Endocrinology* 146:5012–5023.

Hurtado R, Bub G, Herzlinger D (2010). The pelvis-kidney junction contains HCN3, a hyperpolarization-activated cation channel that triggers ureter peristalsis. *Kidney Int* 77:500-508.

Jahn R (2003). SNARE-mediated membrane fusion in the secretory pathway. *Biophysical J* 84:11a-11a.

Jahn R, Lang T, Südhof T (2003). Membrane fusion. *Cell* 112:519–533.

Jahn R, Scheller RH (2006). SNAREs-engines for membrane fusion. *Nat RevMol Cell Biol* 7:631–643.

Johnson GV, Jope RS (1987). Aluminum alters cyclic AMP and cyclic GMP levels but not presynaptic cholinergic markers in rat brain in vivo. *Brain Res* 403:1-6.

Johnson GV, Li XH, Jope RS (1989). Aluminum increases agonist-stimulated cyclic AMP production in rat cerebral cortical slices. *J Neurochem* 53:258-263.

Jorgačevski J, Stenovec M, Kreft M, Bajić A, Rituper B, Vardjan N, Stojilkovic S, Zorec R (2008). Hypotonicity and peptide discharge from a single vesicle. *Am J Physiol Cell Physiol* 295:624–631.

Jorgačevski J, Fošnarič M, Vardjan N, Stenovec M, Potokar M, Kreft M, Kralj-Iglič V, Iglič A, Zorec R (2010). Fusion pore stability of peptidergic vesicles. *Mol Membr Biol* 27:65–80.

Jorgačevski J, Potokar M, Grilc S, Kreft M, Liu W, Barclay WF, Buckers J, Medda R, Hell SH, Parpura V, Burgoyne RD, Zorec R (2011). Munc18-1 Tuning of Vesicle Merger and Fusion Pore Properties. *J Neurosci* 31:9055–9066.

Jorgačevski J, Kreft M, Vardjan N, Zorec R (2012). Fusion pore regulation in peptidergic vesicles.*Cell Calcium* 52:270-276.

Kabaso D, Calejo AI, Jorgačevski J, Kreft M, Zorec R, Iglič A (2012). Fusion pore diameter regulation by cations modulating local membrane anisotropy. *Scientific World Journal*, Article ID 983138, 7 pages doi:10.1100/2012/983138

Kang G, Chepurny OG, Holz GG (2001). cAMP-regulated guanine nucleotide exchange factor II (Epac2) mediates Ca2+-induced Ca2+ release in INS-1 pancreatic beta-cells. *J Physiol* 536:375-385.

Kang G, Joseph JW, Chepurny OG, Monaco M, Wheeler MB, Bos JL, Schwede F, Genieser HG, Holz GG (2003). Epac-selective cAMP analog 8-pCPT-2'-O-Me-cAMP as a stimulus for Ca^{2+}-induced Ca^{2+} release and exocytosis in pancreatic beta cells. *J Biol Chem* 278:8279-8285.

Katz B (1969). The Release of Neural Transmitter Substances. Liverpool University Press, Liverpool.

Kaupp UB, Seifert R (2001). Molecular diversity of pacemaker ion channels. *Annu Rev Physiol* 63:235-257.

Kawasaki H, Springett GM, Mochizuki N, Toki S, Nakaya M, Matsuda M, Housman DE, Graybiel AM (1998). A family of cAMP-binding proteins that directly activate Rap1. *Science* 282:2275-2279.

Kimura K, Kitano J, Nakajima Y, Nakanishi S (2004). Hyperpolarization-activated, cyclic nucleotide-gated HCN2 cation channel forms a protein assembly with

multiple neuronal scaffold proteins in distinct modes of protein-protein interaction. *Genes Cells* 9:631-640.

Klenchin VA, Martin TF (2000). Priming in exocytosis: attaining fusion-competence after vesicle docking. *Biochimie* 82:399-407.

Klyachko VA, Jackson MB (2002). Capacitance steps and fusion pores of small and large-dense-core vesicles in nerve terminals. *Nature* 418:89-92.

Korovkina VP, Stamnes SJ, Brainard AM, England SK (2009). Nardilysin convertase regulates the function of the maxi-K channel isoform mK44 in human myometrium. *Am J Physiol Cell Physiol* 296:C433-C440.

Kostic TS, Tomic M, Andric SA, Stojilkovic SS (2002). Calcium-independent and cAMP-dependent modulation of soluble guanylyl cyclase activity by G protein-couple receptors in pitiitary cells. *J Biol Chem* 277:16412–16418.

Kozlov M, Markin V (1983). Possible mechanism of membrane fusion. *Biofizika* 28:242–247.

Kralj-Iglic V, Heinrich V, Svetina S, Žekš B (1999). Free energy of closed membrane with anisotropic inclusions. *Eur Phys J B* 10:5–8.

Kreft M, Zorec R (1997). Cell-attached measurements of attofarad capacitance steps in rat melanotrophs. *Pflugers Arch* 434:212–214.

Kretschmannova K, Gonzalez-Iglesias AE, Tomić M, Stojilkovic SS (2006). Dependence of hyperpolarisation-activated cyclic nucleotide-gated channel activity on basal cyclic adenosine monophosphate production in spontaneously firing GH3 cells. *J Neuroendocrinol* 18:484-493.

Kretschmannova K, Kucka M, Gonzalez-Iglesias AE, Stojilkovic SS (2012). The expression and role of hyperpolarization-activated and cyclic nucleotide-gated channels in endocrine anterior pituitary cells. *Mol Endocrinol* 26:153-164.

Kwan EP, Gao X, Leung YM, Gaisano HY (2007). Activation of exchange protein directly activated by cyclic adenosine monophosphate and protein kinase A regulate common and distinct steps in promoting plasma membrane exocytic and granule-to-granule fusions in rat islet beta cells. *Pancreas* 35:e45-54.

Lewis AS, Estep CM, Chetkovich DM (2010). The fast and slow ups and downs of HCN channel regulation. *Channels* 4:215-31.

Li L, Chin LS (2003). The molecular machinery of synaptic vesicle exocytosis. *Cell Mol Life Sci* 60:942-960.

Lollike K, Borregaard N, Lindau M (1995). The exocytotic fusion pore of small granules has a conductance similar to an ion channel. *J Cell Biol* 129:99–104.

Lollike K, Lindau M (1999). Membrane capacitance techniques to monitor granule exocytosis in neutrophils. *J Immunol Methods* 232:111–120.

MacDonald PE, Braun M, Galvanovskis J, Rorsman P (2006). Release of small transmitters through kiss-and-run fusion pores in rat pancreatic β cells. *Cell Metabolism* 4:283–290.

Marionneau C, Couette B, Liu J, Li H, Mangoni ME, Nargeot J, Lei M, Escande D, Demolombe S (2005). Specific pattern of ionic channel gene expression associated with pacemaker activity in the mouse heart. *J Physiol* 562:223-234.

Matzel LD, Rogers RF, Talk AC (1996). Bidirectional regulation of neuronal potassium currents by the G-protein activator aluminium fluoride as a function of intracellular calcium concentration. *Neuroscience* 74:1175–1185.

Mei FC, Qiao J, Tsygankova OM, Meinkoth JL, Quilliam LA, Cheng X (2002). Differential signaling of cyclic AMP: opposing effects of exchange protein directly activated by cyclic AMP and cAMP-dependent protein kinase on protein kinase B activation. *J Biol Chem* 277:11497-11504.

Michael D, Cai H, Xiong W, Ouyang J, Chow R (2006). Mechanisms of peptide hormone secretion.*Trends Endocrinol Metab* 17:408–415.

Michels G, Er F, Khan I, Südkamp M, Herzig S, Hoppe UC (2005). Single-channel properties support a potential contribution of hyperpolarization-activated cyclic nucleotide-gated channels and If to cardiac arrhythmias. *Circulation* 111:399-404.

Michels G, Brandt MC, Zagidullin N, Khan IF, Larbig R, van Aaken S, Wippermann J, Hoppe UC (2008). Direct evidence for calcium conductance of hyperpolarization-activated cyclic nucleotide-gated channels and human native If at physiological calcium concentrations. *Cardiovasc Res* 78:466-475.

Miklavc P, Mair N, Wittekindt OH, Hallerb T, Dietla P, Feldera E, Timmlera M, Fricka M (2011). Fusion-activated Ca^{2+} entry via vesicular P2X4 receptors promotes fusion pore opening and exocytotic content release in pneumocytes. *PNAS* 108:14503-14508.

Miller DD, de Ruijter NCA, Emons AMC (1997). From signal to form: aspects of the cytoskeleton-plasma membrane—cell wall continuuum in root hair tips. *J Exp Bot* 48:1881-1896.

Monteggia LM, Eisch AJ, Tang MD, Kaczmarek LK, Nestler EJ (2000). Cloning and localization of the hyperpolarization-activated cyclic nucleotide-gated channel family in rat brain. *Brain Res Mol Brain Res* 81:129-139.

Much B, Wahl-Schott C, Zong X, Schneider A, Baumann L, Moosmang S, Ludwig A, Biel M (2003). Role of subunit heteromerization and N-linked glycosylation in the formation of functional hyperpolarization-activated cyclic nucleotide-gated channels. *J Biol Chem* 278:43781-43786.

Neher E, Marty A (1982). Discrete changes of cell membrane capacitance observed under conditions of enhanced secretion in bovine adrenal chromaffin cells. *Proc Natl Acad Sci USA* 79:6712–6716.

Noam Y, Zha Q, Phan L, Wu RL, Chetkovich DM, Wadman WJ, Baram TZ (2010). Trafficking and surface expression of hyperpolarization-activated cyclic nucleotide-gated channels in hippocampal neurons. *J Biol Chem* 285:14724-14736.

Obermüller S, Lindqvist A, Karanauskaite J, Galvanovskis J, Rorsman P, Barg S (2005). Selective nucleotide-release from dense-core granules in insulin-secreting cells. *J Cell Sci* 118:4271–4282.

Ohara-Imaizumi M, Nakamichi Y, Tanaka T, Katsuta H, Ishida H, Nagamatsu S (2002). Monitoring of exocytosis and endocytosis of insulin secretory granules in the pancreatic beta-cell line MIN6 using pH-sensitive green fluorescent protein (pHluorin) and confocal laser microscopy. *Biochem J* 363:73–80.

Okamoto M, Sudhof TC (1997). Mints, Munc18-interacting proteins in synaptic vesicle exocytosis. *J Biol Chem* 272:31459–31464.

Orci L, Ravazzola M, Amherdt M, Perrelet A, Powell SK, Quinn DL, Moore HP (1987). The trans-most cisternae of the Golgi complex: a compartment for sorting of secretory and plasma membrane proteins. *Cell* 51:1039–1051.

Ozaki N, Shibasaki T, Kashima Y, Miki T, Takahashi K, Ueno H, Sunaga Y, Yano H, Matsuura Y, Iwanaga T, Takai Y, Seino S (2000). cAMP-GEFII is a direct target of cAMP in regulated exocytosis. *Nat Cell Biol* 2:805–811.

Panda SK, Baluska F, Matsumoto H (2009). Aluminum stress signaling in plants. *Plant Signal Behav* 4:592-597.

Pang ZP, Sun J, Rizo J, Maximov A, Südhof TC (2006). Genetic analysis of synaptotagmin 2 in spontaneous and Ca^{2+}-triggered neurotransmitter release. *EMBO J* 25:2039–2050.

Perrais D, Kleppe I, Taraska J, Almers W (2004). Recapture after exocytosis causes differential retention of protein in granules of bovine chromaffin cells. *J Physiol* 560:413–428.

Poller WC, Bernard R, Derst C, Weiss T, Madai VI, Veh RW (2011). Lateral habenular neurons projecting to reward-processing monoaminergic nuclei express hyperpolarization-activated cyclic nucleotid-gated cation channels*. Neuroscience* 193:205-216.

Porter TE, Grandy D, Bunzow J, Wiles CD, Civelli O, Frawley LS (1994). Evidence that stimulating dopamine receptors may be involved in regulatory of prolactin secretion. *Endocrinology* 134:1263-1268.

Postea O, Biel M (2011). Exploring HCN channels as novel drug targets. *Nat Rev Drug Discov* 10:903-914.

Potokar M, Stenovec M, Kreft M, Gabrijel M, Zorec R (2011). Physiopathologic dynamics of vesicle traffic in astrocytes. *Histol Histopathol* 26:277-284.

Pow DV, Morris JF (1991). Membrane routing during exocytosis and endocytosis in neuroendocrine neurones and endocrine cells: use of colloidal gold particles and immunocytochemical discrimination of membrane compartments. *Cell Tissue Res* 264:299-316.

Proenza C, Tran N, Angoli D, Zahynacz K, Balcar P, Accili EA (2002). Different roles for the cyclic nucleotide binding domain and amino terminus in assembly and expression of hyperpolarization-activated, cyclic nucleotide-gated channels. *J Biol Chem* 277:29634-29642.

Provan SD, Yokel RA (1992). Aluminum inhibits glutamate release from transverse rat hippocampal slices: role of G proteins, Ca^{2+} channels and protein kinase C. *Neurotoxicology* 13:413-420.

Puthota V, Cruz-Ortega R, Johnson J, Ownby J (1991). An ultra-structural study of the inhibition of mucilage secretion in the wheat root cap by aluminium. In RJ Wright, VC Baligar, RI' hhrrmann, eds, Plant-Soil Interactions at Low pH. Kluwer Academic Publish- ers, Dordrecht, The Netherlands, pp 779-787

Rahamimoff R, DeRiemer SA, Ginsburg S, Kaiserman I, Sakmann B, Shapira R, Stadler H, Yakir N (1989). Ionic channels in synaptic vesicles: are they involved in transmitter release? *Q J Exp Physiol* 74:1019-1031.

Rahamimoff R, Fernandez JM (1997). Pre- and post-fusion regulation of transmitter release. *Neuron* 18:17–27.

Rahamimoff R, Lev-Tov A, Meiri H (1980). Primary and secondary regulation of quantal transmitter release: calcium and sodium. *J Exp Biol* 89:5-18.

Renström E, Eliasson L, Rorsman P (1997). Protein kinase A-dependent and -independent stimulation of exocytosis by cAMP in mouse pancreatic B-cells. *J Physiol* 502:105–118.

Reusche E, Lindner B, Arnholdt H (1994). Widespread aluminium deposition in extracerebral organ systems of patients with dialysis-associated encephalopathy. *Virchows Arch* 424:105-112.

Rituper B, Flašker A, Guček A, Chowdhury HH, Zorec R (2012). Cholesterol and regulated exocytosis: a requirement for unitary exocytotic events. *Cell Calcium* 52:250-258.

Robinson RB, Siegelbaum SA (2003). Hyperpolarization-activated cation currents: from molecules to physiological function. *Annu Rev Physiol* 65:453-480.

Rohrbough J, Broadie K (2005). Lipid regulation of the synaptic vesicle cycle. *Nature Rev. Neurosci* 6:139–150.

Rupnik M, Zorec R (1995). Intracellular Cl^- modulates Ca^{2+}-induced exocytosis from rat melanotrophs through GTP-binding proteins. *Pflugers Arch* 431:76-83.

Saitow F, Suzuki H, Konishi S (2005). β-Adrenoceptor-mediated long-term up-regulation of the release machinery at rat cerebellar GABAergic synapses. *J Physiol* 565: 487–502.

Sakaba T, Neher E (2001). Preferential potentiation of fast-releasing synaptic vesicles by cAMP at the calyx of Held. *Proc Natl Acad Sci USA* 98:331-336.

Sankaranarayanan S, Simasko SM (1996). A role for a background sodium current in spontaneous action potentials and secretion from rat lactotrophs. *Am J Physiol* 271:C1927–C1934.

Santoro B, Liu DT, Yao H, Bartsch D, Kandel ER, Siegelbaum SA, Tibbs GR (1998). Identification of a gene encoding a hyperpolarization-activated pacemaker channel of brain. *Cell* 93:717-729.

Santoro B, Wainger BJ, Siegelbaum SA (2004). Regulation of HCN channel surface expression by a novel C-terminal protein-protein interaction. *J Neurosci* 24:10750-10762.

Schechter I, Berger A (1968). On the active site of proteases. 3. Mapping the active site of papain; specific peptide inhibitors of papain. *Biochem Biophys Res Commun* 32:898-902.

Schweizer FE, Ryan TA (2006). The synaptic vesicle: cycle of exocytosis and endocytosis. *Curr Opin Neurobiol* 16:298-304.

Sedej S, Rose T, Rupnik M (2005). cAMP increases Ca2+-dependent exocytosis through both PKA and Epac2 in mouse melanotrophs from pituitary slices. *J Physiol* 567:799–813.

Seino S, Shibasaki T (2005). PKA-dependent and PKA-independent pathways for cAMP-regulated exocyosis. *Physiol Rev* 85:1303–1342.

Shafer TJ, Mundy WR (1995). Effects of aluminum on neuronal signal transduction: mechanisms underlying disruption of phosphoinositide hydrolysis. *Gen Pharmacol* 26:889-895.

Shimomura H, Imai A, Nashida T (2004). Evidence for the involvement of cAMP-GEF (Epac) pathway in amylase release from the rat parotid gland. *Arch Biochem Biophys* 431:124-128.

Sikdar SK, Zorec R, Mason WT (1990). cAMP directly facilitates Ca-induced exocytosis in bovine lactotrophs. *FEBS Lett* 273:150–154.

Sikdar SK, Kreft M, Zorec R (1998). Modulation of unitary exocytotic event amplitude by cAMP in rat melanotrophs. *J Physiol* 511:851–859.

Silva VS, Cordeiro JM, Matos MJ, Oliveira CR, Gonçalves PP (2002). Aluminium accumulation and membrane fluidity alteration in synaptosomes isolated from brain cortex following aluminium ingestion: effect of cholesterol. *Neurosci Res* 44:181-193.

Silva VS, Nunes MA, Cordeiro JM, Calejo AI, Santos S, Neves P, Sykes A, Morgado F, Dunant Y, Gonçalves PP (2007). Comparative effects of aluminum and ouabain on synaptosomal choline uptake, acetylcholine release and (Na^+/K^+)ATPase. *Toxicology* 236:158-177.

Simonsen L, Johnsen H, Lund SP, Matikainen E, Midtgård U, Wennberg A (1994). Methodological approach to the evaluation of neurotoxicity data and the classification of neurotoxic chemicals. *Scand J Work Environ Health* 20:1-12.

Smets G, Velkeniers B, Finne E, Baldys A, Gepts W, Vanhaelst L (1987). Postnatal development of growth hormone and prolactin cells in male and female rat pituitary. An immunocytochemical light and electron microscopic study. *J Histochem Cytochem* 35:335–341.

Sollner T, Whiteheart SW, Brunner M, Erdjument-Bromage H, Geromanos S, Tempst P, Rothman JE (1993). SNAP receptors implicated in vesicle targeting and fusion. *Nature* 362:318-324.

Spruce A, Breckenridge L, Lee A, Almers W (1990). Properties of the fusion pore that forms during exocytosis of a mast cell secretory vesicle. *Neuron* 4:643–654.

Staal R, Mosharov E, Sulzer D (2004). Dopamine neurons release transmitter via a flickering fusion pore. *Nat Neurosci* 7:341–346.

Stenovec M, Kreft M, Poberaj I, Betz W, Zorec R (2004). Slow spontaneous secretion from single large dense-core vesicles monitored in neuroendocrine cells. *FASEB J* 18:1270–1272.

Sternweis PC, Gilman AG (1982). Aluminum: a requirement for activation of the regulatory component of adenylate cyclase by fluoride. *Proc Natl Acad Sci USA* 79:4888–44891.

Stojilkovic SS (2005). Ca^{2+}-regulated exocytosis and SNARE function. *Trends Endocrinol Metab* 16:81-83.

Stojilkovic SS, Kretschmannova K, Tomic M, Stratakis CA (2012). Dependence of excitability of pituitary cells on cyclic nucleotides. *J Neuroendocrinol* 24:1183-1200.

Stojilkovic SS, Tabak J, Bertram R (2010). Ion channels and signaling in the pituitary gland. *Endocr Rev* 31:845–915.

Stojilkovic SS, Zemkova H, Van Goor F (2005). Biophysical basis of pituitary cell type-specific Ca2C signaling–secretion coupling. *Trends Endocrinol Metab* 16:152-159.

Su WM, Han GS, Casciano J, Carman GM (2012). Protein Kinase A-mediated Phosphorylation of Pah1p Phosphatidate Phosphatase Functions in Conjunction with the Pho85p-Pho80p and Cdc28p-Cyclin B Kinases to Regulate Lipid Synthesis in Yeast. *J Biol Chem* 40:33364–33376.

Szkudelski T, Nowicka E, Szkudelska K (2005). Leptin secretion and protein kinase A activity. *Physiol Res* 54:79-85.

Takamori S, Holt M, Stenius K, Lemke EA, Grønborg M, Riedel D, Urlaub H, Schenck S, Brügger B, Ringler P, Müller SA, Rammner B, Gräter F, Hub JS, De Groot BL, Mieskes G, Moriyama Y, Klingauf J, Grubmüller H, Heuser J, Wieland F, Jahn R (2006). Molecular anatomy of a trafficking organelle. *Cell* 127:831-846.

Tester M, Zorec R (1992). Cytoplasmic calcium stimulates exocytosis in a plant secretory cell. *Biophys J* 63:864–867.

Thiel G, Battey N (1998). Exocytosis in plants. *Plant Mol Biol* 38:111-125.

Thorn P (2009). New insights into the control of secretion. *Commun Integr Biol* 2:315–317.

Thorn P, Parker I (2005). Two phases of zymogen granule lifetime in mouse pancreas: Ghost granules linger after exocytosis of contents. *J Physiol* 563:433–442.

Tsuboi T, Rutter G (2003). Multiple forms of "kiss-and-run" exocytosis revealed by evanescent wave microscopy. *Curr Biol* 13:563–567.

Tsunoda M, Sharma RP (1999). Altered dopamine turnover in murine hypothalamus after low-dose continuous oral administration of aluminum. *J Trace Elem Med Bio* 13:224-231.

Turner AJ, Tanzawa K (1997). Mammalian membrane metallopeptidases: NEP, ECE, KELL, and PEX. *FASEB J* 11:355-364.

Ulens C, Tytgat J (2001). Functional heteromerization of HCN1 and HCN2 pacemaker channels. *J Biol Chem* 276:6069-6072.

Vaccari T, Moroni A, Rocchi M, Gorza L, Bianchi ME, Beltrame M, DiFrancesco D (1999). The human gene coding for HCN2, a pacemaker channel of the heart1. *Biochim Biophys Acta* 1446:419-425.

Vardjan N, Stenovec M, Jorgačevski J, Kreft M, Zorec R (2007). Subnanometer fusion pores in spontaneous exocytosis of peptidergic vesicles. *J Neurosci* 27:4737–4746.

Vardjan N, Jorgačevski J, Stenovec M, Kreft M, Zorec R (2009). Compound exocytosis in pituitary cells. *Ann N Y Acad Sci* 1152:63–75.

Vardjan N, Jorgacevski J, Zorec R (2012). Fusion Pores, SNAREs, and Exocytosis. *Neuroscientist* 19:160-174.

Varghese A, Tenbroek EM, Coles JJr, Sigg DC (2006). Endogenous channels in HEK cells and potential roles in HCN ionic current measurements. *Prog Biophys Mol Biol* 90:26-37.

Verhage M, Sørensen JB (2008). Vesicle docking in regulated exocytosis. *Traffic* 9:1414-1424.

Wahl-Schott C, Biel M (2009). HCN channels: structure, cellular regulation and physiological function. *Cell Mol Life Sci* 66:470-494.

Wainger BJ, DeGennaro M, Santoro B, Siegelbaum SA, Tibbs GR (2001). Molecular mechanism of cAMP modulation of HCN pacemaker channels. *Nature* 411:805-810.

Walton JR (2004). A bright field/fluorescent stain for aluminum: its specificity, validation, and staining characteristics. *Biotech Histochem* 79:169-176.

Wang CT, Lu JC, Bai J, Chang PY, Martin TFJ, Chapman ER, Jackson MB (2003). Different domains of synaptotagmin control the choice between kiss-and-run and full fusion. *Nature* 424:943–947.

Whittaker VP (1965). The application of subcellular fractionation techniques to the study of brain function. *Prog Biophys Mol Biol* 15:39-96.

Whittaker GM, Angoli D, Nazzari H, Shigemoto R, Accili EA (2007). HCN2 and HCN4 isoforms self-assemble and co-assemble with equal preference to form functional pacemaker channels. *J Biol Chem* 282:22900-22909.

Weise R, Kreft M, Zorec R, Homann U, Thiel G (2000). Transient and permanent fusion of vesicles in Zea mays coleoptile protoplast measured in cell-atached configuration. J Membr Biol 174:15-20.

Wightman RM, Jankowski JA, Kennedy RT, Kawagoe KT, Schroeder TJ, Leszczyszyn DJ, Near JA, Diliberto Jr EJ, Viveros OH (1991). Temporally resolved catecholamine spikes correspond to single vesicle release from individual chromaffin cells. Proc Natl Acad Sci USA 88:10754-10758.

Xue L, Li Y, Han X, Yao L, Yuan J, Qin W, Liu F, Wang H (2012). Investigation of hyperpolarization-activated cyclic nucleotide-gated channels in interstitial cells of Cajal of human bladder. *Urology* 224:e13-18.

Ye B, Nerbonne JM (2009). Proteolytic processing of HCN2 and co-assembly with HCN4 in the generation of cardiac pacemaker channels. *J Biol Chem* 284:25553-25559.

Yokel RA, Allen DD, Meyer JJ (1994). Studies of aluminum neurobehavioral toxicity in the intact mammal. *Cell Mol Neurobiol* 14:791-808.

Yu X, Duan K, Shang C, Yu H, Zhou Z (2004). Calcium influx through hyperpolarization-activated cation channels (Ih channels) contributes to activity-evoked neuronal secretion. *Proc Natl Acad Sci USA* 101:1051–1056.

Zaccolo M, Pozzan T (2003). CAMP and Ca^{2+} interplay: a matter of oscillation patterns. *Trends Neurosci* 26:53-55.

Zhang Y, Liu Y, Qu J, Hardy A, Zhang N, Diao J, Strijbos PJ, Tsushima R, Robinson RB, Gaisano HY, Wang Q, Wheeler MB (2009). Functional Characterization of HCN Channels in Rat Pancreatic β Cells. *J Endocrinol* 203:45–53.

Zhang Y, Zhang N, Gyulkhandanyan AV, Xu E, Gaisano HY, Wheeler MB, Wang Q (2008). Presence of functional hyperpolarisation-activated cyclic nucleotide-gated channels in clonal alpha cell lines and rat islet alpha cells. *Diabetologia* 51:2290-2298.

Zhang W, Lilja L, Bark C, Berggren PO, Meister B (2004). Mint1, a Munc-18-interacting protein, is expressed in insulin-secreting beta-cells. *Biochem Biophys Res Commun* 320:717-721.

Zhang Z, Jackson MB (2008). Temperature dependence of fusion kinetics and fusion pores in Ca^{2+}-triggered exocytosis from PC12 cells. *J Gen Physiol* 131:117–124.

Zhong N, Beaumont V, Zucker RS (2004). Calcium influx through HCN channels does not contribute to cAMP-enhanced transmission. *J Neurophysiol* 92:644-647.

Zimmerberg J, Curran M, Cohen FS (1991). A lipid/protein complex hypothesis for exocytotic fusion pore formation. *Ann N Y. Acad Sci* 635:307–317.

Zorec R, Sikdar SK, Mason WT (1991). Increased Cytosolic Calcium Stimulates Exocytosis in Bovine Lactotrophs. Direct evidence from changes in membrane capacitance. *J Gen Physiol* 97:473–497.